

Institute of Experimental and Clinical Pharmacology and Toxicology
Faculty of Medicine
Saarland University

***In vitro* and *in vivo* functions of TRPC3,
TRPC1 and voltage-gated Ca²⁺ channels
(CaVs) in mouse cortical astrocytes**

Dissertation submitted for obtaining the university degree of
Doctor rerum naturalium

Thabet Belkacemi

Born on 22nd July 1986
Manchester, United Kingdom

September 2016

First referee and “Doktorvater”: Prof. Dr. Veit Flockerzi, MD

Second referee:

Homburg, September 2016

Scientific supervisor: Dr. rer. nat. Andreas Beck

To my family

Acknowledgements

This research project would not have been possible without the support of many people.

I wish to express my gratitude to my supervisors, Dr. Andreas Beck and Prof. Veit Flockerzi who were abundantly helpful and offered invaluable support and guidance.

Special thanks also to Dr. Petra Weißgerber and all members of the animal facility, Dr. Stephan Philipp for his help in FACS, and from Physiology department Prof. Frank Kirchhoff and Dr. Anja Scheller for helping in the surgical experiments.

I would also like to thank Sandra Plant, Stefanie Buchholz, Martin Simon-Thomas, Ute Soltek, Heidi Löhr, Christine Wesely, Tanja Maurer and Tom Janke for their technical assistance, and Claudia Ecker for her administrative help. Many thanks to Barbara Wardas for translating the Summary, and to all my colleagues in the Pharmacology and Toxicology department.

Special thanks to my wife Sara and my parents for their support.

Contributions

I hereby acknowledge the contributions of the following colleagues:

PD. Dr. Stephan Philipp: Helping in the FACS analysis

Stefanie Buchholz: Helping in cloning the TRPC1 VL and TRPC3 cDNAs from astrocytes. Generation of mTRPC3-pcAGGS-IRES-GFP and tetracycline-inducible mTRPC3 MWK mutation in HEK cells.

Laura Hofmann and PD. Dr. Ulrich Wissenbach: Generation of mTRPC1 VL-pcAGGS-IRES-GFP and HEK cells stably expressing the mTRPC1 VL.

Dr. Christina Backes and Prof. Andreas Keller: Transcriptome analysis.

Table of Contents

List of Abbreviations	V
List of Figures.....	VII
List of Tables.....	X
Summary.....	XI
Zusammenfassung.....	XII
1 Introduction.....	1
1.1 Brain injury	1
1.2 Astrocytes	1
1.3 Astrogliosis.....	2
1.4 Calcium (Ca^{2+})	4
1.5 Transient Receptor Potential (TRP) Channels	5
1.6 Transient Receptor Potential Canonical Channels (TRPC).....	7
1.6.1 TRPC1.....	7
1.6.2 TRPC2.....	8
1.6.3 TRPC3.....	8
1.6.4 TRPC4.....	9
1.6.5 TRPC5.....	10
1.6.6 TRPC6.....	10
1.6.7 TRPC7	11
1.6.8 TRPCs in astrocytes.....	11
1.7 Voltage-gated Ca^{2+} channels (CaVs).....	12
1.7.1 The pore-forming $\alpha 1$ subunits	13
1.7.2 The auxiliary subunits.....	14
1.7.3 CaVs in astrocytes.....	16
1.8 Aims	18
2 Materials and Methods	19
2.1 Mouse lines	19
2.2 Isolation and culture of mouse cortical astrocytes and microglia	19

2.3	Human embryonic kidney (HEK) 293 cell culture	21
2.4	HEK cell transfection	22
2.5	Immunocytochemistry	22
2.6	FACS	23
2.6.1	Fluorescence Activated Cell Sorting (FACS).....	23
2.6.2	Fixed and permeabilized cell preparation for FACS	24
2.6.3	Living cell preparation for FACS	24
2.7	Polymerase Chain Reaction (PCR).....	26
2.7.1	Reverse Transcription Polymerase Chain Reaction (RT-PCR).....	27
2.7.2	RNA Isolation.....	27
2.7.3	One-Step Reverse Transcription Polymerase Chain Reaction	28
2.7.4	Gel Electrophoresis	29
2.8	TRPC1 and TRPC3 Full Length Amplification and Cloning.....	30
2.8.1	Two-Steps Reverse Transcription Polymerase Chain Reaction.....	30
2.8.2	Gel Extraction and DNA Purification.....	31
2.8.3	Ligation of Fragments into Vectors.....	31
2.8.4	Transformation	32
2.8.5	DNA Preparation	32
2.8.6	Restriction Analysis	33
2.9	Monitoring of Cytoplasmic Ca^{2+} by Fura-2	33
2.10	Fura-2 Experiment	35
2.11	Electrophysiological recordings.....	36
2.11.1	TRPC3 currents recording.....	37
2.11.2	CaVs currents recording.....	38
2.12	Migration Assay	39
2.13	Cortical stab wound surgery.....	40
2.14	Mice fixation with paraformaldehyde (PFA).....	42
2.15	Immunohistochemistry on brain slices	42
2.16	Pharmacological compounds used in Ca^{2+} imaging and patch clamp experiments	43
2.17	Statistical Analysis	44

2.18	Solutions for Fura-2 and patch clamp experiments	45
3	Results.....	47
3.1	Characterization of mouse cortical astrocyte cultures	47
3.2	TRPC Expression in mouse cortical astrocyte cultures	47
3.3	Analysis of astrocytes by flow cytometry	48
3.4	Sorting astrocytes using preparative FACS	51
3.5	TRPC transcripts expression in the FACS-sorted astrocytes and microglia cells	53
3.5.1	RT-PCR from FACS-sorted astrocytes and microglia cells	53
3.5.2	Transcriptome analysis of TRPCs from GLAST-sorted astrocytes by next generation sequencing.....	54
3.5.3	Expression of TRPC3 and TRPC1 full length transcripts in GLAST-sorted astrocytes.....	56
3.6	TRPC3 in cultured cortical astrocytes	60
3.6.1	Role of TRPC3 in astrocytes	60
3.6.2	OAG-induced Ca^{2+} release and Ca^{2+} Influx in cultured astrocytes	61
3.6.3	OAG-induced Ca^{2+} influx is TRPC3-dependent.....	64
3.6.4	Electrophysiological characterization of TRPC3 current in TRPC3 cDNA expressing HEK293 cells	66
3.6.5	TRPC3 currents in cultured mouse cortical astrocytes.....	67
3.6.6	Role of TRPC3 in astrocytes migration	68
3.6.7	Astrogliosis and glial scar formation in TRPC3 gene-deficient mice	71
3.7	TRPC3 T to A mutation and moonwalker mice (MWK)	74
3.7.1	Expression of the TRPC3 MWK mutant cDNA in HEK 293 cells	74
3.7.2	Astrocytes from moonwalker mice.....	75
3.7.3	Astrocytes reactivity in non-injured MWK mouse brain	76
3.8	TRPC1 in cultured cortical astrocytes	78
3.8.1	Role of TRPC1 in astrocytes	78
3.8.2	Impact of TRPC1 VL on TRPC3 currents in HEK 293 cells	79
3.8.3	Role of TRPC1 in OAG-induced Ca^{2+} oscillations in cultured cortical astrocytes.....	81
3.8.4	Impact of TRPC1 VL on the constitutive TRPC3 MWK	82
3.8.5	Role of TRPC1 in astrocytes migration	85

3.8.6	Astrogliosis and glial scar formation depends on TRPC1 gene-deficient mice	86
3.9	Voltage-gated Ca^{2+} channels (CaVs) in astrocytes	89
3.9.1	Expression of CaVs subunits in cultured mouse cortical astrocytes	89
3.9.2	High potassium depolarization in astrocytes	90
3.9.3	Electrophysiological characterization of voltage-gated Ca^{2+} and Na^{+} channels in cultured cortical astrocytes	91
3.9.4	Impact of $\text{CaV}\beta 3$ deletion on CaVs activity in astrocytes	94
3.9.5	Impact of $\text{CaV}\beta 2$ deletion on CaVs activity in astrocytes	97
3.9.6	Pharmacological characterization of CaVs in astrocytes	99
4	Discussion	102
4.1	Characterization of cultured astrocytes and their transcript expression pattern	102
4.2	Roles of TRPC1 and TRPC3 proteins in astrocytes	104
4.3	Dissection of OAG-induced Ca^{2+} signals in astrocytes	105
4.4	Role of TRPC1 in the OAG-induced TRPC3 channel activity	108
4.5	Role of TRPC1 and TRPC3 in astrocytes migration and astrogliosis	110
4.6	Voltage-gated Na^{+} (NaV) and Ca^{2+} (CaV) channels in astrocytes	112
5	References	117
6	Supplementary Figures	131
	Curriculum Vitae	134

List of Abbreviations

AM	Acetoxymethylester
AUC	Area Under Curve
BAPTA	1,2-bis(o-aminophenoxy)ethane-N,N,N',N'-tetraacetic acid
bp	Base pair
BSA	Bovine-Serum-Albumin
Ca ²⁺	Ca ²⁺ ions
CNS	Central Nervous System
CPA	Cyclopiazonic Acid
DAG	Diacylglycerol
DKO	Double Gene-deficient
DMEM	Dulbecco's modified Eagle's medium
DMSO	Dimethylsulfoxide
DNA	Deoxyribonucleic acid
ER	Endoplasmatic Reticulum
FACS	Fluorescence-activated cell sorting
FCS	Fetal Calf Serum
GFAP	Glial Fibrillary Acidic Protein
GLAST	Glutamate Aspartate Transporter
IP3	Inositol-1,4,5-trisphosphate
IP3R	Inositol-1,4,5-trisphosphate Receptor
K ⁺	Potassium ions
KO	Gene-deficient
min	Minute
mM	Millimolar
ms	millisecond
Na ⁺	Sodium ions
NGS	Normal-Goat-Serum
nm	Nanometer
nM	Nanomolar
OAG	1-Oleoyl-2-acetyl-sn-glycerol
pA/pF	pico Ampere per pico Farad
PBS	Phosphate-Buffered Saline
PIP ₂	Phosphatidylinositol-4,5-bisphosphate
PLC	Phospholipase C
P-L-L	Poly-L-lysine
PMA	Phorbol-12-myristat-13-acetat
pmol	Picomol
Pyr3	Pyrazolium 3
RNA	Ribonucleic acid
ROCE	Receptor-Operated Ca ²⁺ Entry

RT-PCR	Reverse Transcription -Polymerase Chain Reaction
SEM	Standard Error of the Mean
SERCA	Sarcoplasmic/Endoplasmic Reticulum Ca^{2+} ATPase
TG	Thapsigargin
TRPA	Transient Receptor Potential Ankyrin
TRPC	Transient Receptor Potential Canonical
TRPM	Transient Receptor Potential Melastatin
TRPML	Transient Receptor Potential Mucolipin
TRPP	Transient Receptor Potential Polycystin
TRPV	Transient Receptor Potential Vanilloid
μM	Micromolar
CaVs	Voltage-gated Ca^{2+} Channel
NaVs	Voltage-gated Sodium channel
WT	Wild-type

List of Figures

Figure 1-1 Glial scar formation.	3
Figure 1-2 Transient Receptor Potential (TRP) Channel family.	6
Figure 1-3 Topology of voltage-gated Ca^{2+} channel.	13
Figure 2-1 Isolation procedure of mouse cortices.	21
Figure 2-2. Fluorescence Activated Cell Sorting (FACS).	25
Figure 2-3 Loading cells by Fura-2 AM.	34
Figure 2-4 Excitation and emission spectra of Fura-2.	35
Figure 2-5 Whole cell patch clamp recording.	37
Figure 2-6 Voltage ramp protocol for whole cell patch clamp recording. ...	38
Figure 2-7 Voltage ramp and step protocols for whole cell patch clamp recording.	39
Figure 2-8 Migration Assay in 6-well plate.	40
Figure 2-9 Cortical stab wound surgery.	41
Figure 2-10 Cortical stab wound analysis.	43
Figure 3-1. Immunocytochemistry of a mouse cortical astrocyte culture. ..	47
Figure 3-2 TRPC transcripts expression in mouse cortical astrocytes. ...	48
Figure 3-3 Flow cytometry analysis of the fixed and permeabilized astrocytes.	50
Figure 3-4 Preparative FACS of astrocytes and microglia.	51
Figure 3-5 TRPC transcripts expression in astrocytes and microglia.	54
Figure 3-6 Transcriptome analysis of TRPCs in cultured cortical astrocytes.	55
Figure 3-7 Full length amplification of TRPC3 and TRPC1 cDNAs from cultured and sorted astrocytes.	57
Figure 3-8 Restriction analysis of the TRPC1 VL and TRPC3 full length cDNAs in pUC19.	59
Figure 3-9 Ca^{2+} entry in cultured cortical astrocytes from wild-type and TRPC3/C6 gene-deficient mice.	61
Figure 3-10 OAG-induced Ca^{2+} release and Ca^{2+} influx in astrocytes from wild-type mice.	63
Figure 3-11 OAG-Induced Ca^{2+} oscillations in astrocytes are mediated via TRPC3.	65

Figure 3-12 TRPC3 currents in TRPC3 cDNA expressing HEK293 cells....	67
Figure 3-13 TRPC3 currents in astrocytes.....	68
Figure 3-14 Astrocytes migration <i>in vitro</i>.	70
Figure 3-15 Cortical stab wound.....	73
Figure 3-16 Constitutive channel activity of the TRPC3 MWK in HEK293 cells..	75
Figure 3-17 Ca²⁺ imaging in astrocytes from heterozygous MWK mice.....	76
Figure 3-18 GFAP staining of coronal sections from MWK and wild-type mice.....	77
Figure 3-19 Ca²⁺ entry in cultured cortical astrocytes from wild-type and TRPC1 gene-deficient mice.....	78
Figure 3-20 TRPC3 and TRPC3/TRPC1 VL currents in HEK293 cells.....	80
Figure 3-21 Deletion of TRPC1 increases the OAG-induced Ca²⁺ oscillations in astrocytes..	82
Figure 3-22 Effects of TRPC1 VL and TRPC3 on the constitutive TRPC3 MWK currents in HEK 293 cells.).....	84
Figure 3-23 <i>In vitro</i> migration of astrocytes from TRPC1 gene-deficient mice.....	85
Figure 3-24 Cortical stab wound in TRPC1/TRPC5 gene-deficient mice....	87
Figure 3-25 Expression analysis of voltage-gated Ca²⁺ channel subunit genes in cultured cortical astrocytes.....	90
Figure 3-26 Ca²⁺ influx induced by high potassium induced-depolarization in astrocytes.....	91
Figure 3-27 Voltage-gated cation channels in astrocytes..	92
Figure 3-28 Navsubunit α1 and β transcripts of voltage-gated Na⁺ channels in cultured cortical astrocytes..	93
Figure 3-29 CaVs currents in cultured cortical astrocytes.....	94
Figure 3-30 CaV currents in CaVβ3 deficient astrocytes.....	96
Figure 3-31 CaV currents in CaVβ2 deficient astrocytes.....	98
Figure 3-32 Pharmacological characterization CaVs in astrocytes. s.....	99
Figure 3-33 Block of CaV currents in astrocytes in the presence of increasing concentrations of isradipine..	101
Figure 4-1 OAG/DAG-dependent cation entry.....	108

Figure 6-1 TRPC transcripts expression in enriched astrocyte culture...	131
Figure 6-2 TRPC transcripts expression in GLAST-sorted astrocytes..	132
Figure 6-3 TRPC transcripts expression in CD11b-sorted microglia.	133

List of Tables

Table 2-1 Exon-spanning oligodeoxynucleotide primers used in RT-PCR	29
Table 2-2 Oligodeoxynucleotide Primers used to obtain full length TRPC cDNAs	31
Table 2-3 Solutions used in Ca^{2+} imaging experiments	45
Table 2-4 Patch clamp external solutions used for recording of TRPC currents	45
Table 2-5 Patch clamp external solutions used for recording of voltage-gated Ca^{2+} currents	46
Table 2-6 Pipette solutions used for recording of TRPC and CsVs patch clamp experiments	46

Summary

The present study illustrated a strategy to purify the astrocytes for gene expression analysis using FACS, which revealed that TRPC1, TRPC2, TRPC3 and TRPC4 transcript fragments are expressed in FACS-sorted GLAST-positive mouse cortical astrocytes. The full length cDNA of TRPC1 and TRPC3 could be amplified from the purified astrocytes. Fura-2 and patch clamp experiments were used to characterize TRPC3 in astrocytes, which was found to be involved in the DAG- (OAG) mediated Ca^{2+} entry and not in the ORAI-mediated Ca^{2+} entry. The deletion of the TRPC3 gene resulted in a slower astrocytic migration rate measured by the *in vitro* scratch assay, as well as less astrogliosis and cortical edema after brain injury *in vivo*. TRPC1 exerts negative effect on TRPC3 channel activity when co-expressed and astrocytes from TRPC1 gene-deficient mice revealed a faster *in vitro* migration rate and an increased *in vivo* astrogliosis and cortical edema. This correlates with the higher TRPC3 channel activity measured by Fura-2 in astrocytes isolated from TRPC1 gene-deficient mice. The presented results demonstrate an important role of TRPC3 in astrocytes Ca^{2+} signaling in particular after CNS injury as well as of TRPC1 in shaping the TRPC3-mediated Ca^{2+} signals. In the second part of this work, the voltage-gated Ca^{2+} channels (CaVs) in mouse cortical astrocytes were investigated. Transcripts of L-, P/Q- and R-type Ca^{2+} channels as well as $\text{CaV}\beta$ subunits were found to be expressed in GLAST-sorted mouse cortical astrocytes. Patch clamp experiments on cultured cortical astrocytes revealed voltage-gated Na^+ (NaV) and CaV currents. Using specific blockers, L-type Ca^{2+} channels were found to be the major type contributing to the CaV currents in cultured astrocytes, while P/Q-, N- and R-type had minor contributions. Deletion of the $\text{CaV}\beta 3$ subunit gene in astrocytes did not affect the CaV currents; however, the deletion of the $\text{CaV}\beta 2$ subunit gene did reduce the CaV currents in astrocytes. The presented results leave no doubt that mouse cultured cortical astrocytes do express functional voltage-gated Ca^{2+} channels, and that the $\text{CaV}\beta 3$ subunit serves functions beyond modulating CaV currents.

Zusammenfassung

Die vorliegende Arbeit beschreibt eine Strategie zur Isolierung von Astrozyten für Gen-Expressionsanalysen mithilfe der FACS-Methode. FACS-sortierte GLAST-positive kortikale Astrozyten der Maus exprimieren TRPC1, TRPC2, TRPC3 und TRPC4 Transkript-Fragmente, und die vollständige cDNs von TRPC1 und TRPC3 konnte aus ihnen amplifiziert werden. Mithilfe von Fura-2 und Patch Clamp Experimenten wurde TRPC3 in kultivierten Astrozyten charakterisiert und dessen Beteiligung am DAG (OAG)-vermittelten Ca^{2+} -Einstrom gezeigt. Am STIM-vermittelten Ca^{2+} Einstrom ist TRPC3 scheinbar nicht beteiligt. Die Deletion des TRPC3-Gens resultiert in einer reduzierten Migrationsrate der Astrozyten *in vitro*, sowie einer geringeren Astroglie und kortikalen Ödembildung nach einer Hirnverletzung *in vivo*. Die Ko-expression von TRPC1 mit TRPC3 hat einen negativen Effekt auf die TRPC3-Aktivität, da in TRPC1-defizienten Astrozyten sowohl eine schnellere Migrationsrate *in vitro* als auch eine verstärkte Astroglie und Ödembildung *in vivo* beobachtet wurden. Dies korreliert mit der in Fura-2 Experimenten gemessenen erhöhten TRPC3-Aktivität in TRPC1-defizienten Astrozyten. Die Ergebnisse der vorliegenden Arbeit zeigen, dass TRPC3 einen wichtigen Beitrag zu Ca^{2+} -Signalen in Astrozyten leistet, speziell nach Verletzungen im ZNS, und dass TRPC1 die TRPC3-vermittelten Ca^{2+} -Signale moduliert. Im zweiten Teil der vorliegenden Arbeit wurden spannungsabhängige Ca^{2+} -Kanäle (CaVs) in kortikalen Astrozyten der Maus untersucht. In FACS-sortierten GLAST-positiven Astrozyten konnten Transkripte von L-, P/Q-, und R-Typ Ca^{2+} Kanälen, sowie CaV β Untereinheiten nachgewiesen werden. Patch Clamp Experimente zeigten spannungsabhängige Na^+ - und Ca^{2+} -Ströme in kultivierten Astrozyten. Mithilfe spezifischer Blocker konnte der L-Typ Ca^{2+} -Kanal als hauptverantwortlich für den CaV-Strom identifiziert werden. P/Q-, N- und R-Typen trugen nur gering zum CaV Strom bei. Die Deletion der CaV β 3-Untereinheit hatte keinen Einfluss auf den CaV-Strom in den Astrozyten, wohingegen die Deletion der CaV β 2-Untereinheit den CaV-Strom reduzierte. Die Ergebnisse zeigen, dass kultivierte kortikale Astrozyten funktionelle spannungsabhängige Ca^{2+} -Kanäle besitzen, und weisen darüber hinaus darauf hin, dass CaV β 3-Untereinheiten neben der Modulation von CaV-Strömen noch weitere Funktionen ausüben.

1 Introduction

1.1 Brain injury

Brain injury is defined as an injury that occurs in the brain affecting a person physically, emotionally and behaviorally. Statistics showed that the incidence of acute traumatic brain injuries in European countries is about 235 cases per 100000 inhabitants (Tagliaferri et al., 2006). The brain injuries could happen already at birth or later from a disease or trauma and thereby they can be classified as traumatic or non-traumatic brain injuries. Traumatic brain injuries occur when an external force traumatically injures the brain which includes an open head wound, skull fracture or a non-invasive trauma. The non-traumatic brain injury involves no external force, but is rather caused by a primary disease condition like bleeding, lack of oxygen, tumors, infection or inflammation. Brain injuries affect all neuronal and non-neuronal cells in the brain and have different effects on the different cell types. Primary cellular injury is followed by a secondary response that includes changes in cerebral blood flow, local and systemic inflammation, alterations in oxygen delivery and metabolism, and both ischemic and apoptotic death of neural cells (Dutton and McCunn, 2003). Like any other wound, a scar is generated in the area of the damaged tissue that in the brain predominantly consists of astrocytes. Astrocytes, non-neuronal brain cells, are known to play an important role after brain injury where they enter into a reactive state called astrogliosis (Silver and Miller, 2004). This reactive state that astrocytes gain is achieved by the exposure of astrocytes to the damaged neuronal tissue on one side, and on the other side to the blood which finds its way through the brain due to the disruption of the blood brain barrier. This excessive proliferation and migration of reactive astrocytes form what is known as the glial scar.

1.2 Astrocytes

It is suggested that the total number of cells in the human brain is about 10^{12} , where neurons represent 10% whereas 90% of the cells are glial cells of which

the astrocytes are the major type (Kimelberg and Nedergaard, 2010). In 1891, Mihaly von Lenhossek proposed the name astrocytes for a type of cells which were known as neuroglia. The word astrocyte derives from the combination of two Latin words, astro “astron” meaning a star, while cyte “kytos” means a hollow vessel, later a cell (Parpura and Verkhratsky, 2012). The astrocytes can be visualized under the microscope by immunostaining of protein markers such as the Glial Fibrillary Acidic Protein (GFAP), Glutamate Aspartate Transporter (GLAST), S100 Ca²⁺-binding protein B (S100B) and Aquaporin 4 (AQP4). Astrocytes are coupled via gap junctions which allow to exchange small cytoplasmic molecules, such as IP₃, ATP, Ca²⁺ and other ions. They play an indispensable role before and after brain development where they guide the neuronal migration and serve as source of extracellular matrix and adhesion proteins, as well as providing neurotrophic and neurite-promoting factors. The central synapses are ensheathed by astrocytes, where they take up neurotransmitter molecules clearing the synaptic cleft. They also release transmitters itself and thus take part in modulating synaptic signaling and regulate the pH, ion concentration and also the osmolarity of the neuronal environment. The astrocytes are not only communicating with the nervous tissue, but their end-feet cover the entire surface of blood vessels where they secrete and take up transmitters and nutriment molecules. This physical interaction between astrocytes and blood vessels is found to be necessary for angiogenesis in the brain (Maragakis and Rothstein, 2006; Montgomery, 1994). Thus astrocytes are considered one of the major cellular component of the blood brain barrier (Cabezas et al., 2014).

1.3 Astrogliosis

Astrogliosis is a description of astrocytes that became reactive in response to CNS damage that could occur via trauma, infection, ischemia, stroke, autoimmune reaction and neurodegenerative disease. This reactive state causes expressional and morphological changes in astrocytes and subsequently increases the proliferation and the migration of astrocytes. Astrocytes in this activated state will form a glial scar and could inhibit the axonal regeneration in the injury sites (Schachtrup et al., 2010), however other

studies have shown otherwise (Anderson et al., 2016; Sofroniew, 2009). Traumatic injuries are accompanied in most of the case with tissue and cellular damage, blood vessels disruption and subsequent inflammatory reaction. All those events lead eventually to the release of different molecules that trigger the surrounding cells to react to the injury. For the traumatic brain injuries, it is shown that the released molecules after the injury from the damaged tissue and the flux of molecules through the damaged blood brain barrier trigger the surrounding astrocytes to become reactive (Iglesias et al., 2016). Astrocytes in response to those stimuli experience changes in the expression of many genes. In this process Ca^{2+} plays a pivotal role in the signaling cascades downstream of the external stimulus. One of the genes which has been always linked to astrogliosis is GFAP which is upregulated. The GFAP protein as a marker for reactive astrocytes is widely used in the experimental brain injury animal models as well as clinically as a marker for astrogliosis (Anderson et al., 2014). In addition to upregulation of the GFAP gene, the genes of chondroitin sulfate proteoglycans (CSPGs) are also upregulated. CSPGs are a group of proteins that are involved in the cell adhesion, cell growth and cell migration, and which are secreted by astrocytes following injuries (Rhodes and Fawcett, 2004). Those secreted proteoglycans have been shown to inhibit the axonal growth after brain and spinal cord injuries (Schachtrup et al., 2010; Silver and Miller, 2004).

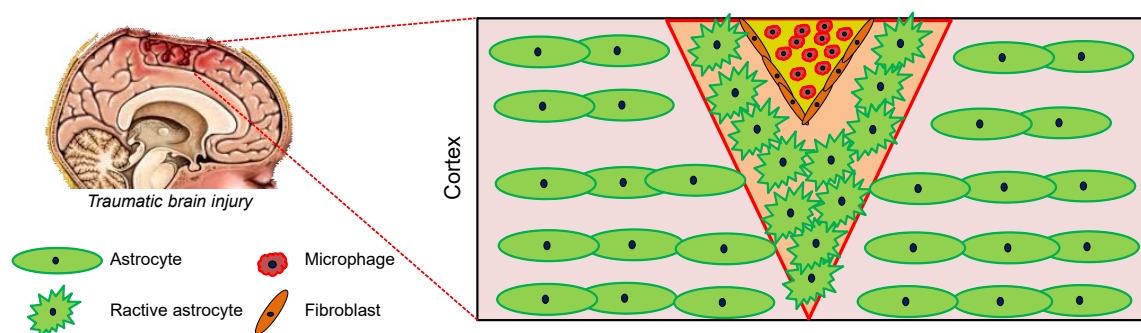


Figure 1-1 **Glial scar formation.** Representative scheme of traumatic brain injury which triggers astrocytes to become reactive and form the glial scar. Images of the head adapted from (<http://emergencymedicinecases.com>).

1.4 Calcium (Ca^{2+})

Calcium is a chemical element which as Ca^{2+} is essential for living organisms, in particular in cell physiology but also as major component in the mineralization of bones and teeth. Within cells, Ca^{2+} plays an important role in signaling; where it acts as a second messenger and regulates neurotransmitters release, muscle contraction, enzymatic activities, gene transcription, as well as division, differentiation, migration and death of cells. The basal cytoplasmic Ca^{2+} concentration in non-stimulated cells ranges between 50 and 150 nM. Upon stimulation, the cytoplasmic Ca^{2+} can rise to tens of μM leading to activation of signaling cascades. The rising in cytoplasmic Ca^{2+} is caused by Ca^{2+} release from the intracellular Ca^{2+} stores and/or Ca^{2+} entry into the cell from the extracellular compartment. The intracellular Ca^{2+} source is represented mainly by the endoplasmic reticulum (ER) which can store Ca^{2+} up to concentrations of 1 mM, but other organelles like mitochondria and, maybe, lysosome-related organelles could also store Ca^{2+} (Clapham, 2007). The ER Ca^{2+} is released into the cytoplasm upon opening of Inositol 1,4,5-trisphosphate receptor channels (IP3Rs) and ryanodine receptor channels. IP3Rs are activated by Inositol 1,4,5-trisphosphate (IP3) which is mobilized upon activation of Gq-coupled receptors or receptor tyrosine kinases: Cleavage of phosphatidylinositol 4,5-bisphosphate (PIP2) by phospholipase C (PLC) into IP3 and diacylglycerol (DAG) occurs. The ER is equipped with a sarco/endoplasmic reticulum Ca^{2+} -ATPase (SERCA) which ensures the Ca^{2+} re-uptake into the ER from the cytoplasm. Another source of Ca^{2+} for the cell is the extracellular space that contains Ca^{2+} at a concentration of 2 mM, and Ca^{2+} enters the cell via selective Ca^{2+} and non-selective cation channels (Reuter, 1986). Many selective and non-selective cation channels have been suggested to be expressed in astrocytes including: Ca^{2+} release-activated Ca^{2+} channels (CRAC) (Kraft, 2015), transient receptor potential channels (Scimemi, 2013), N-methyl-D-aspartate receptors (NMDA) (Conti et al., 1996), α -amino-3-hydroxy-5-methyl-4-isoxazolepropionic acid receptors (AMPA) (Fan et al., 1999), ionotropic purinergic receptors (Neary and Zhu, 1994) and, maybe, voltage-gated Ca^{2+} channels (Burgos et al., 2007). The present work focused on the expression and function of TRP and voltage-gated Ca^{2+} channels.

1.5 Transient Receptor Potential (TRP) Channels

Transient Receptor Potential (TRP) channels represent a large family of ion channel proteins located mostly in the plasma membrane. TRP channels were first discovered in the *Drosophila* photoreceptors where a spontaneous mutation led to a transient, instead of a sustained receptor potential upon light stimulation (Cosens and Manning, 1969). It took then twenty years to identify the gene carrying the mutation, the transient receptor potential gene. It was suggested that its amino acid sequence forms transmembrane segments (Montell and Rubin, 1989). Later in 1995, the first mammalian TRP cDNA, TRPC1, was cloned in the laboratory of Prof. Birnbaumer and Prof. Montell (Wes et al., 1995; Zhu et al., 1995). Today 28 members have been identified in mammalian organisms in which they are expressed in many cell types and tissues. Based on the sequence homology, the TRP channels are classified into 6 subfamilies (Figure 1-2-a): canonical (TRPC1-7), melastatin (TRPM1-8), vanilloid (TRPV1-6), ankyrin (TRPA1), mucolipin (TRPML1-3) and polycystin (TRPP2, 3 and 5) (Wu et al., 2010). It has been suggested that all TRP members share a similar structure of 6 transmembrane spanning segments, including a pore linker between the 5th and the 6th segment (Flockerzi, 2007). In December 2013, the first crystal structure of TRPV1 was published showing a structure of six transmembrane domains and four TRP proteins assembling together in a four-fold symmetry around the central ion permeation path (Cao et al., 2013; Liao et al., 2013). Recently, other groups could show the crystal structures of TRPV1 (Gao et al., 2016), TRPV2 (Zubcevic et al., 2016), TRPV6 (Saotome et al., 2016) and TRPA1 (Paulsen et al., 2015). Most of the TRP channels are non-selective cation channels that are permeable for Ca^{2+} and Na^{+} , except TRPV5 and TRPV6 which are highly Ca^{2+} selective, and TRPM4 and TRPM5 which are highly sodium selective, and which are activated by intracellular Ca^{2+} (Wu et al., 2010). The TRP channels are weakly voltage-sensitive, but they are activated via different mechanism including changes of temperature (heat and cold), pH, extra- and intracellular ligands and they are modulated via second messengers (Freichel et al., 2012). In the recent years extensive work has been conducted to discover modulators for TRP channels i.e., agonists and antagonists, that could be used to study those channels. However, the selectivity of these

modulators for TRP channels has been always an open debate. On the other hand, the emerging of the genetically modified mouse models has given significant boost to TRP channel studies. Many laboratories such as the group of Professor Flockerzi, Birnbaumer and Freichel extensively contributed in the generation of TRP gene-deficient mice and only two TRP channels remained to be knocked out, TRPML2 and TRPP5 (Nilius and Flockerzi, 2014). The generation of gene-deficient mice offered the opportunity to study selectively and accurately the role of TRP channels either in isolated tissues or cells, or in the entire animal. Gene-deficient studies have shown that TRP channels are involved in many cellular functions. For instance, the deletion of TRPV6 gene or the alteration of the TRPV6 channel's Ca^{2+} permeability, by a point mutation in the pore region of all subunits, led to male infertility (Weissgerber et al., 2012). TRPM5 was shown to play a role in insulin secretion, and the TRPM5 gene-deficient mice exhibited a decreased insulin secretion and reduced glucose clearance (Brixel et al., 2010; Colsoul et al., 2010).

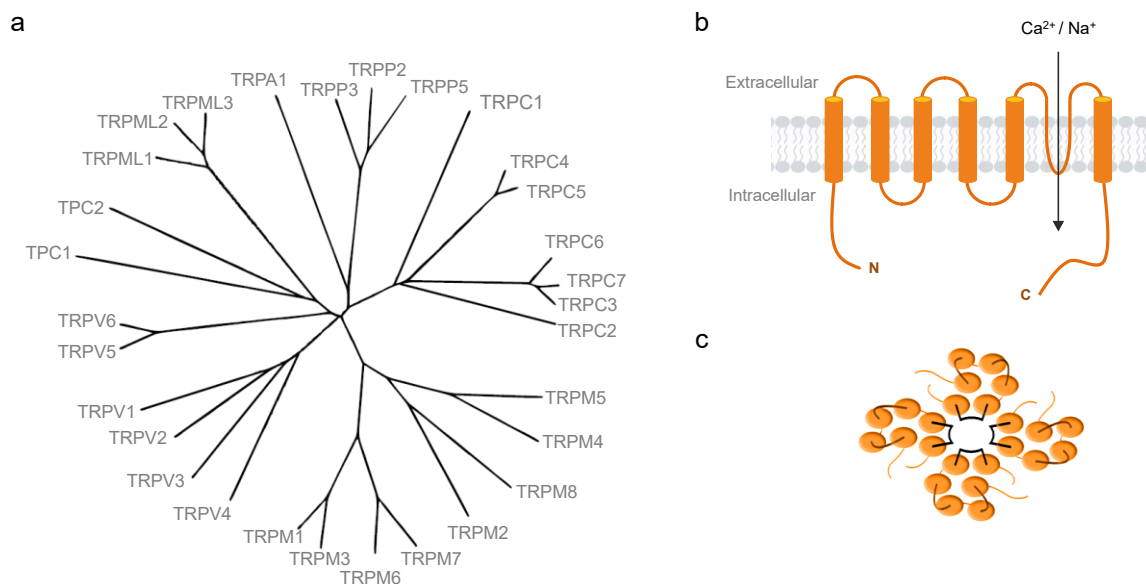


Figure 1-2 Transient Receptor Potential (TRP) Channel family. (a) Evolutionary relation of TRP genes illustrating the 6 subfamilies: TRPC (7 members), TRPV (6 members), TRPM (8 members), TRPA (1 member), TRPML (3 members) and TRPP (3 members). (b) Each TRP protein has 6 transmembrane domains with intracellular C and N termini, and a pore region located between the 5th and the 6th segment which is part of the Ca^{2+} and Na^{+} permeable pore. (c) Four TRP proteins assemble together to form a tetrameric functional channel.

1.6 Transient Receptor Potential Canonical Channels (TRPC)

The TRPC subfamily comprises 7 members that form non-selective cation channels permeable to Ca^{2+} and Na^+ . It has been shown that TRPC channels are activated downstream of phospholipase C (PLC) stimulation, i.e. activation of Gq-coupled receptors or receptor tyrosine kinase (Freichel et al., 2012). The TRPC channels are subdivided into four groups based on their sequence homology TRPC1, TRPC2 which is a pseudogene in humans, TRPC3, TRPC6 and TRPC7 (also called the DAG-sensitive TRPCs), and TRPC4 and TRPC5, however all members have conserved amino acid motifs on the N and C terminus. On the N terminus exist the ankyrin repeats, while on the C terminus the TRP box (EWKFAR) and the calmodulin and IP3 receptor binding site (CIRB) are located, those motifs can be also found in proteins from other TRP subfamilies (Clapham, 2003; Tang et al., 2001).

1.6.1 TRPC1

The TRPC1 was the first mammalian TRP to be cloned (Wes et al., 1995; Zhu et al., 1995); however the mechanism of activation still remains not clear. TRPC1 gene is expressed in many tissues and cell lines including kidney, liver, skeletal muscle, brain, salivary gland (Nesin and Tsiokas, 2014). Very recently Ulrich Wissenbach and Laura Hofmann in our laboratory have identified, in parallel with (Ong et al., 2013), a new starting codon CUG instead of AUG, which results in an extension of the amino terminal by 82 amino acids. Ong et al. have also identified a splice variant TRPC1 ϵ that lack 21 nucleotides which has a functional implication in the ORAI-mediated Ca^{2+} entry. Although TRPC1 is the founding member of TRPCs, the evidence that this protein could form a functional channel by itself is still a matter of debate (Dietrich et al., 2014). Nevertheless, TRPC1 has been shown to interact with its closest homologues TRPCs, but it also does interact with other TRP proteins and other proteins. For instance, the co-expression of TRPC1 with TRPC4 or TRPC5 in HEK293 cells did lead to the change of the current voltage relationship of both channels when compared to the single TRPC4 or TRPC5, concluding that TRPC1 could form functional heteromeric channels with TRPC4 and TRPC5 (Strubing et al., 2001). With the DAG-sensitive TRPC channels, TRPC1 was also shown to form

heteromeric channels with which were less Ca^{2+} permeable, but without changes in their current voltage relationships (Storch et al., 2012). In addition, TRPC1 was shown to interact with ORAI and STIM proteins (Ambudkar, 2014), but the role of TRPC1 in ORAI function has always been controversy and divides the TRP community. For example, the deletion of TRPC1 gene was shown to reduce the Ca^{2+} entry, upon endoplasmic reticulum Ca^{2+} depletion, by 60% in mouse submandibular gland acinar cells (Ambudkar, 2014), and others concluded that TRPC1 is a critical component of the store depletion-mediated Ca^{2+} entry in salivary gland acinar cells (Liu et al., 2007). However, Varga-Szabo et al. reported that platelets isolated from TRPC1 gene-deficient mice did exhibit a normal ORAI function (Varga-Szabo et al., 2008). Perhaps it is important to consider different roles of TRPC1 in different cell types.

1.6.2 TRPC2

TRPC2 is a pseudogene in humans, but it is expressed in rodent vomeronasal organ, testis, brain, spleen, heart, thyroid cells and erythroid cell line (Miller, 2014). This member of TRPC channels is activated via DAG which results from the PLC activation (Lucas et al., 2003). TRPC2 has been described to interact with one of its closest homologue TRPC6 channels, as well as with other Ca^{2+} release and Ca^{2+} influx proteins: IP3 receptor, STIM and ORAI (Kiselyov et al., 2010; Tong et al., 2004). The TRPC2 gene-deficient mice mate normally, however males failed to display male-male aggression towards intruder males (Stowers et al., 2002). In blood cells it was reported that TRPC2 deletion could protect mouse red blood cells from oxidative stress-induced hemolysis (Hirschler-Laszkiewicz et al., 2012).

1.6.3 TRPC3

TRPC3 was cloned in 1996 by Zhu et al., and it was found to be highly expressed in the brain and heart (Camacho Londono et al., 2015; Lichtenegger and Groschner, 2014; Zhu et al., 1996). It shares 69% amino acid sequence identity with TRPC6 and TRPC7 and also the activation mechanism via DAG (Hofmann et al., 1999). TRPC3 was shown to preferentially interact with its closest homologues TRPC6 and TRPC7 (Lichtenegger and Groschner, 2014), but it was also reported to interact with other Ca^{2+} channels such as ORAI in

heterologous expression (Liao et al., 2007). Lintschinger et al. reported that the co-expression of TRPC1 with TRPC3 in HEK cells generated a Ca^{2+} -sensitive OAG-activated channel, while TRPC3 alone exhibited minor Ca^{2+} inhibition (Lintschinger et al., 2000). In addition, the Ca^{2+} selectivity of TRPC3 was shown to decrease when TRPC1 is co-expressed (Storch et al., 2012). The expression of TRPC3 seemed to coordinate with the expression of its closest homologues as shown by Dietrich et al. that TRPC3 gene expression is upregulated in TRPC6 gene-deficient smooth muscle cells, suggesting compensatory effects of TRPC3 after loss of TRPC6 (Dietrich et al., 2005). TRPC3 has been shown to play a role in the mGluR-evoked slow EPSCs in mouse cerebellar Purkinje cells (Hartmann et al., 2008). In the peripheral organs, TRPC3 was reported to be involved in regulation of the myogenic tone of resistance arteries and in controlling arterial blood pressure (Adebiyi et al., 2010). Interestingly, a mutation in the mouse TRPC3 gene (A1903G) has been identified in a mutagenesis screening which led to the replacement of threonine residue at position 635 in the mouse TRPC3 amino acid sequence by an alanine residue. The homozygous mutant mice are not viable, however the heterozygous mutants exhibit motor and coordination abnormalities and loss of Purkinje cells, and thus called moonwalker (MWK) mice (Becker et al., 2009). This phenotype could be because of the altered TRPC3 (T635A) channel gating (Becker, 2014). Like the rest of the TRPC members, TRPC3 is inhibited by the general inhibitors of non-selective cation channels like SKF-96365 and 2-APB (Harteneck and Gollasch, 2011). A selective TRPC3 inhibitor pyrazolium 3 (Pyr3) has been described to have an inhibitory effect on carbachol-induced Ca^{2+} currents in HEK293 cells overexpressing TRPC3 (Kiyonaka et al., 2009). However, Pyr3 also inhibits the ORAI function in astrocytes (own observation, (Schleifer et al., 2012)). Schleifer et al. proposed instead another pyrazole derivative Pyr 10 which was shown to have higher selectivity for TRPC3 versus ORAI.

1.6.4 TRPC4

TRPC4 was first cloned in the laboratory of Prof. Flockerzi (Homburg) in 1996 (Philipp et al., 1996). The closest TRPC homologue to TRPC4 is TRPC5, they share 65% amino acid sequence (Philipp et al., 1998). TRPC4 is expressed in

many organs including brain, eye, heart, lungs and many others, and it is activated downstream $G_{q/11}$ and $G_{\alpha i}$ pathways (Freichel et al., 2014). Deletion of TRPC4 affects the agonist-dependent vasorelaxation and others suggested that TRPC4 is essential in the regulation of blood vessel tone (Freichel et al., 2001). In another study, the gene-deficient of both TRPC4 and TRPC1 was shown to have a preventive affect against maladaptive cardiac remodeling (Camacho Londono et al., 2015). In the brain, the gene-deficient of TRPC4 led to decreased anxiety-like behavior and was related to a subsequent decrease in Gq-dependent responses (Riccio et al., 2014). A gain of function mutation was also described for TRPC4 (TRPC4 G503S) that leads to a constitutive activity of the channel (Beck et al., 2013), however the impact of this mutation *in vivo* has not been described yet. Recently, agonist for TRPC4 (and TRPC5) has been reported (-)-Englerin A which is able to kill renal cancer cells (Akbulut et al., 2015). Nevertheless, a proper analysis of the (-)-Englerin A selectivity has to be conducted.

1.6.5 TRPC5

Almost two years after the cloning of TRPC4, the laboratory of Prof. Flockerzi also cloned TRPC5 which, as mentioned above, shares 69% sequence homology with TRPC4 (Philipp et al., 1998). TRPC5 is predominantly expressed in the central nervous system, however TRPC5 was also detected in other tissues (Zholos, 2014). TRPC5 is also activated downstream of G-protein coupled receptors and it is potentiated by intracellular Ca^{2+} (Gross et al., 2009; Wu et al., 2010). The TRPC5 gene-deficient mice seem to have reduced pilocarpine-induced seizures and subsequent neuronal death (Phelan et al., 2013). In another study, TRPC5 was suggested to play an essential role in amygdala function and fear-related behavior (Riccio et al., 2009). Similar to TRPC4, the G504S mutation which was located within the cytoplasmic linker between transmembrane domain 4 and 5 led also to TRPC5 gain of function (Beck et al., 2013).

1.6.6 TRPC6

The first mammalian TRPC6 was cloned in 1997 by the laboratory of Prof. Birnbaumer from mouse brain (Boulay et al., 1997). TRPC6 shares high

sequence homology with TRPC3 and it is also activated via DAG (Wu et al., 2010). TRPC6 is expressed in lung, stomach, colon, kidney and other organs (Dietrich and Gudermann, 2014). The TRPC6 gene-deficient mice do exhibit a reduced angiotensin II-induced albuminuria, but under normal conditions (without angiotensin II) TRPC6 gene-deficient mice did have similar albumin excretion as wild-type mice (Eckel et al., 2011). Others have shown that TRPC6 may inhibit seizure susceptibility and neuronal vulnerability in the rat (Kim and Kang, 2015). Lysophosphatidylcholine was shown to activate TRPC6 but also TRPC5 (Chaudhuri et al., 2003). In addition, the St. John's wort antidepressant molecule Hyperforin was proposed as a TRPC6 specific activator and has been used since as one (Leuner et al., 2007). However, we could show that hyperforin induces a proton current even totally independent of TRPC6 (Sell et al., 2014). Therefore, the use of hyperforin as a selective TRPC6 agonist has to be reconsidered.

1.6.7 TRPC7

TRPC7 was the last TRPC member to be cloned in 1999 from mouse brain (Okada et al., 1999). This channel also belongs to the DAG-sensitive TRPC channels and shares a high sequence homology with TRPC3 and TRPC6 (Wu et al., 2010). TRPC7 was found to be expressed in different tissues including heart, lungs, eye, brain, spleen and others (Zhang and Trebak, 2014). A recent study using TRPC7 gene-deficient mice showed that TRPC7 is involved in the initiation of seizures both *in vitro* and *in vivo*, and TRPC7 gene-deficient mice seemed to be protected against seizures (Phelan et al., 2014).

1.6.8 TRPCs in astrocytes

In the last decade, several studies have been conducted on the role of TRPC proteins in astrocytes. Different types of astrocytes from different species have been used in those studies including human, mouse and rat astrocytes. All members of the TRPC channels were reported to be expressed in rat cortical astrocytes, but in the rat spinal cord astrocytes TRPC5 and TRPC7 were not detected by PCR (Miyano et al., 2010). TRPC1 was suggested to contribute in intracellular Ca^{2+} dynamics and consequent glutamate release from rat astrocytes (Malarkey et al., 2008). In human astrocytoma cells, TRPC3 was

found to be associated with thrombin-induced morphological changes (Nakao et al., 2008). Another study showed that ATP could induce TRPC3 current in cortical astrocytes was slightly blocked by Pyr3, however control experiments with knockdown or knockout were missing (Streifel et al., 2014). In an intracerebral hemorrhage mouse model, Pyr3 treatment attenuated the astrogliosis after cerebral hemorrhage and was linked to inhibition of TRPC3 (Munakata et al., 2013), however Pyr3 is not a selective TRPC3 blocker (Schleifer et al., 2012). TRPC4 was shown to co-localize with the scaffolding protein ZO-1 in human fetal astrocytes in culture (Song et al., 2005).

1.7 Voltage-gated Ca^{2+} channels (CaVs)

Voltage-gated Ca^{2+} channels (CaVs) are a group of highly selective Ca^{2+} channels that open at depolarized membrane potentials. Their genes are expressed mostly in excitable cells such as neurons, muscle cells or secretory cells. Since the first recording of those channels in 1967 (Reuter, 1967), the CaVs are important targets of drugs, the Ca^{2+} channel blockers, used in the treatment of cardiovascular diseases including hypertension, angina and arrhythmia, as well as neurological diseases such as pain and seizure. The functional CaVs consist of the pore-forming $\alpha 1$ subunit which defines the type and the pharmacology of the channel, and the other subunits β , $\alpha 2\delta$ and, maybe, γ as auxiliary subunits which modulate the properties of the channel (Catterall et al., 2005; Hofmann et al., 1994). CaVs are classified depending on their activation voltages as low voltage activated (LVA) and high voltage activated (HVA). The activation potentials of the HVA Ca^{2+} channels occur between -40 to -10 mV while the activation potentials for the LVA channels occur between -70 to -60 mV (Nowycky et al., 1985). The CaVs are fast activating and inactivating, but not as fast as the voltage-gated sodium channels, and the inactivation happens in a Ca^{2+} -dependent manner and / or in a voltage-dependent manner (Cens et al., 2006; Ulbricht, 2005; Yue, 2004). The activation potentials and the inactivation kinetics are different between the diverse subtypes of CaVs and are therefore used to characterize and distinguish the different members of the voltage-gated Ca^{2+} channels. However,

the characterization of the CaVs is also performed using specific blockers (Olivera et al., 1994; Reuter, 1983).

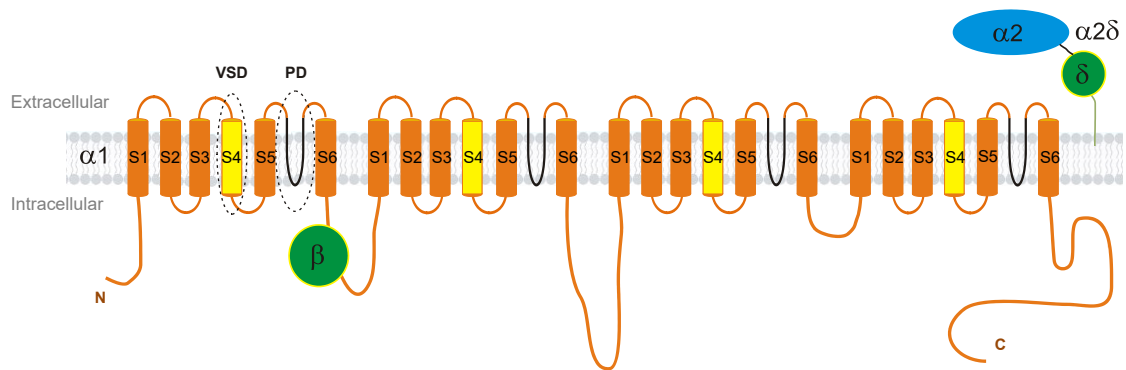


Figure 1-3 Topology of voltage-gated Ca²⁺ channel. Voltage-gated Ca²⁺ channels subunits including the pore forming α1 subunit and the auxiliary subunits β and α2δ. The α1 subunit consists of four homologous repeats, each comprising six transmembrane domains (S1 – S6). The channel pore is situated between the S5 and S6 domains (PD) of each repeat, and the S4 domains represent the voltage sensor (VSD).

1.7.1 The pore-forming α1 subunits

The α1 subunit is the main subunit of the voltage-gated Ca²⁺ channels. It was purified and its cDNA cloned for the first time from rabbit skeletal muscle (Flockerzi et al., 1986; Tanabe et al., 1987) and consists of four homologous domains, each containing six transmembrane segments S1 to S6 (Figure 1-3) (Wu et al., 2015). The pore is located between the transmembrane segments S5 and S6, and the S4 segment which includes positively charged amino acid residues serves as the voltage sensor (Tanabe et al., 1987). Up to date, 10 α1 subunits have been discovered and an alphabetic nomenclature was used to classify them. The α1 cloned from skeletal muscle was given the name α1_S, and the rest were named from α1_A to α1_F. Similarly to the potassium channels, the Ca²⁺ channels were also given the numerical identifier and Ca was used to refer to Ca²⁺ and V to voltage (CaV). The CaV1.1 to CaV1.4 refer to the L-type Ca²⁺ channels formed by α1_S, α1_C, α1_D and α1_F respectively. The CaV2.1, CaV2.2 and CaV2.3 refer to the P/Q-type, N-type and R-type Ca²⁺ channels formed by α1_A, α1_B and α1_E respectively. The CaV3.1 to CaV3.3 refer to the T-type Ca²⁺ channels formed by α1_G, α1_H and α1_I respectively (Ertel et al., 2000). The L-, N-, P/Q- and R-types are considered HVA channels (see 1.7), while the

T-type Ca^{2+} channels are LVA channels (Lipscombe et al., 2004). The L-type Ca^{2+} channels are blocked by diltiazem, by dihydropyridine derivatives such as Amlodipine, Isradipine and Nimodipine and by phenylalkylamine derivatives such as Verapamil. The P/Q-type Ca^{2+} channels are blocked by the funnel web spider venom ω -agatoxin IVA, the N-type Ca^{2+} channels are blocked by the cone snail toxin ω -conotoxin GVIA and related cone snail toxins, and the R-type Ca^{2+} channels are blocked by the synthetic peptide toxin SNX-482 derived from tarantula venom. For the T-type Ca^{2+} channels there are no specific blockers available so far (Catterall et al., 2005). Gene-deficient mice of the various $\alpha 1$ subunit genes have been described and most of them exhibit specific phenotypes if they are viable. For instance, the CaV1.1 gene-deficient mice, which resulted from autosomal recessive mutation in the CaV1.1 $\alpha 1$ subunit die at birth because of asphyxiation (Chaudhari, 1992) and CaV1.2 gene-deficient mice die on embryonic day 14.5 (Seisenberger et al., 2000), while the CaV1.3 gene-deficient are deaf (Platzer et al., 2000) and a spontaneous mutation in the CaV1.4 gene causes night blindness in mice (Chang et al., 2006). The CaV2.1 gene-deficient mice exhibit severe ataxia and die few weeks after birth (Jun et al., 1999), while the CaV2.2 (Saegusa et al., 2001) and CaV2.3 (Pereverzev et al., 2002) gene-deficient mice have mild phenotypes. For the T-type Ca^{2+} channels, the CaV3.1 gene-deficient mice exhibit bradycardia and slow atrioventricular conduction (Mangoni et al., 2006), and were also shown to have hyperalgesia in response to visceral pain (Kim et al., 2003). The CaV3.2 gene-deficient mice have abnormal coronary function and focal myocardial fibrosis (Chen et al., 2003). However the CaV3.2 gene-deficient mice have neurological phenotype characterized by reduced sleep spindles in the thalamus (Astori et al., 2011).

1.7.2 The auxiliary subunits

The auxiliary subunits of the voltage-gated Ca^{2+} channels are required for the trafficking of the pore-forming $\alpha 1$ subunits to the plasma membrane as well as for modulating the gating properties (Arikkath and Campbell, 2003). Those subunits are classified in CaV β subunits, and CaV $\alpha 2\delta$ subunits. The cloning of the first CaV β subunit cDNA was done in 1989 in Homburg, Germany (Ruth et al., 1989), and today four β genes ($\beta 1$ to $\beta 4$) have been characterized. It has

been shown that HVA Ca^{2+} channels have very small membrane expression and subsequently measurable currents in the absence of the β subunits, as those subunits translocate the $\alpha 1$ subunits to the plasma membrane (Buraei and Yang, 2013). Thus, for the high voltage-gated Ca^{2+} channels the β subunits are indispensable for their cellular function. For instance, the $\text{CaV}1.1$ is exclusively associated with the $\beta 1$ subunit and the deletion of $\beta 1$ gene in mice led to the same phenotype as observed is in the $\text{CaV}1.1$ gene deletion: mice die after birth due to asphyxiation (Gregg et al., 1996). The $\beta 2$ subunit of the CaVs plays a vital role in the development of the heart during embryonic phase as illustrated by the work of Weissgerber et al. where they show that homozygous $\beta 2$ gene-deficient embryos die at embryonic day 10.5 due to heart malformation. However, mice were born and could live when the $\beta 2$ gene is deleted in the whole organism except cardiac myocytes (Katiyar et al., 2015; Weissgerber et al., 2006). The $\beta 3$ Gene-deficient mice are viable, but they do exhibit a reduced perception of pain. The mechanism behind this phenotype is probably due to the reduced expression of the N-type Ca^{2+} channel in the $\beta 3$ gene-deficient spinal cord and subsequent reduction in the Ca^{2+} currents (Murakami et al., 2002). Moreover, those mice do also have an increased insulin secretion but the mechanism of this hyperinsulinemia is independent of CaVs and rather related to the IP_3 -induced Ca^{2+} release from the ER, suggesting also Cav-independent functions of the $\beta 3$ subunits (Berggren et al., 2004). The $\beta 4$ gene is not functional in epileptic lethargic mice (lh/lh mice) because of a mutation that leads to exon skipping in the $\beta 4$ gene and induces a premature stop codon. Those mice were reported to have ataxia and seizures as well as spleen and thymic involution (Burgess et al., 1997). The $\alpha 2\delta$ subunits are a group of extracellular proteins consisting of four members: $\alpha 2\delta 1$ to $\alpha 2\delta 4$. The $\alpha 2\delta 1$ cDNA was first cloned in 1988 (Ellis et al., 1988). The $\alpha 2$ and δ polypeptides are linked to each other by disulfide bonds and it was shown that the $\alpha 2\delta$ complex is anchored to the plasma membrane via a glycosphosphatidylinositol (GPI)-anchor at the C-terminal of the δ (Davies et al., 2010). The trafficking of the $\alpha 1$ subunits of the HVA Ca^{2+} channels is mainly mediated via the β subunits, however many reports have shown that the co-

expression of $\alpha 2\delta$ with the $\alpha 1$ and β subunits enhances the Ca^{2+} currents (Dolphin, 2013). The $\alpha 2\delta 1$ has been found to be associated with nerve injury-induced pain where it is upregulated in response to peripheral nerve injury (Newton et al., 2001). A mutation in the $\alpha 2\delta 2$ gene was discovered in the “ducky mice” which leads to the loss of the full length mRNA of this gene and reduces the Ca^{2+} currents in the cerebellar Purkinje cells. This mutation has been associated with the ducky mouse phenotypes of epilepsy and ataxia (Barclay et al., 2001). The $\alpha 2\delta 3$ gene-deficient mice showed impaired transmission of thermal pain-evoked signals from the thalamus to the pain center in the brain (Neely et al., 2010). A mutation in the human $\alpha 2\delta 4$ gene was found in patients diagnosed with night blindness suggesting an involvement of $\alpha 2\delta 4$ in this disease (Wycisk et al., 2006). However, antibody-based purification of CaV channels from brain followed by mass spectrometry analysis revealed $\alpha 1$ and β subunits but not $\alpha 2\delta$ subunits as part of the channel complex (Muller et al., 2010). Among the γ subunits, only $\gamma 1$ subunit is associated with $\alpha 1$ subunit of the CaV1.1 (Chen et al., 2007a; Eberst et al., 1997). Reports have shown that in the absence of the γ subunit the L-type Ca^{2+} current in skeletal muscle cells increases and the inactivation kinetic of the channel is changed (Freise et al., 2000). Most of the other γ subunits interact with the α -amino-3-hydroxy-5-methyl-4-isoxazolepropionic acid (AMPA) receptors and assist the trafficking of these receptors to the plasma membrane. They are therefore called transmembrane AMPA receptor regulating proteins (TARPs) (Nicoll et al., 2006).

1.7.3 CaVs in astrocytes

The presence of functional voltage-gated Ca^{2+} channels in astrocytes has been always a matter of debate. However, some early reports have shown Ca^{2+} currents in cultured astrocytes (MacVicar and Tse, 1988), which were supported by later studies showing mRNA and protein levels of voltage-gated Ca^{2+} channel subunits in cultured astrocytes (Latour et al., 2003). However, electrophysiological measurements *in situ* did not show any Ca^{2+} currents in hippocampal astrocytes (Carmignoto et al., 1998). Apparently, astrocytes change gene expression pattern *in situ* compared to the situation in culture. In

addition, the difference between the *in vitro* and the *in situ* studies is that the *in vitro* studies have used cortical astrocytes while the *in situ* study has used hippocampal astrocytes. This difference has to be taken into consideration since astrocytes from different brain regions could well differ. Up to date, not many studies have discussed the role of CaVs in astrocytes. However, Zeng et al. reported that the spontaneous Ca^{2+} oscillations in astrocytes could be mediated by voltage-gated Ca^{2+} channels (Zeng et al., 2009). In a recent study (Gurkoff et al., 2013), it was shown that administration of CaVs antagonists to rodent models of traumatic brain injury, which involves astrocytes and neurons, reduced cell death and improved cognitive function.

1.8 Aims

The aim of the present work was to study the role of TRPC and CaVs channels in mouse cortical astrocytes. The following aims will be addressed:

1. Establishment and characterization of mouse cortical astrocyte cultures.
2. Expression analysis of TRPC and CaVs channels by the mean of RT-PCR and mRNA deep sequencing from purified (FACS-sorted) mouse cortical astrocytes.
3. Functional characterization of the expressed TRPC3, TRPC1 and CaVs channels by Ca^{2+} imaging and patch clamp experiments.
4. Applying *in vitro* as well as *in vivo* approaches to investigate the physiological role of TRPC3 and TRPC1 in the astrocytes migration and astrogliosis after brain injury.

2 Materials and Methods

2.1 Mouse lines

All animal experiments were performed in accordance with the German legislation on the protection of animals and were approved by the local ethic committee. New born (day 0-3) or adult mice were used from different gene-deficient mice and their corresponding wild-types either from C57BL6/N strain or 129SvJ/C57Bl6/N (mixed) strains. TRPC1 gene-deficient (Dietrich et al., 2007), TRPC3 gene-deficient (Hartmann et al., 2008) and TRPC6 gene-deficient (Dietrich et al., 2005) mice were previously described, the TRPC1/C5 and TRPC3/C6 double gene-deficient mice was generated in our laboratory by crossing the single gene-deficient mice. The gain of function TRPC3 threonine to alanine mutation was first identified by Becker et al. from a mutagenesis screening (Becker et al., 2009), and heterozygous embryos of this mutation so called moonwalker (MWK) mouse were purchased from Harvell Science and Innovation (England) and introduced into the animal facility of the Pharmacology Department in Homburg by Dr. Petra Weissgerber. Cav β 2 gene-deficient mice (Weissgerber et al., 2006) and Cav β 3 gene-deficient mice (Murakami et al., 2002) were generated in the laboratory of Prof. Veit Flockerzi, Pharmacology Department in Homburg.

2.2 Isolation and culture of mouse cortical astrocytes and microglia

The isolation of mouse cortical astrocytes was performed as described before in (T. Belkacemi Master thesis 2012). Mice, aged from 0 to 3 days, were sacrificed by decapitation using scissors, and the cerebral hemispheres were rapidly removed and maintained in a 3.5 cm sterile petri dish containing cold PBS. After the separation of the two hemispheres under a stereomicroscope, hippocampus, amygdala and thalamus were removed and also the meninges were carefully removed in order to avoid fibroblast contamination (Figure 2-1).

The isolated cortices were collected in a 50 ml sterile falcon tube filled with 20 ml of cold DMEM (Dulbecco's modified Eagle's medium) medium (Gibco) supplemented with 1% GlutaMAX (Invitrogen), 100 U/ml Penicillin and 100 µg/ml Streptomycin. After isolation, cortices were gently digested using 5 ml trypsin (5 g/l) (Sigma) per 10 brains for 15 min at 37°C. The trypsin was then inhibited by adding 10 ml DMEM medium supplemented with 10% FCS (Fetal calf serum) (Gibco) and centrifuged for 5 min at 200 g. The supernatant was removed and cortices were suspended in DMEM medium without FCS. The cortices were then triturated by pipetting up and down (10 times) using a 10 ml syringe (B. Braun) with a 20G (0,90 x 40 mm) needle (B. Braun). The obtained suspension was filtered into a new falcon tube using a 40 µm cell strainer (BD Falcon) to get single cells, and centrifuged 5 min at 200 g. Then, cells were resuspended in DMEM medium containing 10% FCS, 1% GlutaMAX, 100 U/ml Penicillin and 100 µg/ml Streptomycin, and plated as 3 brains in 75 cm² poly-L-lysine (P-L-L, 0,1 mg/ml, (Sigma) -coated flasks (BD Falcon) and cultured at 37°C and 5% CO₂ in a humidified incubator (Binder). After 2 to 3 days, the medium was changed to remove dead cells and debris, and afterwards the medium was changed twice a week until cells reached confluency. Cells from single TRPC3 MWK and Cavβ2 gene-deficient mice were prepared and cultured separately until the single mice were genotyped. Microglia cells grow on top of the astrocytes and were separated by gently shaking the flask and subcultured on P-L-L-coated coverslips for Ca²⁺ imaging or patch clamp experiments. Astrocytes are adherent cells and therefore they were detached by first washing the flask (75 cm²) with PBS to remove the medium with FCS and then incubated with 3 ml trypsin (5 g/l) for 3 to 5 min. Afterwards, the flask was knocked by hand in order to detach the cells, and then cells were suspended in 7 ml medium with FCS and plated on P-L-L-coated coverslips for Ca²⁺ imaging or patch clamp experiments.

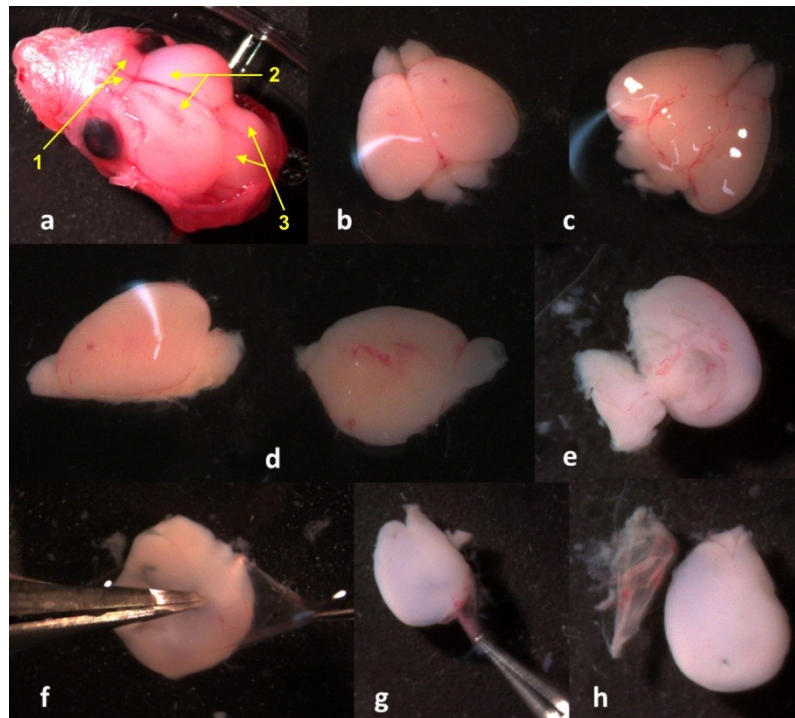


Figure 2-1 Isolation procedure of mouse cortices. (a) Open head of a newborn mouse showing different parts of the CNS (1: olfactory bulbs, 2: cerebral cortices, 3: cerebellum). (b) Extracted brain from the head showing the cerebral cortices from the upper side. (c) The upside down view of the brain. (d) Brain divided into two hemispheres, the cerebral cortex in the left and the hippocampus, amygdala and thalamus in the right. (e) The hippocampus, amygdala and thalamus are being separated from the cerebral cortex. (f & g) The meninges are being removed from the cerebral cortex. (h) The cerebral cortex is separated from the other parts of the brain and ready to be used for astrocyte culturing. Photographs were taken by a color camera (AxioCam, ZEISS). The figure was adapted from (T. Belkacemi Master thesis 2012).

2.3 Human embryonic kidney (HEK) 293 cell culture

HEK-293 cells (ATCC, CRL 1573) are obtained from the American Type Culture Collection (ATCC, Manassas, VA, USA), HEK cells stably expressing the human cDNA TRPC3 were kindly provided by Dr. M.X. Zhu, University of Texas Health Science Center, Houston, HEK cells stably expressing the mouse TRPC1 VL and tetracycline-inducible mouse TRPC3 MWK mutation in HEK cells were generated in our laboratory. For that purpose, nucleotide A at position 1903 was replaced by G in the mouse TRPC3 cDNA and subcloned into pCDNA5/FRT/TO vector. Wild-type HEK cells were cultured in MEM medium and the others were cultured in DMEM medium, supplemented with

10% FCS. The cells were kept in an incubator at 37°C and 5% CO₂, and the medium was changed every third day. Cells were plated on glass coverslips of 1 cm in diameter coated with P-L-L.

2.4 HEK cell transfection

HEK-293 cells were cultured in 3.5 mm petri dishes until they reached 70% confluency. The culture medium was substituted with a fresh medium (MEM supplemented with 10% FCS) prior to the transfection. The transfection mixture was prepared following the manufacturer recommendation using FuGENE HD Transfection Reagent (Promega). For every 3.5 mm petri dish, 2 µg of DNA was mixed with 5 µl of Eugene HD reagent and 100 µl of Opti-MEM medium and incubated at room temperature for 15 min. The transfection mixture was added onto the cells by dropping small droplets all over the petri dish. Afterwards cells were incubated at 37°C and 5% CO₂ for 24 to 48 h and checked under the fluorescence microscope for positive fluorescent cells depending on the transfection DNA. Then, cells were plated on glass coverslips coated with P-L-L for either patch clamp or Ca²⁺ imaging experiments and used for experiment up to 72 h post transfection. The used eukaryotic expression vectors were generated in our laboratory, the full length mTRPC3-pcAGGS-IRES-GFP by Stefanie Buchholz and mTRPC1 VL-pcAGGS-IRES-GFP by Laura Hofmann and Ulrich Wissenbach. The use of IRES will allow the expression and translation of the aimed gene as well as GFP in parallel but separately.

2.5 Immunocytochemistry

Mouse cortical astrocytes were plated on P-L-L-coated coverslips and grown until almost confluency. Cells were fixed with 4% (w/v) paraformaldehyde (PFA) (Sigma) for 15 min at room temperature. After fixation, cells were washed with PBS and permeabilized using 0.5% TritonX-100 (Roth) for 15 min at room temperature. For blocking the unspecific binding sites, cells were washed with PBS and incubated for 60 min at room temperature with 3% Bovine-Serum-Albumin (BSA) Fraction V (Applichem), 1% (v/v) Normal-Goat-Serum (NGS) (Vector) and 0.1% TritonX-100 in PBS solution. Cells were washed and

incubated over night at 4°C with the primary antibodies: Anti-GFAP (glial fibrillary acidic protein) from rabbit to stain astrocytes (Dianova), anti-CD11b (integrin alpha M) (Dianova) from rat to stain microglia. Dilutions (v:v): 1:100 for anti-GFAP and anti-CD11b, and 1:10 for anti-GLAST-PE in PBS containing 1% (w/v) BSA and 0.05% (v/v) TritonX. Next day, cells were washed with PBS and incubated with a fluorescence labeled secondary antibody Goat-Anti-Rabbit-IgG dyelight 488 nm, Goat-Anti-Rat-IgG dyelight 594 nm (Dianova) or Goat-Anti-Rat-IgG dyelight 488 nm (Invitrogen) for 1 hour at room temperature in the dark, the secondary antibody was diluted 1:200 in PBS. After 1 hour, cells were washed with phosphate-buffered saline (PBS) and the nuclei were stained with 1 µg/ml 4',6-diamidino-2-phenylindole (DAPI, Sigma) for 10 min at room temperature, after that, coverslips were washed with PBS and mounted on glass slides covered with mounting medium (Vectashield Vector) and pictures were taken with a fluorescence microscope (Axiovert 200M, ZEISS) equipped with a camera (AxioCam, ZEISS) and light source (HXP 120), using the software AxioVision Rel. 4.7.

2.6 FACS

2.6.1 Fluorescence Activated Cell Sorting (FACS)

Flow cytometry using fluorescent-based separation is a useful scientific instrument which offers fast and accurate quantitative analysis of the fluorescent-labelled cell. Fluorescence activated cell sorting (FACS) is a type of flow cytometry that enables the separation and sorting of different cells into separate containers. The sorting of cells is performed according to their light scattering and fluorescent characteristics. In 1968, Wolfgang Göhde, from the University of Münster, developed the first fluorescence-based device. Afterwards, it was manufactured and commercialized by the German developer Partec through Phywe AG in Göttingen.

In a mixture of cells, different types of cells have different surface markers. These markers can be specifically labelled using fluorescent labels such as fluorescent-coupled antibodies, and thereby become separable FACS. In addition, genetically-modified cells expressing fluorescent proteins could also

be separated from the non-fluorescent cells by FACS. In principle, Cells loaded into FACS will pass through a fast flowing liquid stream for single cells separation. Cells will be then presented in droplets, one cell per droplet, using vibration. They pass afterwards through a laser beam and the scattered light and the fluorescence emissions (upon excitation) of cells are detected. According to the scattered light and the fluorescent proprieties of cells, an electrical charge is applied to the stream immediately before the droplet tears off the stream. The charged droplet falls through an electrostatic deflection system that separates them into different containers according to its charge.

2.6.2 Fixed and permeablized cell preparation for FACS

Around 1.5 million astrocytes cultured for 2 to 3 weeks were trypsinized and suspended into culture medium. Cells were washed with PBS and fixed by incubation with 4% (w/v) PFA in PBS buffer for 10 min. Fixed astrocytes were centrifuged at 200 g for 7 min to remove the PFA solution and incubated in suspension in 0.5% (v/v) TritonX100 in PBS buffer to permeabilize the cells for 10 min. Afterwards, cells were centrifuged at 200 g for 7 min to remove the TritonX100 and resuspended in 0.5% (w/v) BSA in PBS buffer. The cell suspension was divided into 4 tubes; the first one was used as the unstained control, the second and third were incubated for 10 min in the dark separately with anti-GFAP conjugated to Alexa 488 (1:100) (Cell Signaling) or anti-GLAST (1:10) (glutamate aspartate transporter) conjugated to Phycoerythrin (PE; Miltenyi Biotec). The fourth tube was incubated with both antibodies anti-GFAP-Alexa488 and anti-GLAST-PE. After 10 min the tubes were centrifuged at 200 g for 7 min and washed two times, resuspended in fresh 0.5% BSA in PBS buffer and analyzed immediately in the FACS or kept on ice until FACS analysis (Moflo, Beckman Coulter).

2.6.3 Living cell preparation for FACS

Astrocytes cultured for 2 to 3 weeks after isolation were trypsinized and suspended into culture medium. Cells were washed with PBS and resuspended in 0.5% BSA in PBS buffer. The cell suspension was divided into several tubes, one was kept not stained as a control and the other tubes were used for staining of astrocytes and microglia markers. Anti-GLAST-PE (1:10) (Miltenyi

Biotec) was used as a surface marker of astrocytes, while anti-CD11b (1:10) conjugated to Fluorescein isothiocyanate (FITC) (Miltenyi Biotec) was used as a surface marker for microglia. Afterwards, cells were washed with 0.5% (w/v) bovine serum albumin (BSA) in PBS and loaded directly into the FACS (Moflo, Beckman Coulter).

The sorter was first loaded with non-stained cells to characterize their size and granularity. The results obtained from this step showed that the obtained mouse cortical astrocyte culture consisted of two distinct populations in terms of size and granularity. Since astrocytes are bigger when examined under the microscope, the population which is bigger in size and has more granularities was assumed to be the astrocytic population, and the other population would be the microglia. Next, stained cells, with either single antibody or both antibodies against astrocytes and microglia markers, were analyzed in the FACS. The sorting decisions were made from the double stained tubes in respect to three parameters; size, granularity and positivity towards the staining. 100 astrocytes were sorted from the GLAST-positive CD11b-negative population, which is bigger in size and has more granularities, directly into RNase free PCR tubes. While 50 microglia cells were sorted from the GLAST-negative CD11b-positive population, that is smaller in size and has less granularities, directly into RNase free PCR tubes. The PCR tubes were placed immediately in liquid nitrogen and transferred to a -80°C freezer until they were used for RT-PCR.

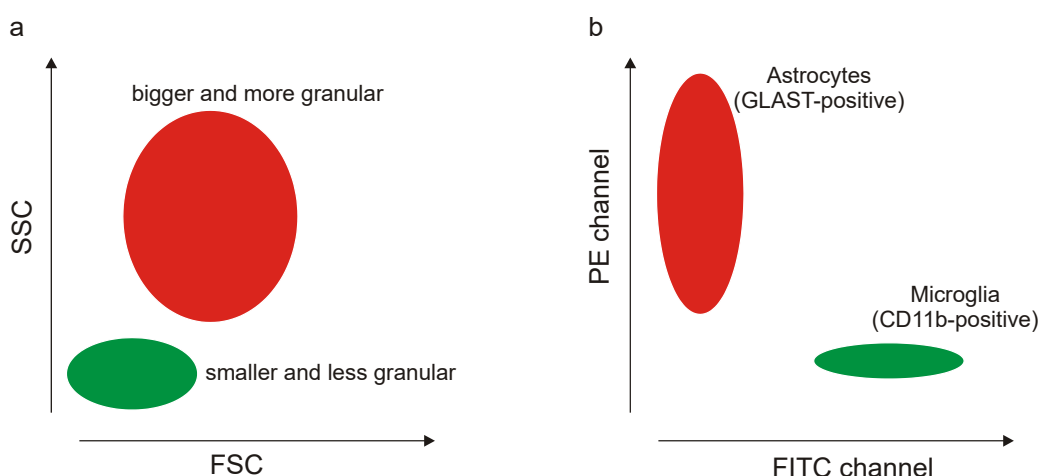


Figure 2-2. **Fluorescence Activated Cell Sorting (FACS).** (a) Scheme of forward (FSC) and side scatter (SSC) analysis of astrocytes culture showing the bigger cells with more granularity in red (astrocytes) and the smaller cells with

less granularity in green (microglia). (b) Scheme of antibody-based fluorescence analysis of stained cells with anti-GLAST-PE (astrocytes in red) and anti-CD11b-FITC (microglia in green).

2.7 Polymerase Chain Reaction (PCR)

In 1971, Dr. Har Gobind Khorana's group described the idea to amplify a DNA (Templeton, 1992). Later on in 1985, Kary B. Mullis invented the Polymerase Chain Reaction (PCR) which is used today in different fields, such as scientific research, clinical diagnostics and criminal investigations. PCR is a molecular biology tool that is used to amplify a fragment of DNA to generate thousands to millions of copies. This technique is based on an enzymatic reaction which is controlled by thermal cycling, where every cycle consists of heating and cooling steps. The generated DNA fragments after every cycle are used as templates for the next cycle. This reaction consists of 5 major components: DNA template, two primers that are complementary to the 3' ends of each strand of the double strand DNA template, heat-stable DNA polymerase, desoxynucleoside triphosphates (dNTPs) and buffer solution. The PCR is performed in 20 to 60 cycles. Each cycle consists of 3 temperature steps ensuring different reactions:

- Denaturation: This step is carried out for 15 – 30 s at 94 – 98°C, causing DNA melting by disrupting the hydrogen bonds between complementary bases and giving two single DNA strands.
- Annealing: Depending on the primers, hydrogen bonds are formed between the primers and single strands of DNA at 55 to 65°C. This step takes around 15-30 s.
- Elongation: After increasing the temperature to about 70°C for 20 to 40 s, the DNA polymerase elongate the primers in 5' - 3' direction to form new DNA strand using dNTPs.

At the end of the cycles, the reaction is kept for a few minutes at 70 - 75°C ensuring a complete extension of any single-stranded DNA. The reaction is stopped by applying low temperature of 10°C.

2.7.1 Reverse Transcription Polymerase Chain Reaction (RT-PCR)

The Reverse Transcription Polymerase Chain Reaction (RT-PCR) is a type of PCR which is used to investigate the gene expression. The RT-PCR uses the RNA as template to amplify a fragment from the studied transcript, but the PCR cannot be done directly on RNA. Thus, a reverse transcription reaction step must be done first to synthesize a complementary DNA (cDNA) which then can be used in the later PCR as a template. The reverse transcription can be done as part of a “RT-PCR” in the PCR tube, which is called one-step RT-PCR, or in two-steps in which the first strand cDNA synthesis is done independently, and the generated first strand is then used as template for PCR in an independent reaction.

2.7.2 RNA Isolation

The RNA could be isolated from cells or tissues using phenol–chloroform extraction, where proteins and DNA are trapped in the organic phase at pH of 4 to 6 and the RNA stays in the aqueous phase (Chomczynski and Sacchi, 1987). Alternatively, silica-based membranes could be also used in which RNA binds specifically and could be eluted after washing out the contaminants i.e. DNA and proteins. In this work, the RNA was extracted using silica-based membrane method. After having the astrocytes, the total RNA was extracted using RNeasy Mini Kit (Qiagen) for samples with more than 5×10^5 cells, and RNeasy Micro Kit (Qiagen) for samples with less than 5×10^5 cells. All steps were performed at room temperature. Cells were disrupted using RLT buffer and the lysate was homogenized by centrifugation through a QIAshredder spin column for 2 min at 17000 g. The flowthrough was mixed with 70% ethanol (equal volume as the RLT buffer used), transferred into an RNeasy spin column and centrifuged at 17000 g for 1 min. After having the flowthrough discarded, RW1 buffer was added to the column, centrifuged at 17000 g for 1 min and the flowthrough was discarded. The spin column was washed twice with RPE buffer each centrifuged at 17000 g for 2 min. The column was centrifuged empty at 17000 g for 1 min to remove any residual ethanol. The RNA was eluted by adding nuclease-free water to the column and centrifugation of 1 min at 17000 g. The yielded RNA was checked by nanodrop (Thermo) and the integrity of the RNA

was assessed in the Experion automated electrophoresis station (BioRad). The RNA quality indicator (RQI) is assessed by the analysis of the ribosomal RNA (rRNA) since it represents more than 80% of the total RNA in the cell and its integrity would represent the one of mRNA. Thus 18S and 28S subunits of the rRNA are visualized by microcapillary electrophoresis, and the RQI is calculated from the 28S, 18S and pre-18S regions. The RQI scores are from 1 to 10, the value 1 indicates that the RNA is totally degraded and value 10 indicates that the RNA is completely intact (Biorad).

2.7.3 One-Step Reverse Transcription Polymerase Chain Reaction

One-step RT-PCR was performed on 100 sorted GLAST-positive astrocytes or 50 sorted CD11b-positive microglia using SuperScriptTM One-Step RT-PCR with Platinum^R *Taq* (Invitrogen^R). Each 25 µl reaction contained 12.5 µl 2X Reaction Mix (0.4 mM dNTP, 24 mM MgSO₄), 0.5 µl RT/Platinum *Taq* DNA Polymerase, 0.75 µl forward primer (10 pmol/µl), 0.75 µl reverse primer (10 pmol/µl) and 10 µl RNase- DNase-free H₂O. The thermal cycle profile of the reverse transcription and the PCR were done as following:

1.	1st Strand Synthesis	50°C	30 min	
2.	PCR	94°C	2 min	
		94°C	15 s	1 st to 15 th cycle
		62°C	15 s	1 st to 15 th cycle
		70°C	20 s	1 st to 15 th cycle
		94°C	15 s	16 th to 45 th cycle
		62°C	15 s	16 th to 45 th cycle
		70°C	20 s + 2 s/cycle	16 th to 45 th cycle
		72°C	5 min	
		4°C	∞	

Forward and reverse primers used are specific for mouse TRPC1, TRPC2, TRPC3, TRPC4, TRPC5, TRPC6, TRPC7 and HPRT1 DNAs and are shown in table 2-1.

Table 2-1 **Exon-spanning oligodeoxynucleotide primers used in RT-PCR**

Gene	Forward (5'→3')	Reverse (5'→3')	Product size
TRPC1	TAAAGATTTGCTCGCACA AGCCC	TTTGACTGGGAGACAAAC TCCTTCTGG	171 bp
TRPC2	TCTGCCAGCTCACGAATC GC	TTTCGTTGAAATTGCCTAG CTTCTCG	173 bp
TRPC3	CAGCATTCTCAATCAGCC AACACG	AAGATGGCTAATTCTCTCC GTCGC	198 bp
TRPC4	TGAGAAGGAAGCCAGAAA GCTTCG	CCTTAACATTCTCCTCCGT CAAGCC	168 bp
TRPC5	GTGGGCGATGCATTACTC TACGC	GTGGGCTGCCAACATAAT GGG	168 bp
TRPC6	TCCAGGAAATTGAGGATG ATGCG	TTGGAAGCCTTGCTTTTGA CCC	197 bp
TRPC7	AGGCCAAACGCTGTGAAA ACG	CCGCTTCATGATCTTCTG GTATCTGG	152 bp
HPRT	GTCAACGGGGGACATAAA AGTTATTGG	GCTTGCAACCTTAACCATT TTGGG	160 bp

2.7.4 Gel Electrophoresis

Agarose gel electrophoresis was used to separate the DNA fragments by size. Hereby, 2% agarose gels were used because the expected size of the amplified DNA fragments was around 150 – 200 bp. The agarose gel was prepared by dissolving agarose standard (CarlRoth) in Tris/Borate (90 mM) EDTA (2 mM) buffer (1X TBE) and boiled for 2 to 3 min in a microwave. After cooling, ethidium bromide (0.5 µg/ml) was added and then the agarose loaded onto the gel tray. Samples were applied with loading buffer into the gel wells and run at 100 – 150 V (Consort EV 261 Sigma-Aldrich). The loading buffer (6X) consisted of (w/v) 15% Ficoll 400 (Sigma), 0.25% Bromophenol blue (Sigma) and 0.25% Xylencyanol (Sigma). Bands were visualized using UV light (312 nm) and photos were taken using (HeroLab UVT-28 ME-HC) equipped by a camera (Herolab B1228-U5).

2.8 TRPC1 and TRPC3 Full Length Amplification and Cloning

2.8.1 Two-Steps Reverse Transcription Polymerase Chain Reaction

Reverse transcription is a reaction that uses the RNA as template to synthesis a complementary DNA which then can be used as template in an independent PCR experiment. This reaction is carried out in the presence of reverse transcriptase, primers that can hybridize on the RNA and dNTPs.

The first strand cDNA was synthesized from RNA isolated from astrocytes using the Maxima first strand cDNA synthesis kit (Thermo Scientific). 734.51 ng of RNA (104.93 ng/ μ l) was mixed with 4 μ l 5X Reaction Mix (reaction buffer, dNTPs, oligo (dT) and random hexamer primers), 2 μ l Maxima Enzyme Mix (Reverse Transcriptase and Thermo Scientific RiboLock RNase Inhibitor) and 7 μ l of nuclease-free water. The mixture was incubated for 10 min at 25°C followed by 15 min at 50°C. The reaction was terminated by heating the mixture at 85°C for 5 min. The generated first strand cDNA was stored at -20°C.

The PCR was performed using KOD Xtreme™ Hot Start DNA Polymerase (Merck Millipore). Every reaction contains 25 μ l of PCR mix which consists of 3 μ l cDNA (obtained from reverse transcription of 734.51 ng of RNA, see above), 12.5 μ l 2X Xtreme Buffer, 5 μ l dNTPs (0.4 mM), 0.75 μ l forward primer (10 pmol/ μ l), 0.75 μ l reverse primer (10 pmol/ μ l), 2.5 μ l nuclease-free H₂O and 0.5 μ l KOD-Xtreme polymerase (1 U/ μ l). Forward and reverse primers specific to full length sequence i.e. the 5' and 3' ends of the protein-coding DNAs of mouse TRPC1 VL and TRPC3 are shown in table 2-1. The PCR amplification consists of 40 cycles, with cycle profile as following:

94°C	2 min	
98°C	10 s	1st to 40th cycle
62°C	30 s	1st to 40th cycle
68°C	3 min	1st to 40th cycle
68°C	5 min	
4°C	∞	

Oligodeoxynucleotide Primers used in the PCR reaction were specific for mouse TRPC1 VL and TRPC3 and cover the 5'- and 3'-DNA sequence which encodes full length of TRPC1 VL and TRPC3, as shown in table 2-2.

Table 2-2 **Oligodeoxynucleotide Primers used to obtain full length TRPC cDNAs**

cDNA	Forward (5'->3')	Reverse (5'->3')	Product size
TRPC1 VL(*)	[Phos]GATGACGTGAGGAG AAAGCC	[Phos]TTAATTTCTTGGATAA AACATAGC	2880 bp(*)
TRPC3	[Phos]ATGTCCACCAAGGTC AAGAAG	[Phos]TCACTCACATCTCAG CACACTG	2733 bp

(*) the primers used to amplify TRPC1 VL DNA were 201 nucleotides upstream the new start codon CTG. Thus the coding sequence is 2679 bp.

2.8.2 Gel Extraction and DNA Purification

Samples were separated by gel electrophoresis (0.8% agarose gel) and DNA fragments of the expected sizes were excised from the gel. After that, DNA fragments were separated from the gel using Wizard SV Gel and PCR Clean-Up System (Promega) which uses the ability of DNA to bind to silica membranes in the presence of guanidine isothiocyanate. 10 mg of excised gel was incubated with 10 µl of membrane binding solution at 50-65°C until the gel slice was completely dissolved. The dissolved gel was transformed and incubated for 1 min at room temperature into SV Minicolumn and then centrifuged at 16000 g for 1 min. The flow-through was discarded and the column was washed two times by adding 700 µl of membrane wash solution and centrifuged at 16000 g for 1 min. The column was incubated with 50 µl nuclease-free water for 1 min followed by centrifugation at 16000 g for 1 min to elute the DNA in a new nuclease-free tube.

2.8.3 Ligation of Fragments into Vectors

The vector used for ligation was pUC19 which consists of 2686 bp and contains an ampicillin resistance gene. The vector was cut using the SmaI restriction enzyme which cuts at 5'....CCC/GGG....3'. DNA fragments were incubated overnight at 14°C with the vector (ratio sample/vector is 3/1 estimated by

running both on an agarose gel) in the presence of 1.5 µl ligase buffer, 1 µl of T4 DNA ligase (NEB) and H₂O to achieve 15 µl as final volume.

2.8.4 Transformation

Transformation was carried out using competent *E.coli* cells by heat shock. 15 µl of the ligation reaction of each DNA samples were added to 300 µl of *E.coli* and incubated on ice for 30 min. Mixtures were exposed to heat shock at 42°C for 1 min and then chilled on ice for 2 min. Samples were supplemented with 700 µl of LB medium and incubated at 37°C in a shaker incubator for 1 h. On each sample, 200 µl 5-bromo-4-chloro-indolyl-β-D-galactopyranoside (XGal 40 mg/ml) and 50 µl Isopropyl-β-D-thiogalactopyranosid (IPTG 0.1 M) were added and then they were plated onto LB-ampicillin agar plates and incubated at 37°C overnight. XGal (colorless) and IPTG were used to distinguish the colonies which have been transformed with the DNA fragments from those which have not. The *E.coli* contains lacZΔM15 mutant gene (β-galactosidase is coded by lacZ) and the vector contains the complementary α-peptide-coding sequence. When the DNA fragment is inserted at the multiple cloning site, the *E.coli* cells are not able to produce the β-galactosidase and therefore are not able to hydrolyze the XGal (white colonies). The others, i.e. *E.coli* carrying empty vector or the insertion was not at the multiple cloning site, are able to produce functional β-galactosidase and thus the XGal will be hydrolyzed and gives a blue color (blue colonies). This is called blue-white selection of colonies.

2.8.5 DNA Preparation

Using the Mini prep kit (Sigma - Aldrich), single white *E.coli* colonies from procedure 2.8.4) were inoculated into 5 ml LB-ampicillin medium for each colony and incubated overnight at 37°C in a shaker incubator. 1.5 ml of cell suspension was spun down at 12000 g for 2 min and the supernatant was discarded. Cells were lysed by adding 200 µl of lysis buffer (Sigma - Adrich) and gently inverted in the tubes for 6-8 times. 350 µl of neutralization/binding buffer was added and samples were centrifuged at 12000 g for 10 min. The supernatant was transferred into a Miniprep Binding Column and centrifuged at 12000 g for 1 min (flow-through liquid was discarded). 500 µl of wash solution 1 (Sigma - Adrich) was added and samples were centrifuged at 12000 g for 1 min

(flow-through liquid was discarded). The previous step was repeated with wash solution 2. The column was transferred into a new collection tube, 100 µl of elution solution was added to the column and centrifuged at 12000 g for 1 min. DNA samples were stored at -20°C.

2.8.6 Restriction Analysis

For analyzing the TRPC1 VL and TRPC3 cDNAs in the pUC19 vector using the Accelrys Gene software, four restriction enzymes were chosen. For TRPC1 VL, KpnI and XhoI were used; positive clones should yield two distinct bands. In the case of sense insertion, 3078 and 2488 bp fragments will be obtained, and in the case of antisense 5174 and 392 bp will be obtained for TRPC1 VL. For TRPC3, XbaI and PshAI cuts yield in the case of sense insertion, 3690 and 1729 bp fragments and in the case of antisense 4397 and 1022 bp. The restriction reactions were analyzed by gel electrophoresis and positive clones were sequenced on both strands by SeqLab sequencing service in Göttingen, Germany.

2.9 Monitoring of Cytoplasmic Ca²⁺ by Fura-2

In 1985, Roger Tsien's group has developed a fluorescent Ca²⁺ indicator called Fura-2 (Grynkiewicz et al., 1985). Since then many other ion selective fluorescent dyes have been developed. Today, the most common way to measure changes of Ca²⁺ in the cytoplasm is using fluorescent dyes as e.g. Fluo-4 and Fura-2. In the present study, Fura-2 was used to study Ca²⁺ concentration changes in mouse cortical astrocytes. Because Fura-2 is polar and thus not membrane permeable, ester form, Fura-2-AcetoxyMethyl (Fura-2-AM), was used which is membrane permeable (nonpolar). Once it is inside the cell it will be de-esterified by intracellular esterases and becomes trapped and able to bind free Ca²⁺ (Figure 2-3).

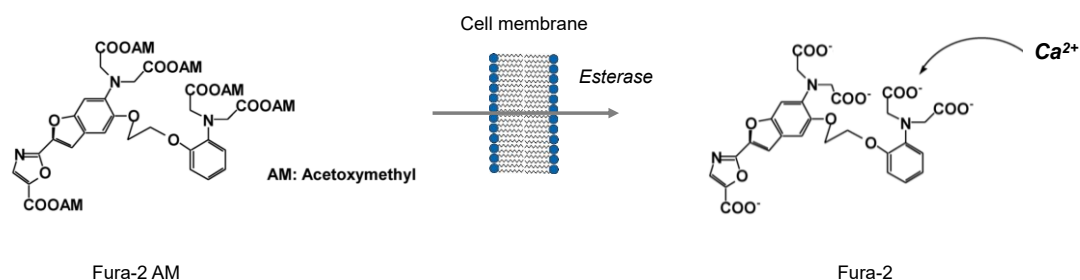


Figure 2-3 **Loading cells by Fura-2 AM.** Fura-2 AM is nonpolar and Ca²⁺-insensitive and membrane permeable. Once it is inside the cell, it is hydrolyzed by cytoplasmic esterases into the polar, Ca²⁺-sensitive form.

Fura-2 is a fluorescent dye changing its excitation spectrum due to the binding of Ca²⁺ ions. Upon Ca²⁺ binding the excitation peak shifts from 380 nm towards 340 nm, the emission spectrum stays independent of Ca²⁺ with a peak at about 510 nm. At the excitation wavelength of 360 nm, Fura-2 fluorescence intensity is Ca²⁺-independent; this wave length is called isosbestic wavelength. The more Ca²⁺ is bound to Fura-2, the fluorescence emission at 340 nm excitation increases and the fluorescence emission at 380 nm decreases (Figure 2-4). Thus, Fura-2 is used in a dual excitation system, which measures separately the fluorescence emission for both excitation wavelengths, and therefore the changes at cytoplasmic Ca²⁺ concentrations are expressed as the ratio F340/F380. Since the F340 increases with Ca²⁺ binding and the F380 decreases, the ratio F340/F380 increases when the cytoplasmic Ca²⁺ rises (Figure 2-4). Therefore, the use of ratiometric measurement eliminates the differences in the amount of Fura-2 loading of the different cells.

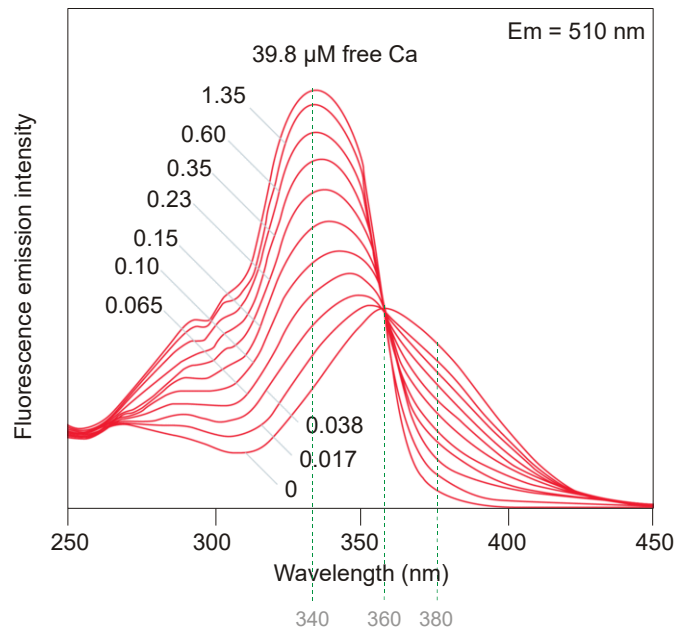


Figure 2-4 **Excitation and emission spectra of Fura-2.** The fluorescence emission intensity for Fura-2 depends on the excitation wavelengths and on the Ca^{2+} concentration. The excitation peak shifts from 380 nm towards 340 nm upon Ca^{2+} binding. The fluorescence emission at 360 nm stays independent of Ca^{2+} binding is called isosbestic wavelength and is a direct measure of the amount of Fura-2 per cell (adapted from Leica).

2.10 Fura-2 Experiment

Primary astrocytes, cultured for 2 to 3 weeks, were subcultured for 4 to 6 days on glass coverslips coated with P-L-L. Before imaging, cells were loaded for 40 min with 5 μM Fura-2-AM in medium and incubated in the dark in the presence of 5% CO_2 at 37°C. Afterwards, cells were washed with 0 or 2 mM Ca^{2+} -based solution (Table 2-3) and the coverslip was fixed in an open or closed chamber either for direct application of solutions into the bath or for perfusion, respectively. The perfusion system consisted of 8 channels; these channels were filled with the appropriate external solutions. Different compounds were dissolved in the desired channel, and an aspirating pump was used to generate a stable flow of approximately 3 ml/min. The chamber was placed on a monochromator (Polychrome V, TILL-Photonics) equipped inverted microscope (Axivert S100, Carl Zeiss). Every 2 s Fura-2 was alternately excited at 340 nm and 380 nm for 30 ms each and the emitted fluorescence (~ 510 nm) were recorded with a charge-coupled device (CCD) camera (Imago, TILL-Photonics,

Germany). Ratio images were calculated from 340 and 380 nm pictures after background correction i.e. subtraction of the fluorescence intensity at 340 and 380 nm excitation of a cell-free region prior to calculate the ratio. Single cells were marked as regions of interest and F340/F380 was plotted versus time. The monochromator, camera acquisition and analysis were controlled by Till-Vision software (TILL-Photonics).

2.11 Electrophysiological recordings

The patch clamp technique allows the recording of single or multiple ion channels activities in cells. This technique was first developed by Erwin Neher and Bert Sakmann, who were awarded the Nobel Prize in Physiology or Medicine for his achievement in 1991. Patch clamp recording uses a glass micropipette called a patch pipette as a recording electrode, and another electrode in the bath around the cell, as a reference ground electrode (Figure 2-5). Several configurations could be used to measure ion channels including, the cell-attached, the inside-out, outside-out and the whole cell mode. In this work, the whole cell mode was employed which allows the recordings from all active ion channels in the plasma membrane. The patch pipette is filled with a solution of defined ion composition and concentrations depending on the aimed ion channel, and contains the measuring electrode as well. To begin the measurements, the cytoplasm of the measured cell has to be exchanged by the pipette solution allowing access to the measuring electrode which is also used to control the membrane potentials. To achieve this configuration, the patch pipette is brought in very close contact with the cellular membrane to get a gigaseal i.e. the pipette resistance at this stage has gigaohm (GΩ) readings, then light sucking is applied to break into the cell.

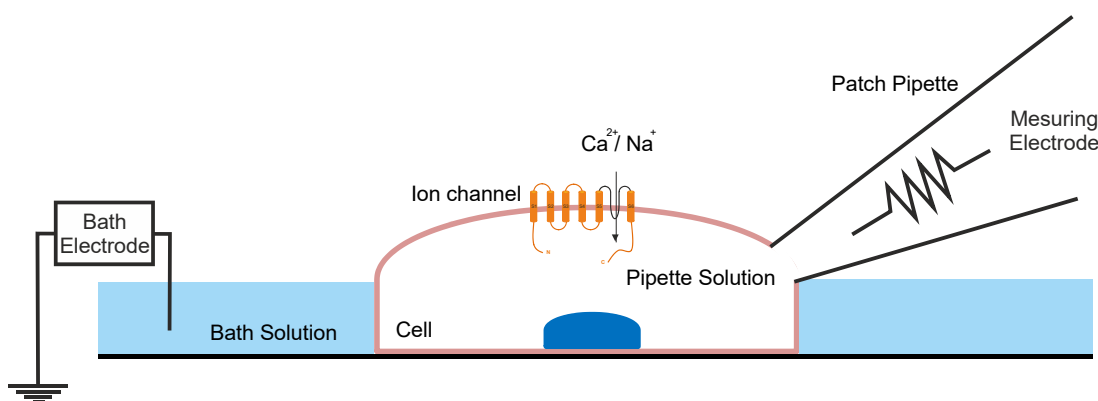


Figure 2-5 **Whole cell patch clamp recording.** Representative schema of the whole cell patch clamp shows two electrodes, one as a bath electrode and another one as a measuring electrode in the patch pipette. The pipette solution replaces the cytoplasm upon break-in and the flow of ions upon channels activation is measured as a current.

2.11.1 TRPC3 currents recording

Membrane currents were recorded in the tight seal whole-cell patch clamp configuration using an EPC-9 amplifier (HEKA Electronics, Lambrecht, Germany). Patch pipettes were pulled from glass capillaries GB150T-8P (Science Products, Hofheim, Germany) at a vertical Puller (PC-10, Narishige, Tokyo, Japan) and had resistances between 2 and 4 M Ω when filled with standard internal solution (pipette solution). The different used solutions are listed in section (2.18). The compounds used for external application were diluted into the extracellular solution to achieve the final concentration as indicated. All modified solutions were directly applied onto the patch-clamped cell via an air pressure-driven application pipette. Osmolarity of all solutions were controlled to range between 290 and 310 mOsm. Voltage ramps of 400 ms duration spanning a voltage range from -100 to 100 mV were applied at 0.5 Hz from a holding potential (V_h) of 0 mV over the period of the measurements using the PatchMaster software (HEKA). All voltages were corrected for a 10 mV liquid junction potential. Currents were filtered at 2.9 kHz and digitized at 100 ms intervals. Capacitive currents and series resistance were determined and corrected before each voltage ramp using the automatic capacitance compensation of the EPC-9. Inward and outward currents were extracted from each individual ramp current recording by measuring the current amplitudes at -80 and +80 mV, respectively, and plotted versus time. Basic currents before an

application were subtracted to get the net developing current. Current-voltage (IV) relationships were extracted at indicated time points. Currents were normalized to the initial size i.e. capacitance of the cell to obtain current densities (pA/pF).

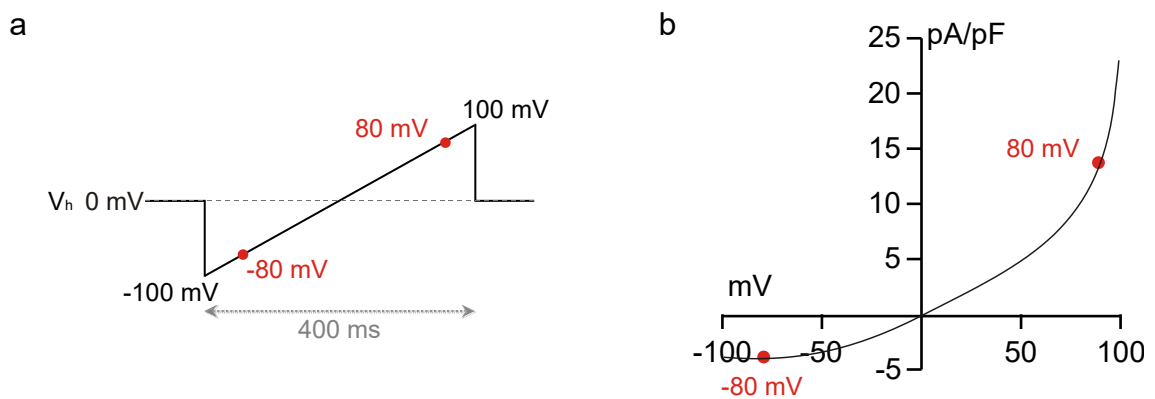


Figure 2-6 Voltage ramp protocol for whole cell patch clamp recording. (a) Representative scheme of a 400 ms voltage ramp spanning from -100 to 100 mV from a holding potential (V_h) of 0 mV, used to measure whole cell currents by patch clamp experiments. (b) Example trace of a current-voltage relationship where inward and outward currents could be extracted at -80 and +80 mV from each individual ramp current and plotted versus time.

2.11.2 CaVs currents recording

The same setup and general configurations as described for TRPC3 current recordings (2.11.1) were used to measure the CaVs, however different bath solution were employed (Table 2-5 and Table 2-6). Voltage ramps of 50 ms duration spanning a voltage range from -100 to 100 mV were applied at 0.5 Hz from a holding potential (V_h) of -60 mV over the period of the measurements using the PatchMaster software (HEKA). After measuring for 3 to 5 min in the ramp protocol, voltage steps of 400 ms duration were applied from -70 to 90 mV in 10 mV increase from a holding potential of -60 mV. All voltages were corrected for a 5 mV liquid junction potential. Currents were filtered at 2.9 kHz and digitized at 100 ms intervals, and linear leak was subtracted by auto-leak subtraction feature from PatchMaster software (HEKA). Capacitive currents and series resistance were determined and corrected before each voltage ramp using the automatic capacitance compensation of the EPC-9. The maximum current-voltage (IV) relationships were extracted from the ramp protocol and

normalized to the initial size of the cell to obtain current densities (pA/pF). In the step protocol, the current-voltage (IV) relationships were constructed from plotting the peak currents of each step versus the applied voltages and normalized to cell size. In addition, the current of the maximum step was plotted versus the step time in ms to obtain the inactivation kinetics. The activation (τ_{act}) and inactivation (τ_{inact}) kinetics were calculated from the maximum current obtained from the step protocol using the following single exponential equation:

$$y = y_0 + A \frac{-(x-x_0)}{\tau}$$

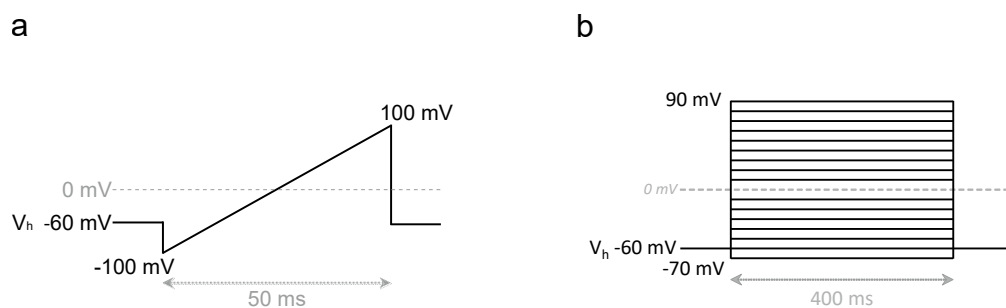


Figure 2-7 Voltage ramp and step protocols for whole cell patch clamp recording. (a) Representative scheme of a 50 ms voltage ramp spanning from -100 to 100 mV from a holding potential (V_h) of -60 mV, used to measure whole cell voltage-gated ion currents by patch clamp experiments. (b) Representative scheme of voltage steps used to measure whole cell voltage-gated ion currents by patch clamp experiments showing steps of 400 ms from -70 to 90 mV (10 mV increments) and holding potential (V_h) of -60 mV.

2.12 Migration Assay

Astrocytes migration was analyzed using a scratch assay in which the migration rate of cells is assessed by their speed in covering a defined scratched area on a confluent cell layer. Cells were plated in 6-well plates which were previously coated with poly-L-lysine and scratched from the outside bottom using a needle as an external marker to help taking pictures from the exact same region (Figure 2-8 blue lines). All migration experiments were always performed with TRPC deficient and the corresponding wild-type astrocytes at the same time. Once cells reached confluency, two scratches were performed in every well (vertical to the needle scratch) using a 200 μ l pipette tip. Wells were washed with PBS to remove the detached cells and incubated with 0% FCS medium to

inhibit the proliferation at 37°C 5% CO₂. At 0, 4, 8 and 24 hours, 4 pictures per well (Figure 2-8) were taken from the scratches, at the crossing between the scratch line and the external needle scratch, using a phase-contrast light microscope (Axiovert 40C, ZEISS) equipped with a camera (AxioCam, ZEISS). Migration was quantified as the average of the cell-free scratch areas reoccupied by the migrated cells using Image J software. All the measured areas were normalized to the 0 hour area (100% cell-free area).

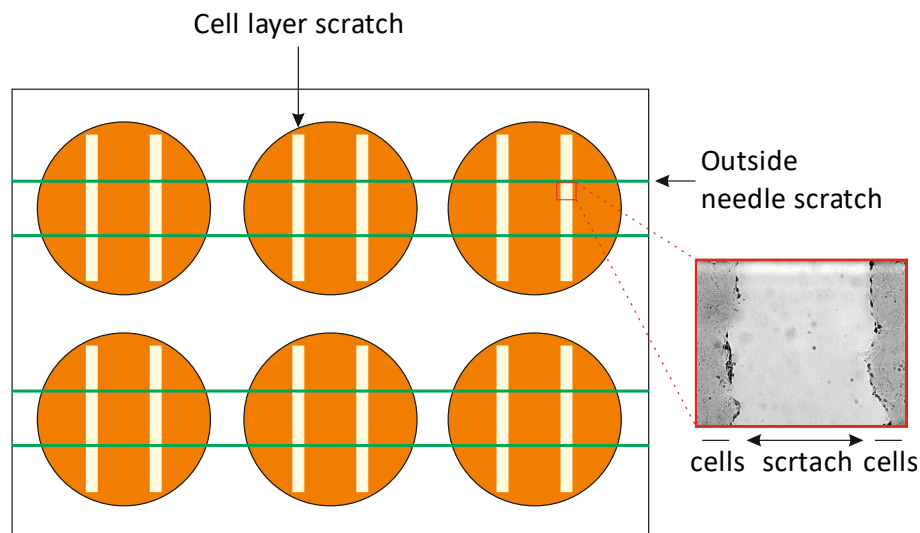


Figure 2-8 Migration Assay in 6-well plate. 6-well plate scratched from the outside bottom with a needle (green horizontal lines) as markers for pictures. The cell scratches on the confluent cell layer were made with 200 µl pipette tip (white vertical lines). After the scratches, the 10% FCS medium was substituted with a 0% FCS medium to stop proliferation and photos are taken from the area where the cell and needle scratches meet (red box).

2.13 Cortical stab wound surgery

The cortical stab wound experiment is a surgical technique used to study the astrogliosis and glial scar formation in the cortex (Saadoun et al., 2005). All experiments were performed in the laboratory of Prof. Frank Kirchhoff under the supervision of Dr. Anja Scheller in the Department of Physiology at Saarland University. I obtained the approval to perform the stab wound surgery from state of Saarland under the name: "Einfluss von TRPC3 Kationenkanälen auf die Wundheilung im ZNS" AZ C1-2.4.2.2/11-2015. Mice were anesthetized using ketamine (87 mg/kg body weight) and xylazine (13 mg/kg body weight) via

intraperitoneal injection and kept inside cages until the complete loss of reflection upon application of pressure on the rear feet. Anesthetized mice were then transferred onto a stereotaxic instrument equipped with heating plate set at 35°C to prevent anesthesia-induced hypothermia. After having wiped the top of the head with 70% ethanol, a 1 cm long incision in the skin was made in the middle of the head following the sagittal plane using a sharp scalpel. The membrane which covers the skull was removed with forceps. Using an electric drill, the skull was thinned (3 to 4 mm length), in the right hemisphere region located 2 mm from the sagittal suture and 4 mm from the olfactory lobe, followed by an insertion of a 3 mm wide scalpel in the thinned region 2 mm deep into the cortex (Figure 2-10) directed by a stereotactic arm. After cleaning the blood, the skin was sutured and animals received buprenorphine (0.05 mg/kg) via subcutaneous injection to relieve the pain; animals were kept in cages on a heating plate until they regained consciousness. Then they were transferred in the mice-housing room. Mice were kept and monitored for three days; afterwards the following procedure was performed.

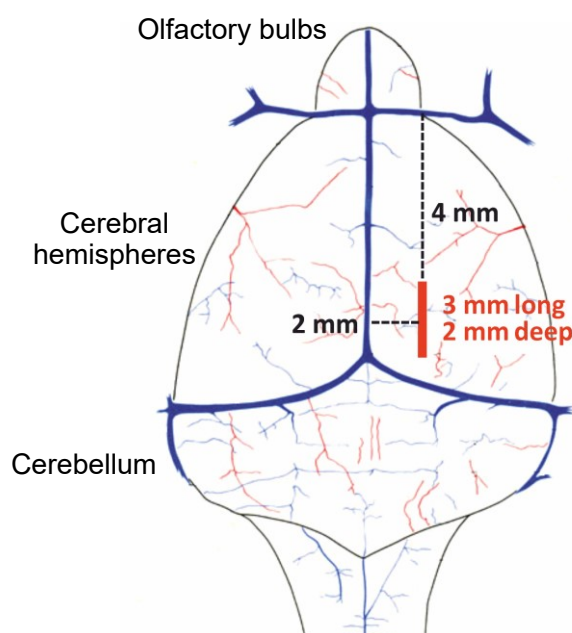


Figure 2-9 **Cortical stab wound surgery.** Schematic representation of the position of the wound performed on the mouse cerebral cortex of the right hemisphere 4 mm away from the olfactory bulb and 2 mm from the sagittal suture. The wound is parallel to the sagittal suture and has a length of 3 mm and 2 mm in depth. Image adapted from “The Anatomy of the Laboratory Mouse” Margaret J. Cook.

2.14 Mice fixation with paraformaldehyde (PFA)

Three days after the surgery, mice were again anesthetized via intraperitoneal injection using ketamine (87 mg/kg body weight) and xylazine (13 mg/kg body weight) and kept inside cages until the complete loss of reflex upon application of pressure on the rear feet. Mice were fixed onto a plate and the thorax was opened using sharp scissors. Under the hood 30 ml PBS followed by 30 ml 4% PFA were perfused by inserting a 25 G needle into the left ventricle and opening the right atrium. The perfused brains were removed and kept fixed further overnight in 4% PFA solution and used later for immunohistochemical analysis.

2.15 Immunohistochemistry on brain slices

Brains incubated overnight in 4% PFA were washed with PBS, trimmed with scalpel and mounted caudal side-down on a vibratome (Leica) with tissue glue (Loctite). 35 µm thick coronal sections were made in the wound region and 4 representative sections were taken from each brain for immunostaining. Slices were placed in 48 well plate and incubated with 3% (v/v) TritonX (Roth) / 5% (v/v) donkey serum in PBS to permeabilize the tissue and block the unspecific binding sites for 1 hour at room temperature. Then the blocking solution was removed and replaced by the same solution containing the primary rabbit anti-GFAP antibody (Dako) (1:1000) and incubated overnight at 4°C. The next day, slices were washed 3 times with PBS and incubated at room temperature for 1 hour with the secondary antibody donkey anti-rabbit Alexa 555 antibody (Invitrogen) (1:1000) to visualize the primary anti-GFAP antibody, and 1 µg/ml DAPI to stain the nuclei. Then, slices were washed and mounted on glass slides with a mounting medium (Thermo) and pictures were taken with a fluorescence microscope (Axiovert 200M, ZEISS) equipped with a color camera (AxioCam, ZEISS), using the software AxioVision Rel. 4.7 as mosaic images with 10% overlap. Images were analyzed with AxioVision by measuring three parameters: the area of reactive astrocytes (GFAP-stained cells), cortex edema as the increase in the cortex thickness, and distribution of reactive astrocytes

measured from the fluorescence intensity of the GFAP staining along the cortex (Figure 2-10).

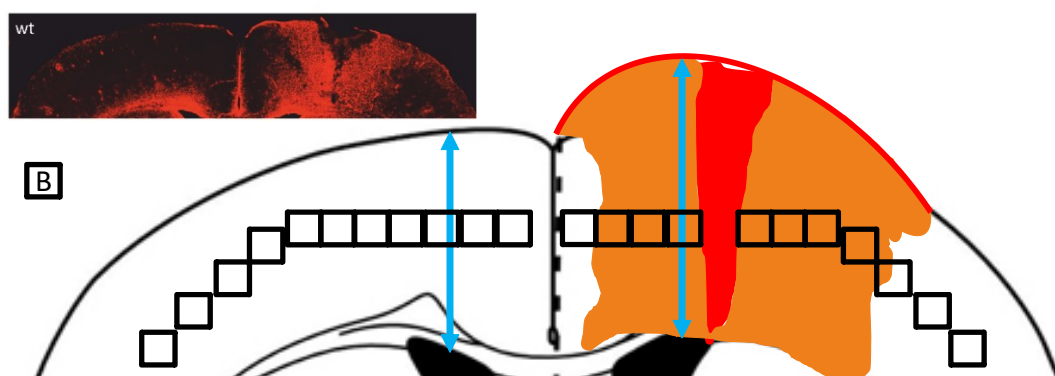


Figure 2-10 **Cortical stab wound analysis.** The cortical wound was analyzed 3 days after the surgery. As early as possible after immunostaining against GFAP (inset), the area of reactive astrocytes i.e. area of GFAP-stained astrocytes (orange area) was determined. The cortical edema was measured from the increase in the cortex thickness (blue arrows). The distribution of the reactive astrocytes is obtained from the GFAP fluorescence intensity of the boxes along the cortex (injured and non-injured) after subtracting the background intensity (box B).

2.16 Pharmacological compounds used in Ca^{2+} imaging and patch clamp experiments

Compound	Provider	Used at final concentration of
<i>Thapsigargin (TG)</i>	Invitrogen	2 μM
<i>Cyclopiazonic Acid (CPA)</i>	Calbiochem	10 μM
<i>1-Oleoyl-2-acetyl-sn-glycerol (OAG)</i>	Calbiochem	100-300 μM
<i>Phorbol 12-myristate 13-acetate (PMA)</i>	Calbiochem	1 μM
<i>Nifedipine</i>	Sigma-Aldrich	10 μM
<i>Verapamil</i>	Tocris	10 μM
<i>Isradipine</i>	Tocris	1-100 μM
<i>ω-Agatoxin-IVA</i>	Tocris	2 μM
<i>ω-Conotoxin-GVIA</i>	Tocris	1 μM
<i>SNX482</i>	Tocris	300 nM
<i>Tetrodotoxin (TTX)</i>	Tocris	10 μM

2.17 Statistical Analysis

Data were analyzed using Till-Vision (Till Photonics), PatchMaster software (HEKA), Microsoft Excel, Igor Pro 5.1 (WaveMetrics), AxioVision Rel. 4.7 (ZEISS) and ImageJ (NIH). Data are shown as mean \pm SEM with (xx/y) indicating the number of analyzed cells, scratches or mice (xx) per performed experiments (y). To estimate the significance of differences, Student's t-test for two groups and one way ANOVA followed by Bonferroni test for more than two groups. The difference was found significant if the P-value < 0.05 (*), < 0.01 (**) or < 0.001 (***).

2.18 Solutions for Fura-2 and patch clamp experiments

All prepared solution were adjusted to a pH of 7.2 with NaOH or CsOH for Na⁺- or Cs⁺-based solutions respectively, and only solution with an osmolarity between 290 to 310 mOsm were used.

Table 2-3 **Solutions used in Ca²⁺ imaging experiments**

Compound (mM)	Solutions			
	2 mM Ca²⁺	0 Ca²⁺	50 mM K⁺	0 K⁺
NaCl	140	140	94	140
KCl	4	4	50	0
MgCl ₂	1	3	1	1
HEPES	10	10	10	10
Glucose	10	10	10	10
CaCl ₂	2	0	2	2

Table 2-4 **Patch clamp external solutions used for recording of TRPC currents**

Compound (mM)	Solutions	
	1 mM Ca²⁺	0 Ca²⁺
NaCl	140	140
KCl	0	0
MgCl ₂	1	3
HEPES	10	10
Glucose	10	10
CaCl ₂	2	0

Table 2-5 **Patch clamp external solutions used for recording of voltage-gated Ca^{2+} currents**

Compound (mM)	Solutions		
	10 mM Ba^{2+}	0 Ba^{2+}	0 Na^+
NaCl	102	130	0
MgCl_2	1	1	1
CsCl	5.4	5.4	107.4
TEACl	20	20	20
HEPES	5	5	5
Glucose	10	10	10
BaCl_2	10	0	10

Table 2-6 **Pipette solutions used for recording of TRPC and CsVs patch clamp experiments**

Compound (mM)	Solutions	
	100 nM Ca^{2+}	0 Ca^{2+}
CsMs	140	140
NaCl	8	8
MgCl_2	1	1
HEPES	10	10
CaCl_2	3.1	0
BAPTA	10	10

- Ms stands for methanesulfonate.
- TEA stands for Tetraethylammonium
- BAPTA stands for 1,2-bis(o-aminophenoxy)ethane-N,N,N',N'-tetraacetic acid
- The 100 nM free Ca^{2+} was calculated with Webmaxc Standard (<http://web.stanford.edu/~cpatton/webmaxcS.htm>).

3 Results

3.1 Characterization of mouse cortical astrocyte cultures

It is well accepted that primary astrocyte cultures contain noticeable percentages of microglia and oligodendrocytes. However the presence of other cell types could indicate a contamination from other tissue, for instance the presence of fibroblast in the astrocyte culture means that the meninges were not completely removed. To estimate the purity of the mouse cortical astrocyte culture, confluent cultures in flasks obtained from mouse cortices were plated on glass coverslips and stained with antibodies against glial fibrillary acidic protein (GFAP), an astrocyte specific marker and CD11b, a microglia specific marker. 90% of the cells were GFAP-positive, 9% of the cells were CD11b positive and 1% of the cells were neither stained with GFAP nor with CD11b antibodies, analyzed from 4 images. There was no co-staining of both antibodies in the same cells; however some microglia cells were on top of astrocytes which appeared as co-staining but in fact it was not (Figure 3-1).

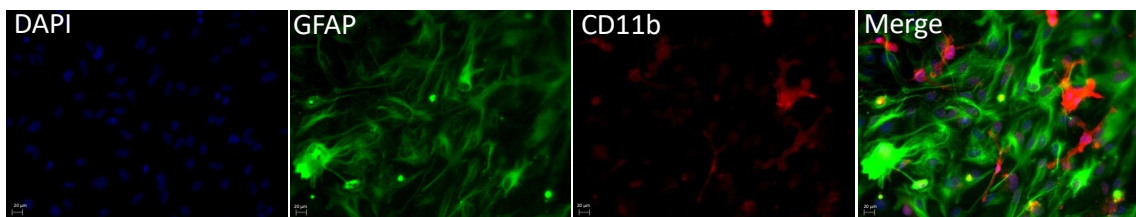


Figure 3-1. **Immunocytochemistry of a mouse cortical astrocyte culture.** Cells are stained with antibodies against GFAP (green) for astrocytes and DAPI (blue) to visualize the nuclei, CD11b (red) for microglia. The merge image shows no co-staining between the astrocytic and microglia markers, except some microglia cells were on top of astrocytes that gave a yellow color.

3.2 TRPC Expression in mouse cortical astrocyte cultures

RNA was extracted from three independent astrocyte cultures which were shown to contain 90% astrocytes; the extracted RNA was used for RT-PCR. Fragments for TRPC1, TRPC2, TRPC3, TRPC4, TRPC6, TRPC7 and HPRT transcripts were amplified at the expected sizes except for TRPC5 that revealed

a band at about 75 bp instead of 168 bp (Figure 3-2). The amplified fragments of TRPC transcripts were visualized on 2% agarose gel. Although the astrocyte cultures contained around 87% astrocytes, this does not mean that the non-astrocytic cells will not contribute to the RNA extracted from the cultures. Therefore, a second strategy was used to ensure that transcripts are only derived from astrocytes.

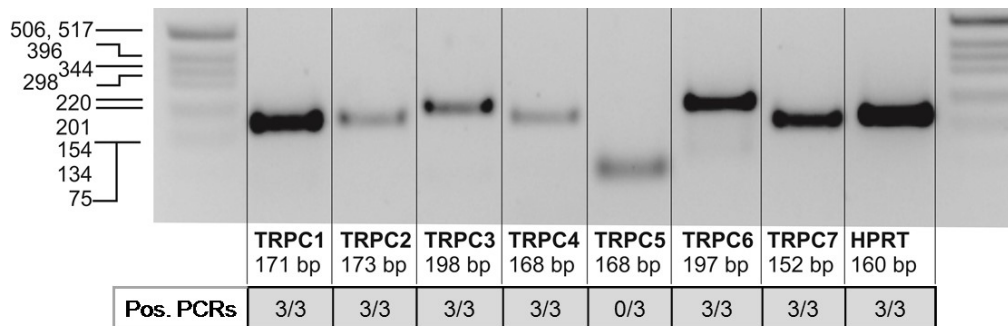


Figure 3-2 TRPC transcripts expression in mouse cortical astrocytes. Agarose gels from three independent RT-PCRs performed with RNA extracted from enriched astrocyte cultures. DNA-fragments of the expected sizes, were amplified by and one-step RT-PCR for HPRT (160 bp), TRPC1 (171 bp), TRPC2 (173 bp), TRPC3 (198 bp), TRPC4, (168 bp), TRPC6 (197 bp), TRPC7 (152 bp), but not for TRPC5 (168 bp) and run on a 2% agarose gel. All three RT-PCR gels are shown in supplementary figure S1.

3.3 Analysis of astrocytes by flow cytometry

Fluorescence-activated cell sorting (FACS) was used to separate the astrocytes from contaminating cells. The fluorescent anti-GFAP antibody cannot be used for FACS because GFAP is a cytoplasmic protein and cell permeabilization is required stain with a specific antibody. The glutamate aspartate transporter (GLAST) is localized in the cell membrane and can also be used as an astrocytes marker (Jungblut et al., 2012). Thereby, intact living cells can be sorted and thereafter be used for RNA extraction or one-step RT-PCR. First we check whether the same cell population is stained by the anti-GFAP and the anti-GLAST antibodies. After shaking off most of the microglia cells, fixed and permeabilized astrocytes were stained with anti-GLAST conjugated with PE and anti-GFAP conjugated with FITC either separately or combined. Therefore, the cells were analyzed by analytical fluorescence-activated cell sorting. The

analysis of the forward (FSC) and side scattered (SSC) light (Figure 3-3-a) indicates that the fixed and permeablized cells are still intact and not fragmented, and the non-stained cells do not exhibit any fluorescence in the FITC and PE channels (Figure 3-3-b). Most of the cells stained with anti-GFAP-FITC shifted towards the FITC channel (R18, Figure 3-3-c); they were spread along the channel which indicates differences in the amount of the GFAP protein in these cells. The amount of GFAP defines fluorescence intensity. Cells stained with anti-GLAST-PE shifted towards the PE channel (R15, Figure 3-3-d), but under this condition cells accumulated in a small area indicating a more homogeneous amount of GLAST than of GFAP in astrocytes. GFAP and GLAST are proposed to be astrocyte-specific markers and fixed and permeablized astrocytes were stained with both anti-GFAP-FITC and anti-GLAST-PE antibodies. 96% of the cells shifted towards the right upper corner (R16 in Figure 3-3 e) of the flow cytometer analysis window which shows that these cells are stained with both antibodies. This result confirms the result obtained by the anti-GFAP and anti-CD11b staining of the astrocytes culture and the counting under the microscope (Figure 3-1). It also shows that shacking off the microglia increases the percentage of astrocytes.

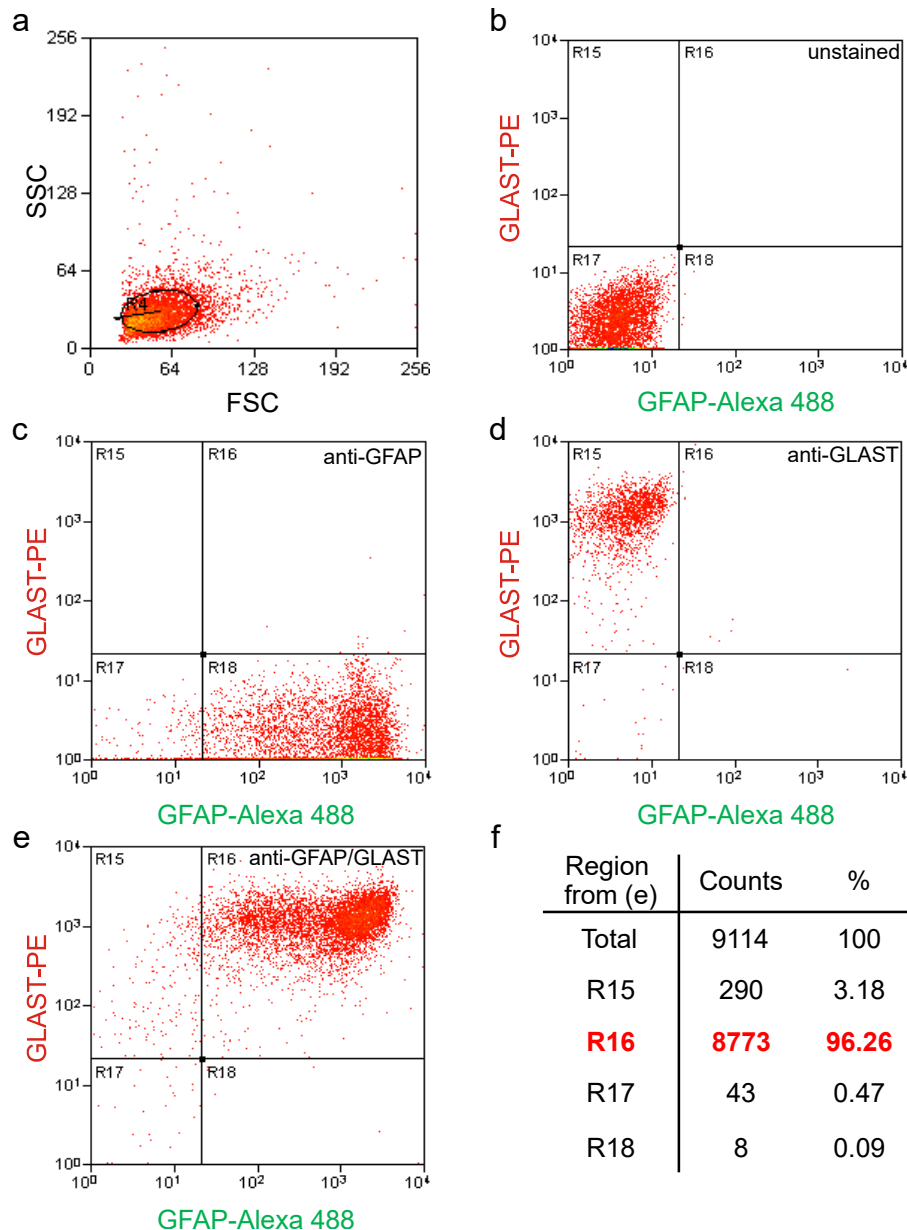


Figure 3-3 Flow cytometry analysis of the fixed and permeabilized astrocytes. (a) Forward (FSC) and side scatter (SSC) analysis of the fixed and permeabilized astrocytes showed one population. (b) Analysis of the non-stained astrocytes on the PE and FITC channels where it shows no reactivity from those cells in both channels (R17). (c) Cells stained with only anti-GFAP-FITC did migrate towards the FITC channel (R18), and (d) cells stained with only anti-GLAST-PE did migrate towards the PE channel (R15). (e) 96% of the cells stained with both anti-GFAP-FITC and anti-GLAST-PE did migrate toward the upper left corner of the analysis window indicating that those cells are actually reactive to both channels due to the expression of GFAP and GLAST markers (R16).

3.4 Sorting astrocytes using preparative FACS

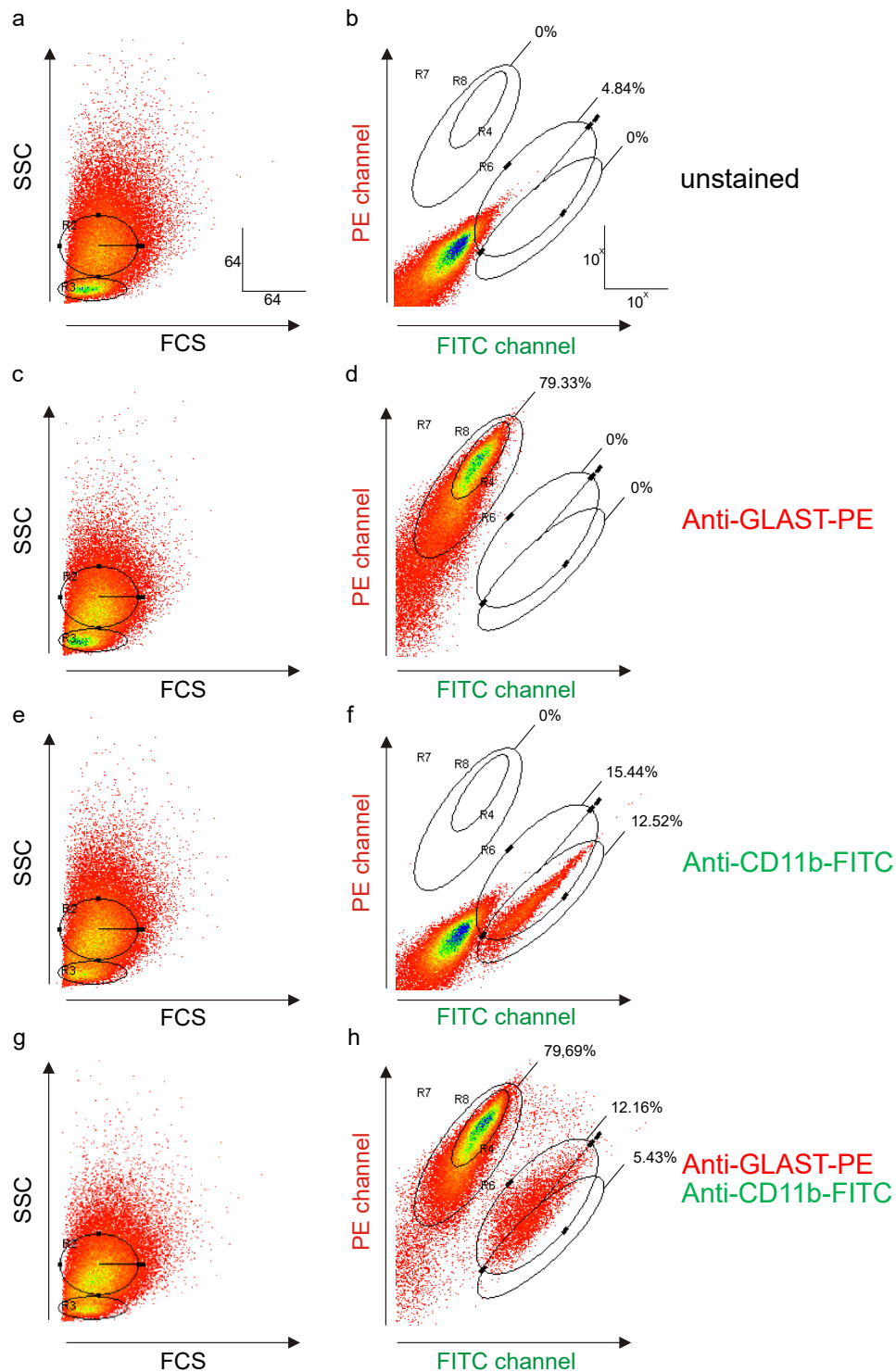


Figure 3-4 Preparative FACS of astrocytes and microglia. (a, c, e and g) representative experiments from 5 experiments of the forward (FSC) and side (SSC) scatter of cells from the staining conditions showed a consistency in terms of the existing and the size of two populations. (b) The fluorescence analysis of the unstained cells shows no reactivity towards the PE and the FITC channels. (d) Staining cells with anti-GLAST-PE led to a shift of 79% of the cells

towards the PE channel (R7). The selection of the stained population is based on a clear separation from the unstained population. (f) The anti-CD11b-FITC staining led to a shift of about 12% of the cells towards the FITC channel (R6). (h) The combination of both antibodies anti-GLAST-PE and anti-CD11b-FITC led to a clear separation of the cells into two distinct populations with the same percentages obtained from the single staining; however, there was a slight upper shift in the CD11b population in the presence of anti-GLAST-PE (R4 and R6). The sort decision for astrocytes was made from the inner circle of the GLAST population (R8), and for the microglia cells from lower right circle which has 5% of cells (R6).

As previously shown in the immunostaining and the flow cytometry analysis the astrocyte cultures contained 9% of microglia. These cells will contribute to the RNA isolated from the cultures. Therefore, the preparative fluorescence-activated cell sorting was employed to specifically sort pure astrocytes. To sort living cells the anti-GLAST-PE and anti-CD11b-FITC antibodies were used for labelling as described above. Unstained astrocytes were first analyzed in terms of their size (FSC) and granularity (SSC) which revealed two different populations that differ slightly in size and the one that was bigger in size had also more granularity (R2 in Figure 3-4-a). The fluorescence analysis of the unstained cells showed no signals in the PE channel or in the FITC channel (Figure 3-4-b). Cells were then stained with anti-GLAST conjugated with PE. The majority of cells did migrate towards the PE channel with 79.33% (R7 in Figure 3-4-d) of cells exhibit strong staining and no signal was detected in the FITC channel. When cell were stained with microglia marker anti-CD11b conjugated with FITC, only 12.52% (R4 in Figure 3-4-f) of the cell migrated towards the FITC channel and no signal was seen in the PE channel. In the condition where both marker antibodies were used, anti-GLAST-PE and anti-CD11b-FITC, two distinct populations were observed. However the CD11b population did shift slightly towards the center indicating possible weak unspecific staining by the anti-GLAST antibody, but this population could be easily separated from the GLAST-labelled population. For the GLAST-labelled population, no shift was observed and the percentage of strongly stained cells remained at 79.69% (R7 in Figure 3-4-h). The sorting decision for the astrocytes includes cells that showed more granularity and bigger size and which were stained by anti-GLAST antibody but not by the anti-CD11b antibody. Astrocytes

were sorted in single RNase-free PCR tubes at 100 cells per tube for one-step RT-PCR. The remaining astrocytes were sorted in a 14 ml tube to be used for total RNA extraction. The microglia cells were defined as the less granular and small sized cells labelled by anti-CD11b but not by anti-GLAST antibodies. The microglia cells were sorted at 50 cells per tube for RT-PCR.

3.5 TRPC transcripts expression in the FACS-sorted astrocytes and microglia cells

3.5.1 RT-PCR from FACS-sorted astrocytes and microglia cells

PCR tubes containing either sorted-astrocytes or microglia cells were stored at -80°C and the one-step RT-PCR mix were added to the tubes immediately after taking them from the freezer. 13 independent RT-PCR from 5 independent sortings were performed with astrocytes to check for the expression of TRPC transcripts. TRPC1 and TRPC2 were amplified 10 times from 13 PCRs, TRPC3 was always detected in all 13 PCRs, while TRPC4 was amplified in 11 out of 13 reactions. The other TRPC members TRPC5, TRPC6 and TRPC7 were not detectable in all performed PCRs. The HPRT transcript was used as control. The HPRT reaction was always the last one to be pipetted, and the HPRT DNA fragment was always amplified (Figure 3-5-a-c). For the microglia 3 independent RT-PCRs were performed and only TRPC4 was detected in 3 PCRs, while TRPC2 was detected one time out of 3 PCRs. HPRT was again used as control and was always detected (Figure 3-5-b-c).

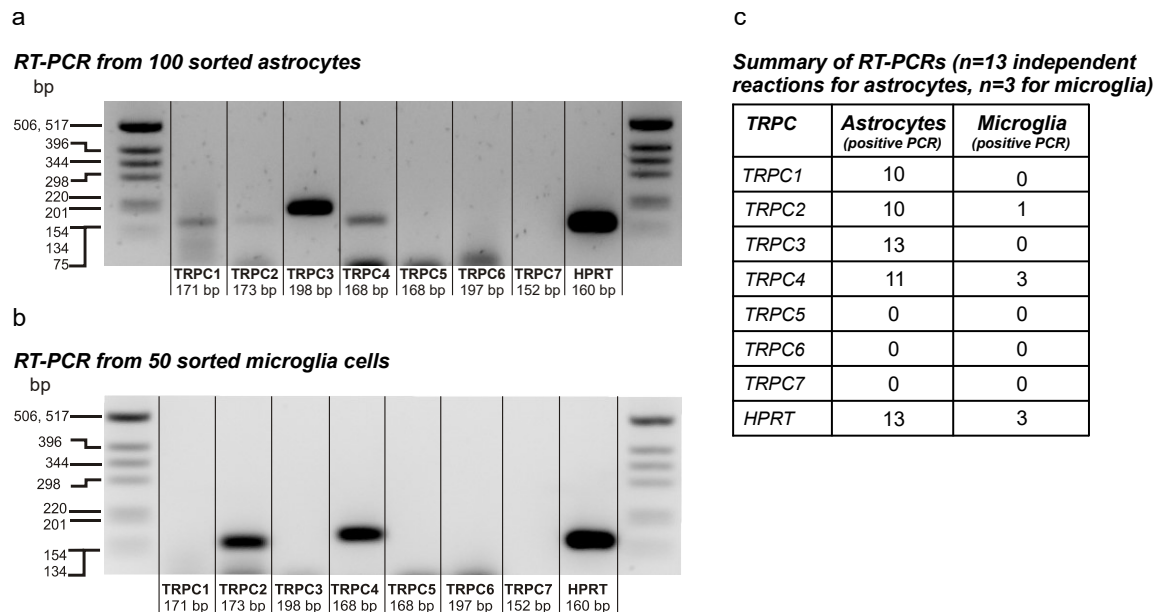


Figure 3-5 TRPC transcripts expression in astrocytes and microglia. (a) Example gel from 13 independent RT-PCRs performed from GLAST-sorted astrocytes showing the amplification of TRPC1, TRPC2, TRPC3, TRPC4 and HPRT DNA fragments of the expected sizes. (b) Example gel from 3 independent RT-PCRs performed from CD11b-sorted microglia showing the amplification of TRPC2, TRPC4 and HPRT fragments. (c) Summary of all RT-PCR results from the FACS-sorted astrocytes (n=13 reactions) and microglia cells (n=3 reactions). All performed RT-PCR gels are shown in supplementary figure S2 (astrocytes) and S3 (microglia).

3.5.2 Transcriptome analysis of TRPCs from GLAST-sorted astrocytes by next generation sequencing

The RNAs used for the transcriptome analysis were extracted from three independent FACS sortings i.e. GLAST-positive astrocytes, from three independent cultures. The transcriptome analysis was performed in collaboration with Prof. Andreas Keller and Dr. Christina Backes from the Clinical Bioinformatics department at Saarland University. The samples were sequenced in Illumina HiSeq (paired-end, 75 bp) and the obtained reads were compared to the mouse genome (NCBI). Ca^{2+} signaling- and astrocytes-related genes were extracted and analyzed, including: TRPC, ORAI, STIM, ITPR, AMPA, KAR, NMDA, GRM and astrocyte markers (GFAP, GLAST and S100b) genes. TRPC1, TRPC2, TRPC3 and TRPC7 were detected while TRPC4, TRPC5 and TRPC6 had very low FPKM (Fragments Per Kilobase of transcript per Million mapped reads) values. TRPC1, TRPC2 and TRPC3 were detected

with both approaches i.e. RT-PCR and transcriptome, whereas TRPC4 in the transcriptome revealed low FPKM value and was detected 10 times from 13 RT-PCRs. Surprisingly, TRPC7 was never detected in RT-PCR (TRPC7 primers gave positive band in Figure 3-2) but in the transcriptome analysis it was the most expressed among the TRPCs, however, it is unclear yet the exact cause behind it.

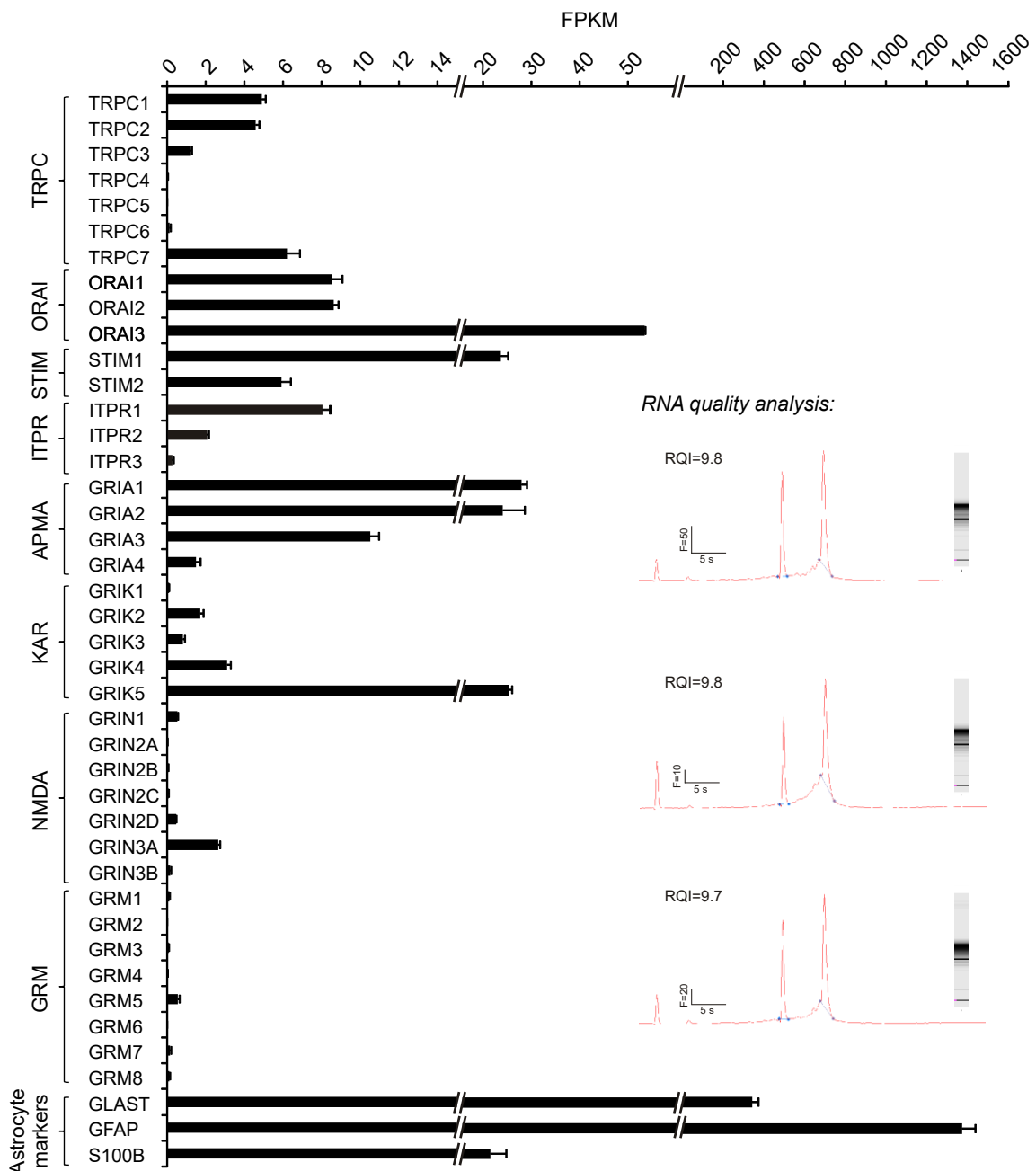


Figure 3-6 Transcriptome analysis of TRPCs in cultured cortical astrocytes. Bar graph representing transcriptome data, from the GLAST-sorted astrocytes RNA, of the TRPC, ORAI, STIM, ITPR, AMPA, KAR, NMDA, GRM and astrocyte markers. The values are expressed in FPKM (Fragments Per

Kilobase of transcript per Million mapped reads) as mean \pm SEM of three independent experiments from three independent cultures. The inset illustrates the RNA quality analysis of the three independent RNA samples from sorted astrocytes, showing the 18S and 28S peaks (red trace) and fragments, and RNA quality indicator (RQI) number.

3.5.3 Expression of TRPC3 and TRPC1 full length transcripts in GLAST-sorted astrocytes

The results from the RT-PCR showed that the TRPC3 transcripts are consistently amplified from GLAST-sorted astrocyte RNA. TRPC3 fragments were amplified in 13 of 13 PCRs. The amplified fragment comprises 198 bp. To provide the evidence that the full length transcript of 2733 bp is expressed, primers covering the full length TRPC3 transcript were employed. As template, the total RNA isolate from the GLAST-sorted astrocytes was reverse transcribed into cDNA. The full length of 2733 bp TRPC3 cDNA was amplified from the GLAST-sorted astrocytes (Figure 3-7-b). In addition the expression of TRPC1 full length cDNA in astrocytes was investigated. The TRPC1 fragments was identified in 10 out of 13 PCRs and it is shown to interact with TRPC3, TRPC4 and other TRP proteins (Storch et al., 2012). Laura Hofmann and Ulrich Wissenbach in our laboratory have found that the TRPC1 start codon is CUG which is actually 246 bp upstream of the AUG start codon which has been published (Wes et al., 1995; Zhu et al., 1995), leading to an extension of the amino terminus by 82 amino acids. Because of its extended length this variant of TRPC1 was called TRPC1 very long (VL). The primers used to amplify TRPC1 VL cover the TRPC1 sequence including the extension. The TRPC1 VL cDNA was amplified from the sorted astrocytes; the DNA fragment runs slightly lower than the 3000 bp marker which fits to the full length cDNA sequence of TRPC1 VL of 2880 bp (Figure 3-7-a). The coding sequence of TRPC1 VL is 2679 bp, however the used primers initiate the amplification 201 bp upstream the new start codon. Ong et al have also shown that TRPC1 starts from another start codon upstream the AUG, and they have also discovered a functional splice variant which lacks 21 nucleotides and an EcoRV restriction site; they called this variant TRPC1 ϵ (Ong et al., 2013). After having purified the amplified TRPC1 VL DNA (not subcloned), it was incubated with EcoRV and thereafter by agarose gel electrophoresis analyzed (Figure 3-7-c-d). Three DNA fragments of

2880, 1737 and 1143 bp were identified. Apparently, two variants are present in GLAST-sorted astrocytes; the TRPC1 ϵ (non-cut) and the TRPC1 VL (two bands at 1737 and 1143 bp).

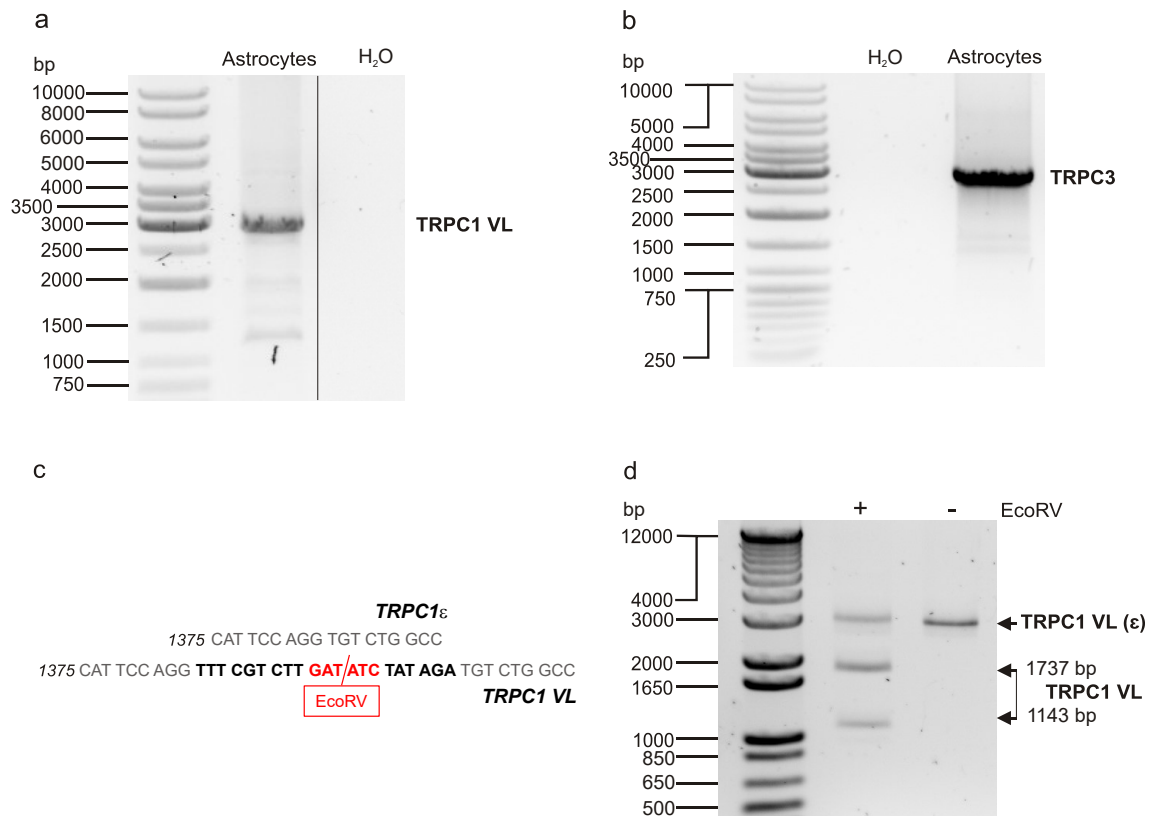


Figure 3-7 Full length amplification of TRPC3 and TRPC1 cDNAs from cultured and sorted astrocytes. Agarose gel showing TRPC1 VL (a) and TRPC3 (b) full length cDNAs amplified from GLAST-sorted astrocytes. (a) For TRPC1 VL, the amplified DNA is running between the marker DNA fragment of 2500 and 3000 bp and corresponds to the full length size of 2880 bp. (b) For TRPC3, the amplified DNA is running between the marker DNA of 2500 and 3000 bp and corresponds to the full length size of 2733 bp. (c) Sequences of TRPC1 VL with the 21 nucleotides (including the EcoRV restriction site) and absent in TRPC1 ϵ is shown in bold black. (d) Agarose gel showing the restriction cut of TRPC1 VL by EcoRV which resulted in three distinct fragments: the first between 2000 and 3000 bp corresponding to TRPC1 ϵ (non-cut), the second between 1650 and 2000 bp and the third between 1000 and 1650 bp corresponding to the 1737 and 1143 bp fragments of TRPC1 VL.

In the next step the full length TRPC3 and TRPC1 VL cDNAs were excised from the gels purified and subcloned into pUC19. After transformation of *E. coli*, positive colonies were picked; DNA was extracted and analyzed by restriction enzymes (Figure 3-8). XbaI and PshAI cut of the TRPC3 cDNA should give two

bands running at 1729 bp and 3690 bp for sense orientation, or 1022 bp and 4397 bp for antisense orientation. Twelve clones were analyzed and all of them yield two fragments and the higher one is between 3500 and 4000 bp (3690 bp). However, clones number 5, 6 and 10 have lower bands running far below the 1500 bp DNA marker whereas the rest of clones have the second band running at 1729 bp. This suggests that clones 1-4, 7-9, 11 and 12 are correct whereas clones 5, 6 and 10 could be splice variants (Figure 3-8-b). Clones 5 to 10 were send for sequencing on both strands: The sequences of clone 7, 8 and 9 did correspond to the DNA sequence of mouse TRPC3. Clone 5 consists of only the 5' sequence, clone 6 lacks the last part of the 3' sequence and clone 10 lacks the sequence encoding transmembrane domains 2, 3, 4 and part of 5. For TRPC1 VL, KpnI and XhoI enzymes were employed which, in the case of sense insertion, should generate two distinct fragments of 3078 and 2488 bp, and 5174 and 392 bp in the case of the antisense insertion. Clones 1, 2, 3, 6, 7 and 8 were sequenced and only clone 2 corresponds to the TRPC1 VL. All other clones (1, 3, 6, 7 and 8) lacked exon 3; in addition clones 1, 7 and 8 lacked the 21 bp containing the EcoRV site. In summary and according to the sequence data these full-length TRPC1 cDNA were isolated, cloned and sequenced: TRPC1 VL, TRPC1 VL Δ exon3 and TRPC ϵ Δ exon3 (Figure 3-8-a).

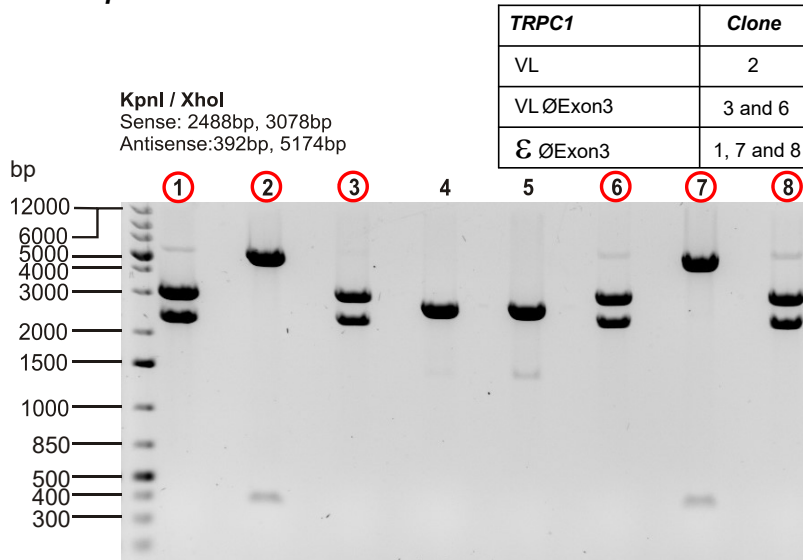
a Independent TRPC1 cDNA clones**b Independent TRPC3 cDNA clones**

Figure 3-8 Restriction analysis of the TRPC1 VL and TRPC3 full length cDNAs in pUC19. (a) Agarose gel showing analysis of 8 clones from TRPC1 VL in pUC19 digested with KpnI and XhoI. Clones 1, 3, 6 and 8 show two bands which correspond to the fragments obtained from clones in the sense orientation. Clone 2 and 7 also show two bands that have an upper one running at less around 5000 bp and a lower one running at around 400 bp which correspond to the antisense cut that should result in two bands at 5174 and 392 bp. (b) Agarose gel showing analysis of 12 TRPC3 in pUC19 digested with XbaI and PshAI. All clones two fragments have been identified that have an upper one running at less than 4000 bp and a lower one (except clone 5, 6 and 10) running between 1500 and 2000 bp which correspond to the sense orientation. Clone 5, 6 and 10 had the second lower band running below 1500 bp. Tables in a and b illustrate the summary of sequencing results from TRPC1 VL and TRPC3 cDNA.

3.6 TRPC3 in cultured cortical astrocytes

3.6.1 Role of TRPC3 in astrocytes

When the intracellular Ca^{2+} stores of the endoplasmic reticulum (ER) are depleted by IP₃-induced Ca^{2+} release, ER STIM proteins assemble, and interact with the plasma membrane Ca^{2+} channels ORAI; these channels open and allow Ca^{2+} influx into the cell. Then the SERCA pump in the membrane of the ER pumps Ca^{2+} back into the ER. Blockers of the SERCA pump, such as thapsigargin (TG) or cyclopiazonic acid (CPA) prevent the SERCA activity. Because there is a continuous Ca^{2+} leak from the ER into the cytoplasm which is counteracted by consistent Ca^{2+} uptake via the SERCA pump. This results in the depletion of the ER- Ca^{2+} stores independently of IP₃, and thereby ORAI channels will be activated as described above. To monitor the cytoplasmic Ca^{2+} changes in astrocytes, Fura-2 was used as an indicator of Ca^{2+} concentration: The Fura-2 F340/F380 ratio is proportional to the Ca^{2+} concentration in the cytoplasm. After applying 2 μM of the SERCA pump blocker thapsigargin in the absence of extracellular Ca^{2+} an increase in the intracellular $[\text{Ca}^{2+}]$ was observed that is caused by Ca^{2+} leakage from the ER into the cytoplasm. This $[\text{Ca}^{2+}]$ decreased overtime because of its transport out of the cell by other pumps and exchangers. Upon readdition of extracellular Ca^{2+} , the $[\text{Ca}^{2+}]$ increased because of the Ca^{2+} influx through ORAI channels (Figure 3-9-a). The fluorescence ratio decreased over time to reach a steady state but does not go back to the basic value because the continuous inhibition of the SERCA pump which in turn keeps the ORAI channels in an active state. In addition to ORAI (Feske et al., 2006), members of the TRPC channel subfamily have been suggested to contribute to the Ca^{2+} entry (Venkatachalam et al., 2002). Because cultured mouse cortical astrocytes express the TRPC3 gene, TRPC3 could contribute to this Ca^{2+} entry. Therefore astrocytes from wild-type and from mice deficient in TRPC3 and TRPC6 genes were used in the following experiment (Figure 3-9). The depletion of the ER Ca^{2+} stores by thapsigargin in the absence of extracellular Ca^{2+} leads to increase of Ca^{2+} in the cytoplasm. When extracellular Ca^{2+} was readded (5 mM) Ca^{2+} entry occurs which was not different in astrocytes from wild-type or TRPC3/TRPC6 deficient mice. These

results suggest that TRPC3 and TRPC6 are not involved in Ca^{2+} entry by this pathway (Figure 3-9 a c).

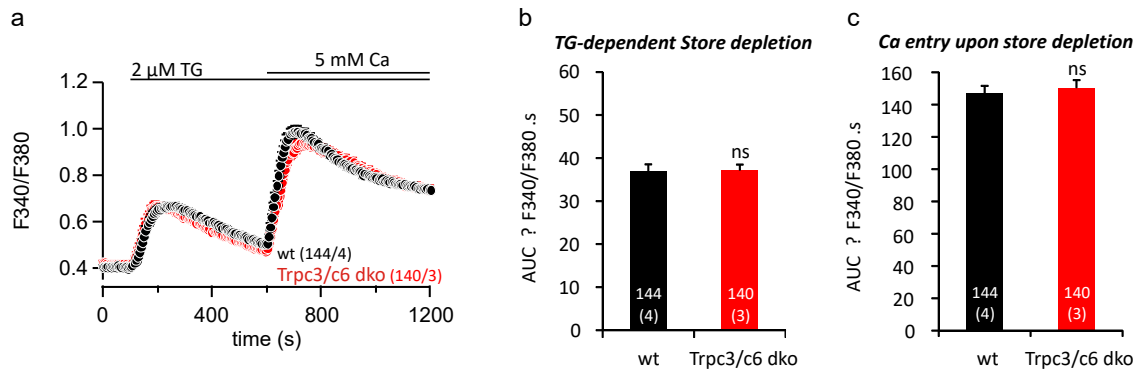


Figure 3-9 Ca^{2+} entry in cultured cortical astrocytes from wild-type and TRPC3/C6 gene-deficient mice. (a) Fura-2 experiments showing changes in the cytoplasmic Ca^{2+} concentration as changes of F340/F380 ratio. In the absence of extracellular Ca^{2+} , 2 μM thapsigargin was applied to deplete the ER by blocking the SERCA pump. Readdition of 5 mM Ca^{2+} provokes an increase in the Ca^{2+} signal which is due to Ca^{2+} entry in wild-type astrocytes (black). Astrocytes from TRPC3/TRPC6 gene-deficient mice (red) did behave in the same manner as the wild-type cells and showed no difference in terms of response to TG or Ca^{2+} readdition. Summary: Area under the curves of the store depletion (100 s to 500 s) (b) and Ca^{2+} entry (500 s to 1200 s) (c) from both genotypes show no significant differences. Results represent mean \pm SEM from four (wt) and three (TRPC3/C6 dko) independent measurement with 144 and 140 cells respectively (ns = not significant).

3.6.2 OAG-induced Ca^{2+} release and Ca^{2+} Influx in cultured astrocytes

TRPC channels have been shown to be activated downstream of PLC activation which involves the generation of diacylglycerole (DAG) and inositol 1,4,5-triphosphate (IP₃). TRPC2, TRPC3, TRPC6 and TRPC7 are activated by DAG leading to Ca^{2+} and sodium influx (Hofmann et al., 2000). OAG, an analogue of DAG, can be used experimentally to activate the DAG-sensitive TRPCs. The application of 100 μM OAG in the presence of 2 mM extracellular Ca^{2+} on astrocytes induced Ca^{2+} oscillations measured by Fura-2, but no Ca^{2+} signal was observed in microglia (Figure 3-10-a-b). However when the extracellular Ca^{2+} was removed, the astrocytes did still exhibit Ca^{2+} oscillation which were obviously generated from intracellular Ca^{2+} stores, as the readdition

of Ca^{2+} in absence of OAG led to steep increase in Ca^{2+} signal (Figure 3-10-c). Hisatsune et al., showed that OAG can also activate PLC and thereby leads to IP3 production which in turns induces Ca^{2+} release from the ER (Hisatsune et al., 2005). The observed Ca^{2+} oscillation in the absence of extracellular Ca^{2+} might be caused by the activation of PLC in the presence of OAG which makes it difficult to distinguish whether OAG is able to induce any Ca^{2+} influx via TRPC channels in astrocytes. Therefore, a separation of Ca^{2+} influx into the cytoplasm from the extracellular space and the ER Ca^{2+} release is necessary to investigate whether TRPCs are involved in OAG-induced Ca^{2+} signaling in astrocytes. In order to separate the Ca^{2+} influx from the Ca^{2+} release induced by OAG, the SERCA pump inhibitor cyclopiazonic acid (CPA) was used at a concentration of 10 μM in the presence of 2 mM extracellular Ca^{2+} to deplete the internal stores and induce a steady state Ca^{2+} entry. At this stage the IP3 will not be able to induce any further Ca^{2+} release. On top of this protocol, 100 μM of OAG was applied to directly activate TRPC channels (Figure 3-10-d). Since the internal stores were already depleted and Ca^{2+} entry through ORAI reached a steady state, the additional increase of cytoplasmic Ca^{2+} (Figure 3-10-d) is most probably mediated by Ca^{2+} influx via Ca^{2+} channels activated by OAG. OAG is well known as activator of protein kinase C (PKC) (Nishizuka, 1984) as well as of MUCK 13 (Brose and Rosenmund, 2002), which imposes the question, whether the observed additional Ca^{2+} influx in astrocytes upon OAG application is mediated via PKC which subsequently activate a Ca^{2+} channel in the membrane or by direct channel activation. Phorbol-12-myristat-13-acetat (PMA) was used instead of OAG and did not induce any additional Ca^{2+} signal (Figure 3-10-e), which indicates that the OAG-induced Ca^{2+} influx in astrocytes is PKC- and MUN 13-independent. The next experiments were done to answer the question whether channel activated by OAG in the above protocol is TRPC3.

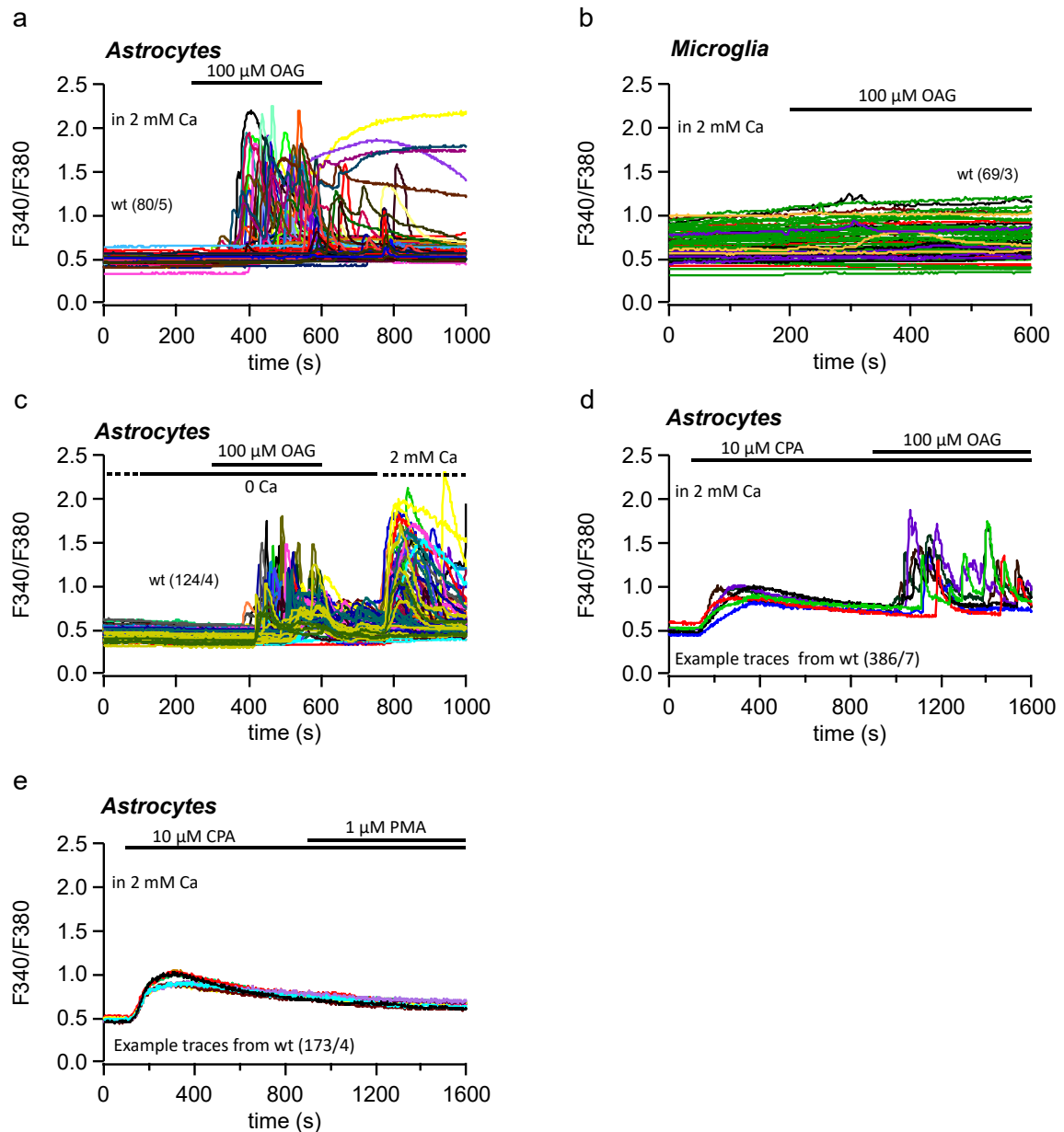


Figure 3-10 OAG-induced Ca^{2+} release and Ca^{2+} influx in astrocytes from wild-type mice. (a) The application of 100 μ M OAG in the presence of 2 mM extracellular Ca^{2+} induces Ca^{2+} oscillations in astrocytes but not in microglia (b) measured by Fura-2. (c) In the absence of extracellular Ca^{2+} , 100 μ M OAG induces also Ca^{2+} oscillations but the amplitude and frequency of peaks were notably less comparing to the experiment in the presence of extracellular Ca^{2+} . (d,e) In the presence of 2 mM extracellular Ca^{2+} , Ca^{2+} release and Ca^{2+} entry are induced in the presence of CPA. Adding OAG on top (d) leads to additional Ca^{2+} oscillations; these oscillations do not occur if PMA is added instead (e). Figure a, b and c show numbers of measured cells per number of experiments, and figure d and e show example traces from 386/7 and 173/4 wild-type astrocytes, respectively.

3.6.3 OAG-induced Ca^{2+} influx is TRPC3-dependent

As shown in the previous section, OAG increases the astrocytic cytoplasmic Ca^{2+} concentration by Ca^{2+} influx. This is probably due to the activation of DAG-sensitive TRPC channels. By PCR, TRPC2 and TRPC3 transcripts were amplified from the GLAST-sorted astrocytes; however TRPC7 was only detected in the RNA sequencing analysis and not in RT-PCR. Thus those channels could be the candidate channels responsible for the OAG-mediated Ca^{2+} influx. I used astrocytes from TRPC channel gene-deficient mice to investigate their contribution in the OAG-induced Ca^{2+} influx. Astrocytes isolated from wild-type, TRPC3-, TRPC6- and TRPC3/TRPC6 gene-deficient mice were used in the following experiments (Figure 3-11). The deletion of the TRPC3 gene resulted in a significant decrease by about 30% in the number of OAG-responding astrocytes when compared to wild-type astrocytes in which around 85% of the cells did respond to OAG (Figure 3-11-a-b-e). However, even within the OAG-responding astrocytes from TRPC3 gene-deficient mice the oscillation frequency was significantly reduced to 1.5 oscillations per cell compared to around 3.5 oscillations per astrocytes from wild-type mice within the 700 s of OAG application (Figure 3-11-a-b-f). Despite the fact that TRPC6 transcripts were not identified in the GLAST-sorted astrocytes, astrocytes from TRPC6 gene-deficient mice were also tested for their OAG response. As expected, those astrocytes isolated from TRPC6 gene-deficient mice did not show any difference in the OAG response when compared to wild-type astrocytes neither in the number of responding cells nor in the oscillation frequency (Figure 3-11-a-c-e-f). On the other hand, the astrocytes originating from TRPC3/TRPC6 gene-deficient mice show similar response to OAG as in the astrocytes isolated from TRPC3 gene-deficient mice in terms of responding cell number and oscillation frequency (Figure 3-11-b-d-e-f). These results show that cultured cortical astrocytes do exhibit a functional TRPC3 channels.

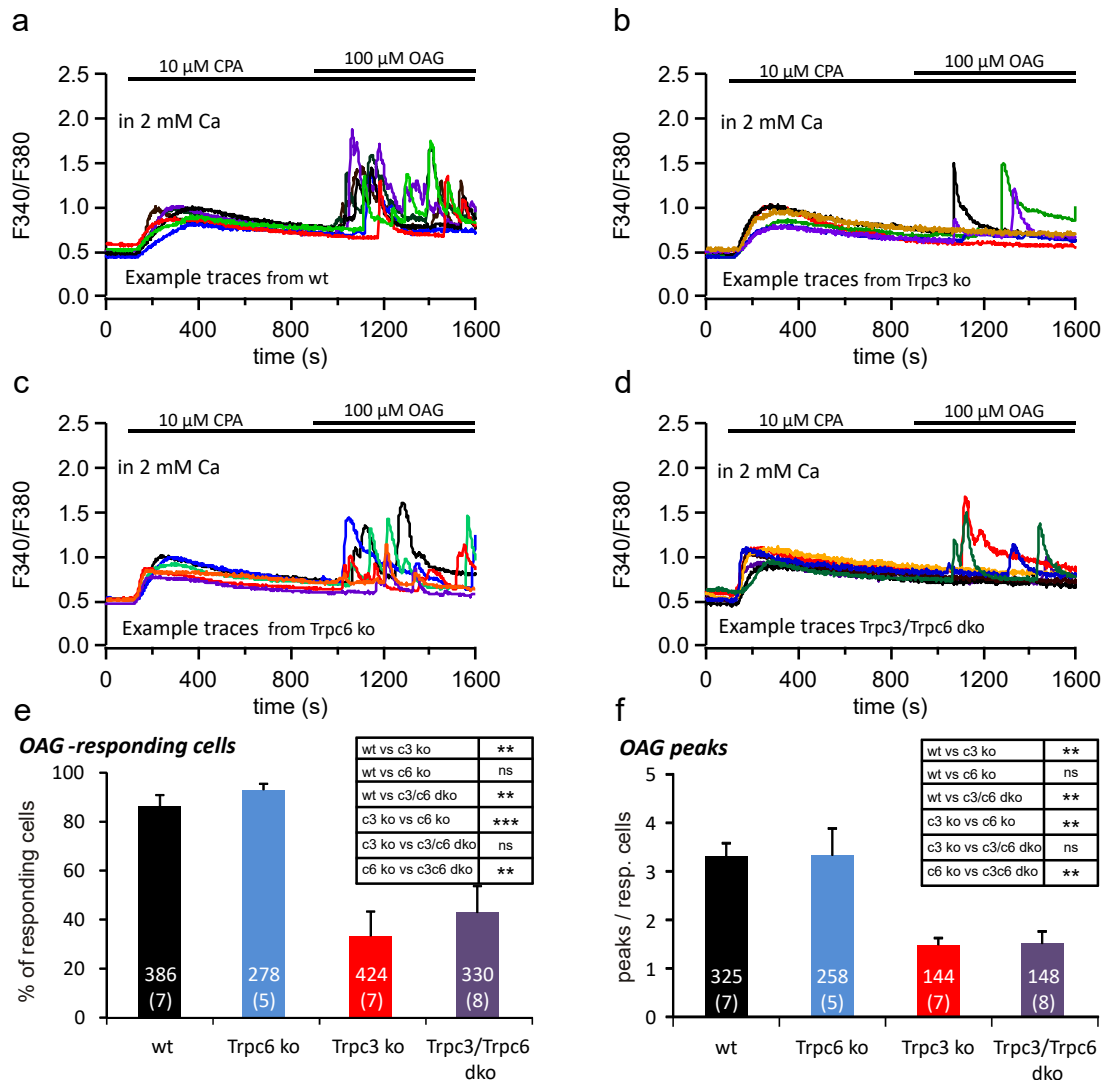


Figure 3-11 OAG-Induced Ca^{2+} oscillations in astrocytes are mediated via TRPC3. (a, b, c and d) In the presence of 2 mM extracellular Ca^{2+} , Ca^{2+} release and Ca^{2+} entry are induced in the presence of CPA and OAG was additionally applied. 100 μM OAG, on top of CPA, induced Ca^{2+} oscillations in astrocytes isolated from wild-type (a, same as in Figure 3-10-d), TRPC3- (b), TRPC6- (c) and TRPC3/C6 gene-deficient (d) mice. (e) Summary of the number of OAG responding cells shows that only 30% of astrocytes from TRPC3 gene-deficient (red) and TRPC3/TRPC6 gene-deficient (violet) mice did respond to OAG application while 85% of astrocytes responded in wild-type (black) and TRPC6 gene-deficient (blue). (f) Summary of the number of oscillations per cell within the 700 s of OAG application shows that astrocytes from TRPC3 gene-deficient (red) and TRPC3/TRPC6 gene-deficient (violet) mice exhibited 1.5 oscillations per cell while astrocytes obtained from wild-type (black) and TRPC6 gene-deficient (blue) mice revealed around 3.5 oscillations per OAG-responding cell. Figure a, b, c and d show example traces, and e and f show mean \pm SEM (number of cells/number of experiments) of the percentage of OAG-responding cells and number of OAG peaks respectively from wild-type (386/7), TRPC6-

(278/5), TRPC3- (424/7) and TRPC3/TRPC6 gene-deficient (330/8) astrocytes. Tables in figure e and f reveal the statistical comparison between the different genotypes using one way ANOVA followed by Bonferroni test (** for p value ≤ 0.01 , *** for p value ≤ 0.001 and ns for non-significant).

3.6.4 Electrophysiological characterization of TRPC3 current in TRPC3 cDNA expressing HEK293 cells

TRPC3 is a non-selective cation channel which is permeable to Ca^{2+} and sodium. The activation of TRPC3 can be measured as a current by whole cell patch clamp technique. A voltage ramp from -100 mV to 100 mV during 400 ms was applied every 2 s from a holding potential (V_h) of 0 mV (Figure 3-12-a). External application of 100 μM OAG was used to activate TRPC3 in a HEK 293 cell line stably expressing the human TRPC3 cDNA. Using 1 mM Ca^{2+} in the extracellular solution and 100 nM free Ca^{2+} in the patch pipette induced only very small whole cell currents during the application of 100 μM OAG (Figure 3-12-b-c-d). Several Ca^{2+} channels are known to inactivate in the presence of Ca^{2+} such as voltage-gated Ca^{2+} channels or the TRPV6 channel (Niemeyer and Lummis, 2001). Therefore, intra- and extracellular Ca^{2+} concentrations were changed in the whole cell patch clamp experiments to optimize the condition for TRPC3 current recording. First, the extracellular Ca^{2+} was removed (nominally Ca^{2+} -free) and the intracellular (pipette) Ca^{2+} was kept at 100 nM (buffered with BAPTA). When OAG was applied no obvious increase in the current amplitude occurred comparing with the previous condition (1 mM / 100 nM Ca^{2+}). However, in the presence of 1 mM extracellular Ca^{2+} and buffering the intracellular Ca^{2+} to zero (1 mM / 0 Ca^{2+}), outward and inward currents with a similar current-voltage relationship as the published for TRPC3 currents were induced in the presence of 100 μM OAG. Interestingly, when both the extra- and intracellular Ca^{2+} were removed (0 mM/ 0 nM), OAG did induce even a Larger current compared to the previous condition (Figure 3-12-b-c-d). These results strongly suggest that TRPC3 is a Ca^{2+} sensitive channel that could be inhibited by either intracellular and/or extracellular Ca^{2+} .

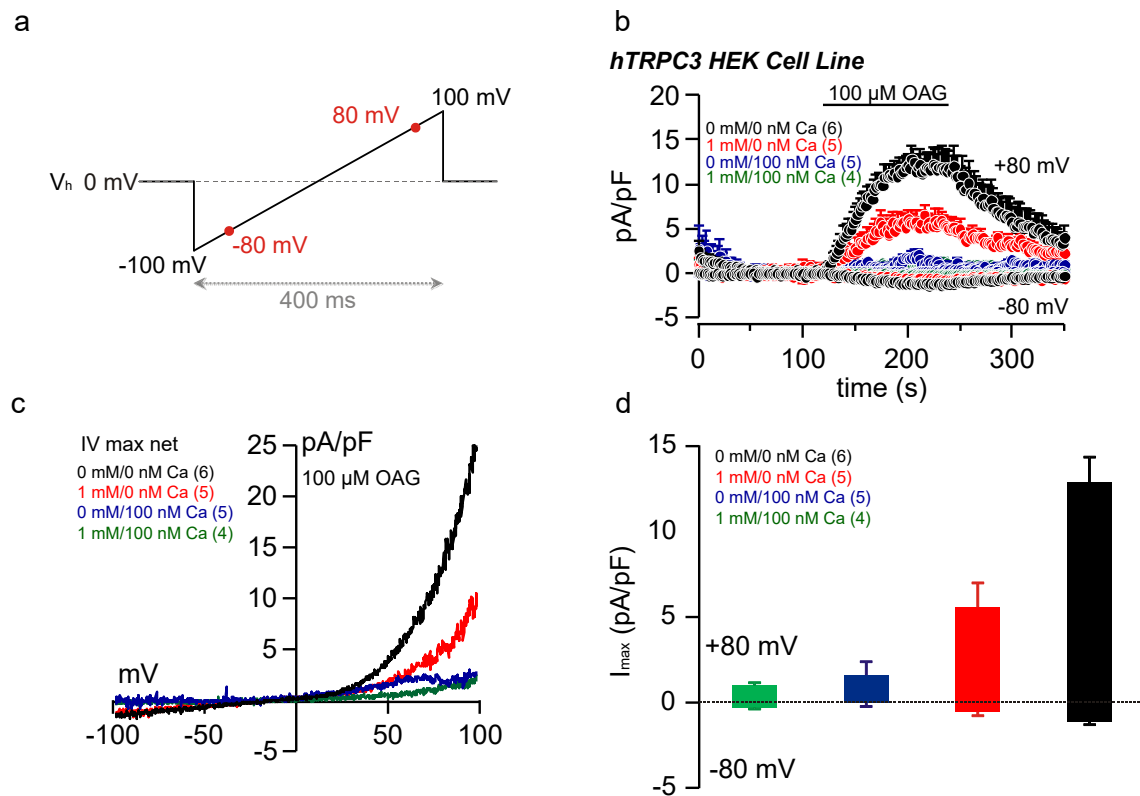


Figure 3-12 **TRPC3 currents in TRPC3 cDNA expressing HEK293 cells.** (a) Voltage ramp protocol used to measure TRPC3 currents. Voltage ramps were applied every 2 s over a duration of 400 ms from -100 to 100 mV from a holding potential of 0 mV. (b) Currents at -80 and 80 mV and plotted versus time showing the current (pA/pF) before, during and after OAG application after subtracting the basic current i.e. current before application. (c) Current-voltage relationships were extracted from the maximum current during OAG application after subtracting the basic current. (d) Summary of the I_{max} at -80 and 80 mV during application of 100 μM OAG showing the Ca²⁺ dependent inhibition of TRPC3 currents at different Ca²⁺ concentrations (external/internal): 1 mM / 100 nM (green), 0 mM / 100 nM (blue), 1 mM / 0 nM (red) and 0 mM / 0 nM (black). Figure b and d are mean \pm SEM of the indicated number of measured cells.

3.6.5 TRPC3 currents in cultured mouse cortical astrocytes

As shown in Figure 3-11, OAG activates TRPC3-dependent Ca²⁺ entry measured by Fura-2. Now, the optimized patch clamp conditions were employed to measure the native TRPC3 currents in astrocytes. However, the amount of the TRPC3 protein in astrocytes is expected to be much less as compared to HEK293 cells expressing TRPC3 cDNA, and therefore the TRPC3 currents could be much smaller. For this reason, 300 μM OAG was used instead of 100 μM OAG to increase the chance to measure the native TRPC3

currents in astrocytes. Under this condition, OAG induced inward and outward currents in astrocytes and the current-voltage relationship (Figure 3-13-b) was very similar to the one of TRPC3 currents in HEK293 cells (Figure 3-12-c). Although the current is very small and only in few cells responded to OAG, this further proves that TRPC3 is a functional channel in astrocytes. Because of the low success rate, comparison with astrocytes from TRPC3 gene-deficient mice was not performed.

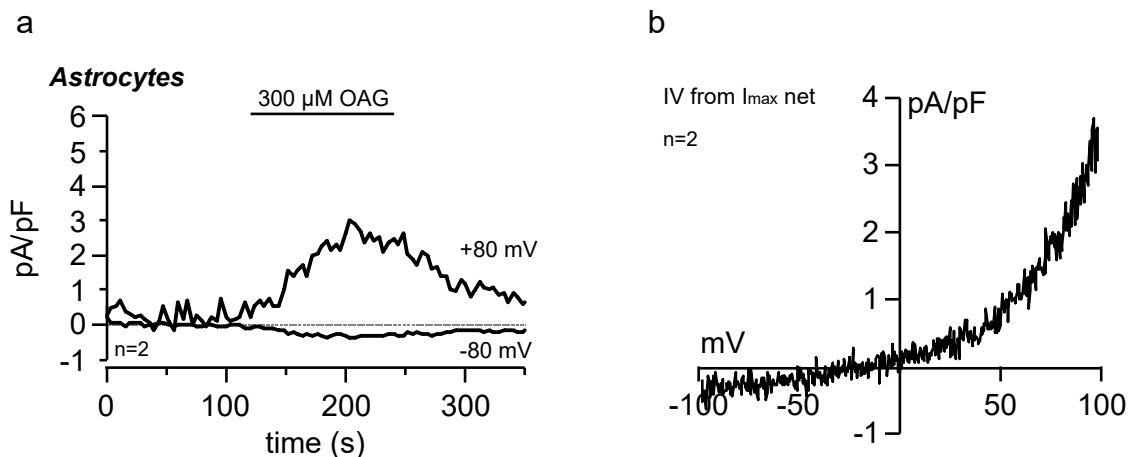


Figure 3-13 **TRPC3 currents in astrocytes.** (a) Currents measured in astrocytes extracted at -80 and 80 mV and plotted versus time. The application of 300 μ M OAG led to the development of inward and outward currents in astrocyte. (b) The current-voltage relationships of the maximum current during the application of 300 μ M OAG exhibit a similar shape as the one for TRPC3 currents in HEK293 cells.

Expression analysis, Ca^{2+} imaging and patch clamp experiment provide clear evidence that TRPC3 is functionally expressed in cultured mouse cortical astrocytes. In response to brain injury, astrocytes become reactive and experience increased proliferation and migration (Fawcett and Asher, 1999). Ca^{2+} has been always linked to cellular migration and was shown to be involved in the astrocytic migration (Striedinger and Scemes, 2008). In the following experiment, role of TRPC3 in astrocyte migration will be addressed.

3.6.6 Role of TRPC3 in astrocytes migration

The so called scratch or *in vitro* wound healing assay is an assay which is used to mimic an injury on cultured cells and learn how cells migrate in culture. Astrocytes isolated from wild-type and different TRPC gene-deficient mice were

transferred into a 6 well plate and cultured until reaching confluency. Afterward, the cell monolayer was scratched with a 200 µl pipette tip and pictures were taken at 0, 4, 8 and 24 hours after the scratch from the same region. After scratching, the culture medium was substituted with an FCS-free medium to avoid cell proliferation. Migration was quantified by measuring the area of scratch re-covered by migrated cells again at 4, 8 and 24 h, which was normalized to the size of the scratch area at 0 hour. 4 hours after the scratch, about 10% of all the scratch area was occupied again by astrocytes isolated from wild-type mice but only 5% coverage was observed in astrocytes from TRPC3 gene-deficient mice. After 8 hours, about 18% of the scratch was covered with astrocytes from wild-type mice, and 7% of the scratch was covered in astrocytes from TRPC3 gene-deficient mice. At 24 hours, 30% coverage was observed in wild-type astrocytes, while astrocytes from TRPC3 gene-deficient mice covered only 18% of the total scratch area after 24 hours. This suggests that TRPC3 and/or Ca^{2+} influx via TRPC3 plays a role in the astrocytic migration. In the Fura-2 experiment, astrocytes from TRPC6 gene-deficient mice behaved similarly to the wild-type and cells isolated from TRPC3/TRPC6 gene-deficient did behave like the TRPC3 gene-deficient. Therefore, astrocytes were isolated from TRPC6 and TRPC3/TRPC6 gene-deficient mice and used for migration assay. As expected, the migration rate of astrocytes isolated from TRPC6 gene-deficient mice did not differ from the one of wild-type astrocytes after 4, 8 and 24 hours, while the astrocytes from TRPC3/TRPC6 gene-deficient mice were very similar to the astrocytes from TRPC3 gene-deficient mice after 4, 8 and 24 hours (Figure 3-14). Those results prove the role of TRPC3 in the *in vitro* migration of cortical astrocytes.

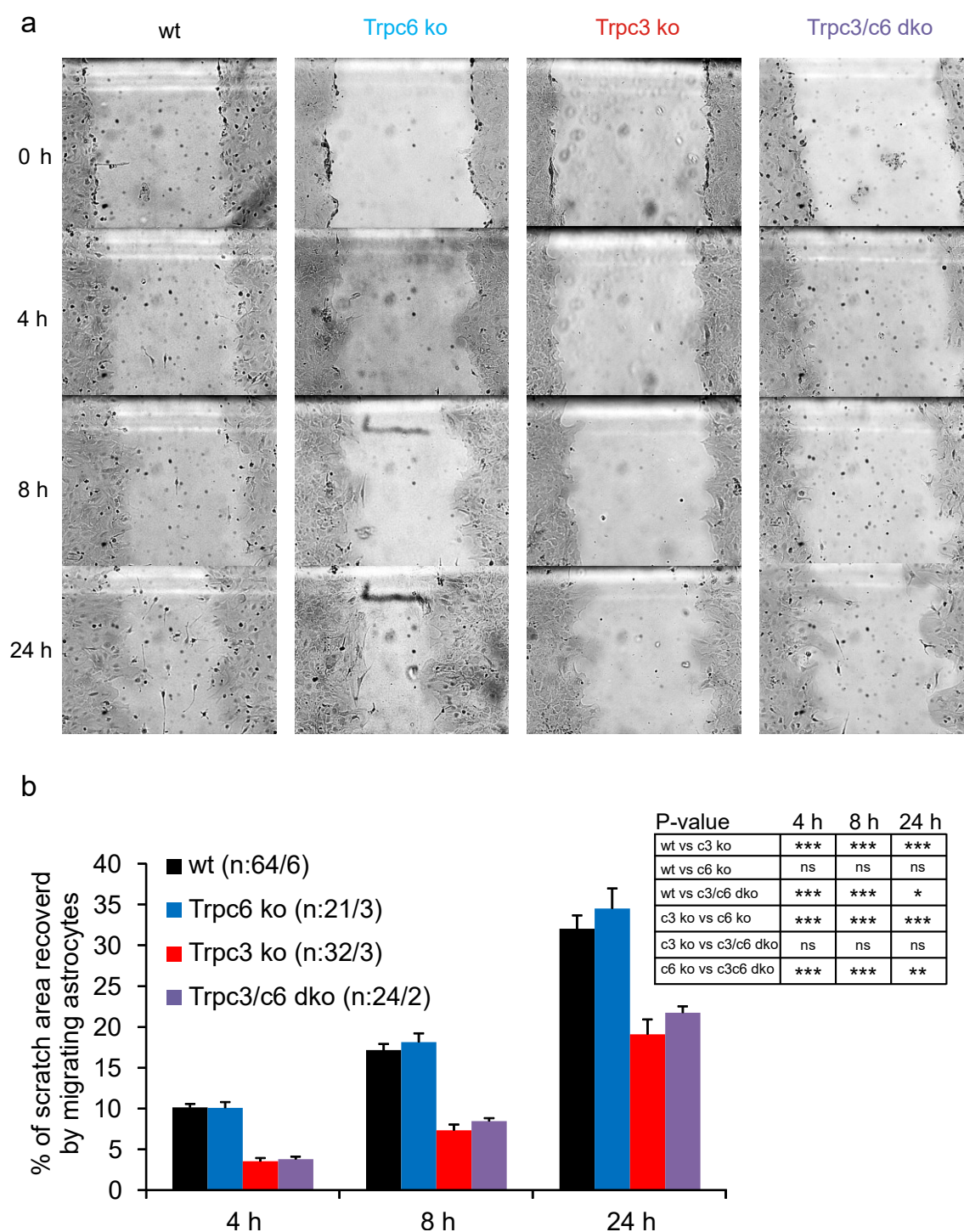


Figure 3-14 **Astrocytes migration *in vitro***. (a) Representative images of the astrocytes at 0 and 4, 8 and 24 hours after scratch from wild-type, TRPC3-, TRPC6- and TRPC3/TRPC6 gene-deficient mice. (b) Summary of the migration data. Scratch area at time "0" is 100%; area recovered by migrating astrocytes after 4, 8 and 24 h are indicated. Different colors are used for each genotype as indicated. Data represent mean \pm SEM of the indicated number of scratches from number of experiments (scratches/experiments) and table in figure b reveals the summary of the different genotypes statistical comparison (*, p value ≤ 0.05 , **, p value ≤ 0.01 , ***, p value ≤ 0.001 and ns for non-significant).

The previous experiment showed how the deletion of TRPC3 gene affected negatively the *in vitro* migration of astrocytes; which is more pronounced in the astrogliosis state. Thus in the following experiment, the role of TRPC3 in the *in vivo* migration and glial scar formation will be investigated.

3.6.7 Astrogliosis and glial scar formation in TRPC3 gene-deficient mice

In response to brain injury, astrocytes enter into a reactive state leading to the formation of the glial scar which involves excessive proliferation and migration of astrocytes into the injury site (Saadoun et al., 2005; Silver and Miller, 2004). This reactive state leads to the upregulation of the GFAP gene, and thus the GFAP protein is used as an indicator for astrogliosis. Experimentally, cortical stab wound surgery is used as a model to study the astrogliosis and glial scar formation after brain injury. In this work wild-type and TRPC3 gene-deficient male mice (8 weeks old) were used to address the role of TRPC3 in astrogliosis and glial scar formation. The surgery was performed under anesthesia on the right hemisphere of the cerebral cortex and both genotypes (wild-type and TRPC3 gene-deficient mice) were used in parallel. 3 days after the surgery mice were sacrificed and fixed with 4% PFA and 35 μm coronal sections were made from the injured region and stained against GFAP (Figure 3-15-a). The analysis of the wound images showed that the absence of TRPC3 led to a significant decrease in the GFAP positive area 2.5 mm^2 compared to 3.2 mm^2 in wild-type mice (Figure 3-15-b). This result shows that astrogliosis is less pronounced in TRPC3 gene-deficient mice. This was confirmed by the analysis of the fluorescence intensity in which the fluorescence intensity of the anti-GFAP antibody bond was measured from equally sized rectangles placed along the injured and non-injured cortex (Figure 3-15-c inset). The results of this analysis showed that in the non-injured hemisphere there was no significant difference in the GFAP-fluorescence intensity between TRPC3 gene-deficient and wild-type mice. However on the injured hemisphere, TRPC3 gene-deficient mice exhibited significant reduction in the GFAP-fluorescence intensity when compared to the wild-type mice. Even more, the width of the GFAP staining (i.e. distribution of GFAP staining along the cortex) was much smaller in the TRPC3 gene-deficient mice compared to the wild-type (Figure 3-15-c). Like in any other

injury, an edema was observed in the injured cerebral cortex and was quantified by measuring the cortex width of the injured hemisphere and normalized to the contralateral side. The TRPC3 gene-deficient mice showed after cortical stab injury an increase of about 5% in the cortex size which was significantly smaller when compared to the wild-type mice where they had an increase of about 12% in the cortex size after brain injury (Figure 3-15-d). This result indicates that TRPC3 plays a role in the reactivity of astrocytes as well as in the inflammatory reaction following brain injury.

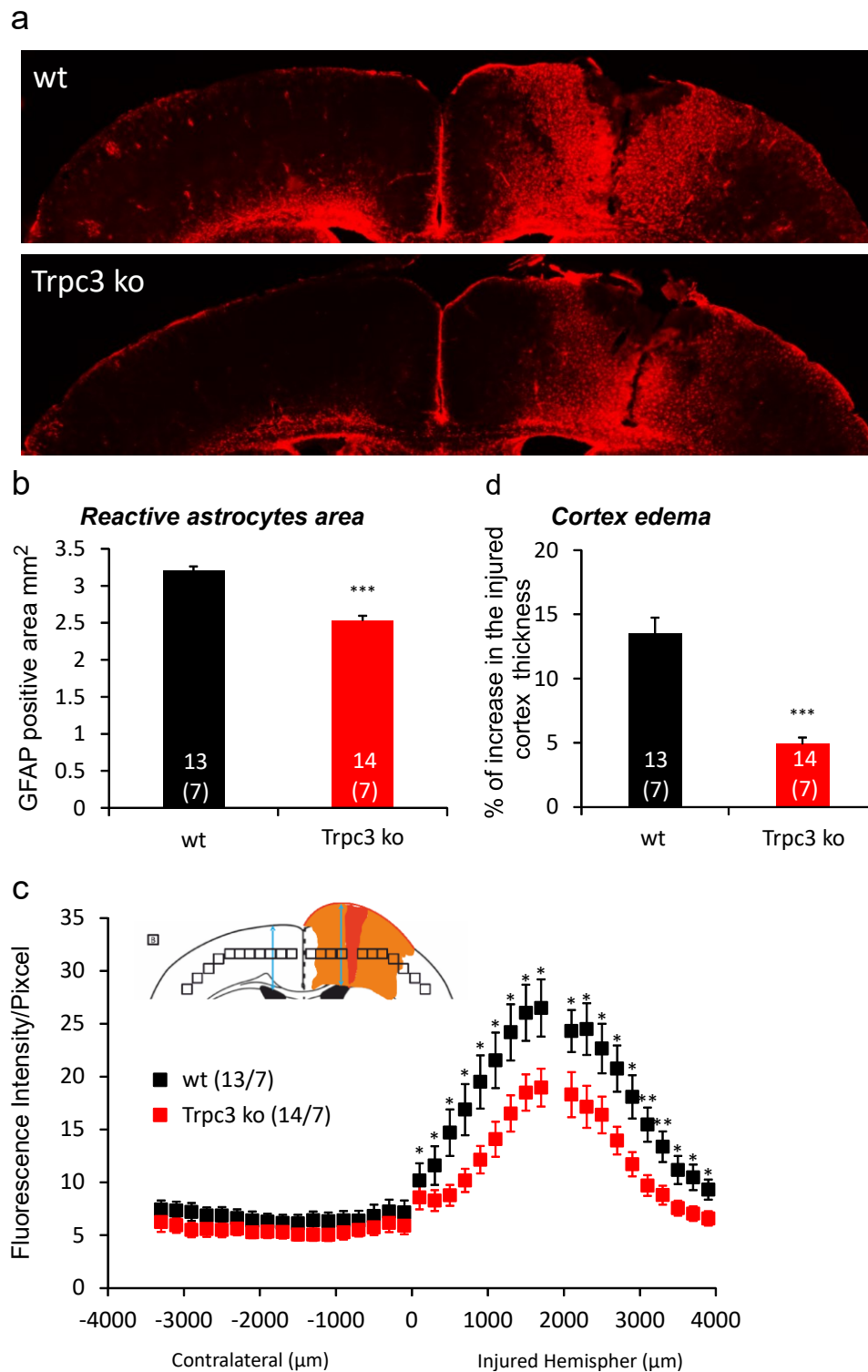


Figure 3-15 Cortical stab wound. (a) Example images of the cortical stab injury from wild-type and TRPC3 gene-deficient mice as 35 μm sections stained anti-GFAP antibody to visualize the reactive astrocytes. (b) Summary of the area of reactive astrocytes (in mm^2) showing significant smaller area of GFAP staining in TRPC3 gene-deficient mice (red) compared to wild-type (black). (d) Analysis of the cortical edema after brain injury measured from the cortical width where the TRPC3 gene-deficient mice had less cortical edema compared

to wild-type mice. (c) Diagram showing the distribution of the reactive astrocytes obtained (inset) from measuring the anti-GFAP fluorescence intensities of rectangles along the cortex. Data shows again the TRPC3 gene-deficient mice had less intensity and distribution of astrocytes compared to wild-type. Data represent mean \pm SEM from 7 wild-type mice (13 sections) and TRPC3 gene-deficient mice (14 sections) (* for p value ≤ 0.05 , and *** for p value ≤ 0.001).

3.7 TRPC3 T to A mutation and moonwalker mice (MWK)

3.7.1 Expression of the TRPC3 MWK mutant cDNA in HEK 293 cells

As already described in the introduction and material and methods (sections 1.6.3 and 2.3), I refer to the TRPC3 A1903G mutation, which is a TRPC3 gain of function mutation, as TRPC3 MWK in this study. The overexpression of the TRPC3 MWK cDNA in HEK 293 cells lead to cell death (observed in our laboratory) due probably to the increase of the cytoplasmic Ca^{2+} concentrations to a level beyond the cellular counterregulatory mechanisms. Therefore, a HEK cell line was generated in which the expression of TRPC3 MWK cDNA is induced in the presence of tetracycline (see section 2.3). Already 2 hours after induction by 1 $\mu\text{g/ml}$ tetracycline, currents could be measured in whole cell patch clamp experiments upon break-in using the same ionic conditions than outlined in (Figure 3-12). The outward current at 80 mV after break-in was ~ 20 pA/pF (Figure 3-16-a-b inset) and currents kept increasing over time reaching ~ 60 pA/pF after 150 seconds (Figure 3-16-a-b). The current-voltage relationship shows an inward and an outward current which has some similarity with the one of wild-type TRPC3 (Figure 3-12) and the shape of the current did not change over time (Figure 3-16-b). In Fura-2 experiments (Figure 3-16-c), the readdition of 2 mM Ca^{2+} induced an increase in the F340/F380 ratio already 2 hours after induction of TRPC3 MWK cDNA expression also indicating that the mutation rendered the TRPC3 open (Figure 3-16-c). The previous experiments were performed 2 hours after tetracycline treatment, however increasing the time after tetracycline addition led to a strong decrease in the number of surviving cells to about 70% after 6

hours (observed during Fura-2 measurement), indicating that the cells dye due to the constitutive Ca^{2+} influx and Ca^{2+} overload (Figure 3-16-d).

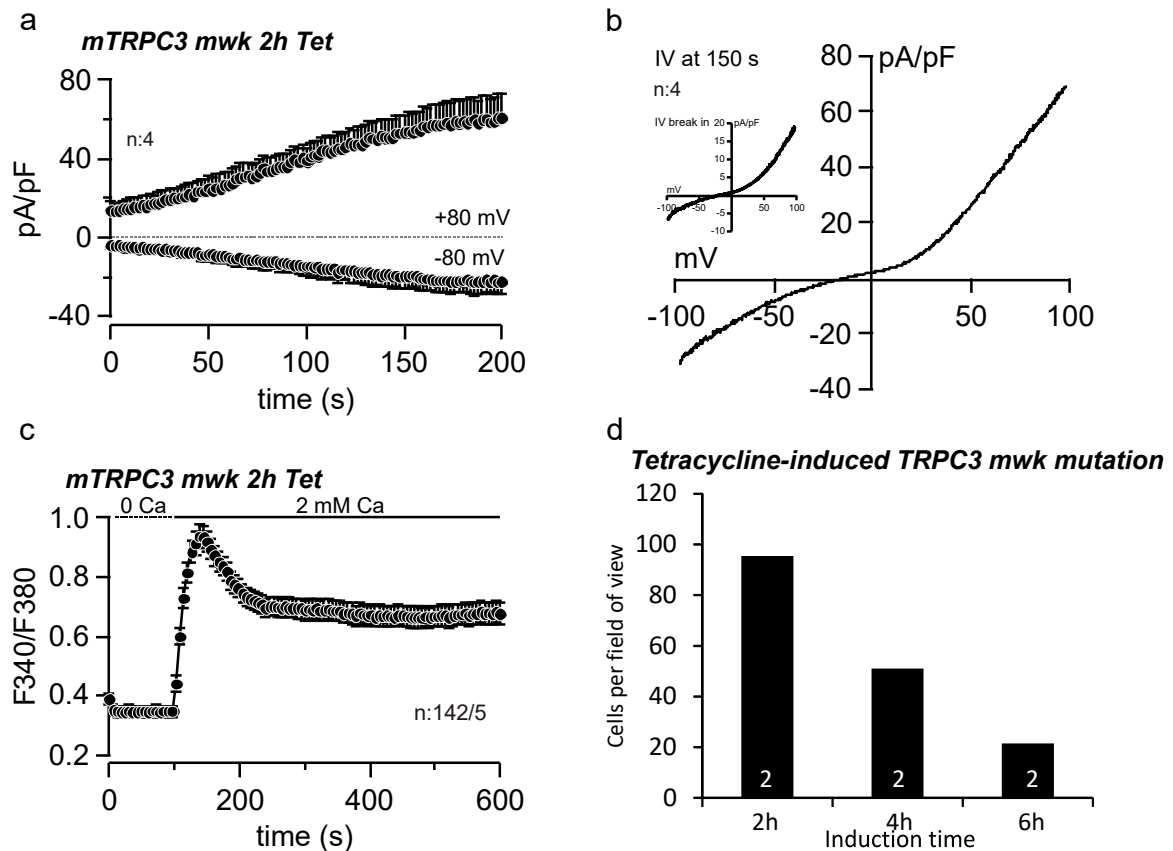


Figure 3-16 Constitutive channel activity of the TRPC3 MWK in HEK293 cells. (a) Currents at -80 and +80 mV versus time showing constitutive currents which were already present upon break-in in absence of any agonist. Current-voltage relationships of the break-in current (b inset) and the current after 150 s (b) showing a similar shape as the TRPC3 wild-type current (Figure 3-12). (c) Fura-2 experiment shows after adding tetracycline cells were kept in 0 extracellular Ca^{2+} , after 100 s 2 mM Ca^{2+} was added to the bath leading to Ca^{2+} entry. (d) Cells stained with Fura-2 observed under the microscope and counted. Times after adding tetracycline are indicated. The data represent mean \pm SEM of the number of cells in patch clamp and number of cells per number of experiments in Fura-2.

3.7.2 Astrocytes from moonwalker mice

Because TRPC3 gene is expressed in mouse cortical astrocytes, astrocytes from heterozygous MWK mice were isolated and analyzed (will be referred as MWK astrocytes). These astrocytes exhibit a higher basal Ca^{2+} levels in the presence of 2 mM extracellular Ca^{2+} when compared to the astrocytes isolated from their wild-type littermates mice (Figure 3-17-a). In the Ca^{2+} readdition

protocol (Figure 3-17-b), the MWK astrocytes did have a higher basal Ca^{2+} level which was dropping to the wild-type levels in the absence of extracellular Ca^{2+} . Upon readdition of 2 mM Ca^{2+} , mutant astrocytes revealed a significant increase of the F340/F380 ratio compared to the wild-type astrocytes which showed a rather small Ca^{2+} increase if at all (Figure 3-17-b).

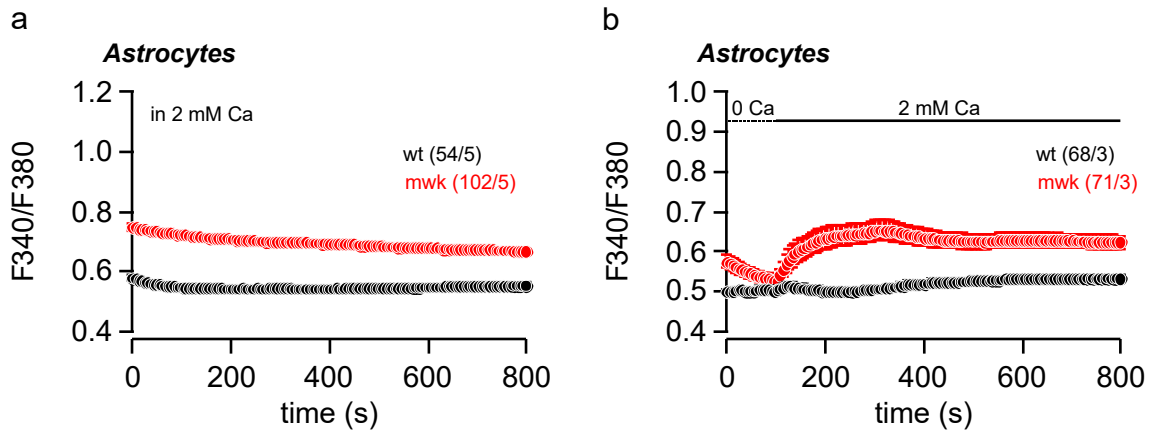


Figure 3-17 **Ca^{2+} imaging in astrocytes from heterozygous MWK mice.** (a) Fura-2 experiment in the presence of 2 mM Ca^{2+} showing the increased basal Ca^{2+} level in the astrocytes from MWK (red) compared to cell from wild-type mice (black). (b) Readdition of 2 mM Ca^{2+} led to an increase in the Ca^{2+} signal in astrocytes isolated from MWK mice (red) compared to cell from wild-typelittermates (black). Data represent mean \pm SEM of the indicated number of cells per number of experiments.

3.7.3 Astrocytes reactivity in non-injured MWK mouse brain

As shown in Figure 3-14 and Figure 3-15, the deletion of TRPC3 gene led to reduction in the reactivity of astrocytes and the size cortical edema after brain injury. We asked the question could the constitutively open TRPC3 has an astrocytic effect, i.e. it leads to astrogliosis even without injury? To address this question wild-type and MWK mice were analyzed for astrogliosis without stab wound surgery by sectioning their brains and staining them anti-GFAP antibody. Images from the GFAP staining showed that there is no obvious difference between TRPC3 MWK and wild-type mice in terms of GFAP staining (Figure 3-18). This suggests that only activation of TRPC3 alone is not sufficient to trigger astrogliosis without injury.

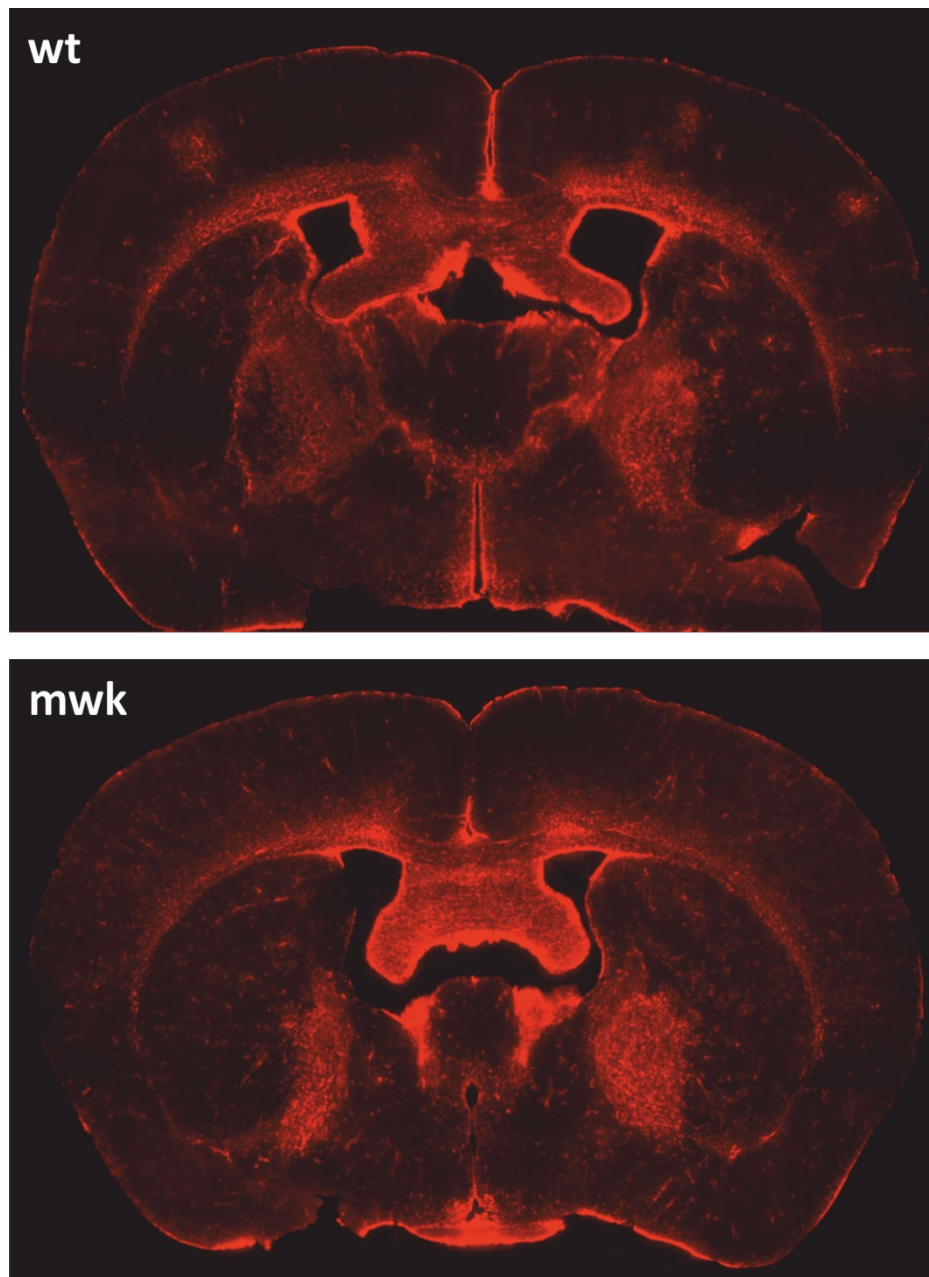


Figure 3-18 **GFAP staining of coronal sections from MWK and wild-type mice.** Brain coronal section obtained from heterozygous TRPC3 MWK and wild-type mice stained with anti-GFAP in red to visualize the reactive astrocytes. No obvious difference in GFAP staining could be observed in the cortex. Those images are obtained from one mouse from each genotype and representative sections are shown.

3.8 TRPC1 in cultured cortical astrocytes

3.8.1 Role of TRPC1 in astrocytes

TRPC1 has been repeatedly reported to be associated with STIM and ORAI which are expressed in astrocytes (see Figure 3-6) (Brechard et al., 2008; Dietrich et al., 2007; Liu et al., 2007). Therefore, astrocytes from TRPC1 gene-deficient mice were used in Fura-2 experiments. Intracellular Ca^{2+} stores were depleted in the presence 10 μM CPA that leads to a transient increase in the cytoplasmic Ca^{2+} due to the continuous Ca^{2+} leak out of the ER which is not reversed by the SERCA pump because it is blocked. Comparing astrocytes from wild-type and TRPC1 gene-deficient mice revealed that TRPC1 deficient astrocytes had significantly smaller Ca^{2+} release from the ER upon CPA treatment in the absence of extracellular Ca^{2+} (Figure 3-19-a-b). Upon readdition of 2 mM extracellular Ca^{2+} , the cytoplasmic Ca^{2+} increases because of ORAI-dependent Ca^{2+} influx. When applying the same protocol on astrocytes isolated from TRPC1 gene-deficient mice no obvious difference was observed when looking at the Fura-2 traces. However, when analyzing the area under the curve of the traces obtained in the presence of 2 mM Ca^{2+} TRPC1 gene-deficient astrocytes had slightly larger area under the curve as compared to the wild-type astrocytes (Figure 3-19-a-c). Those observations in TRPC1 deficient astrocytes upon CPA treatment indicate that TRPC1 could have an ORAI/STIM-independent effect in astrocytes.

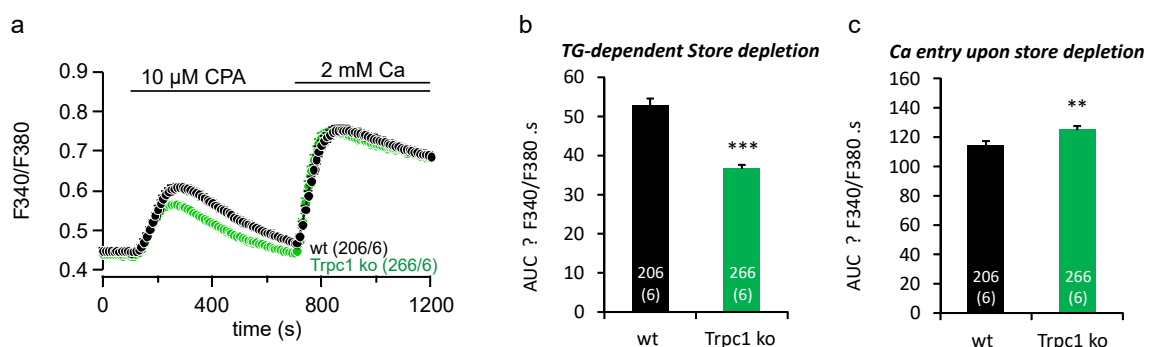


Figure 3-19 Ca^{2+} entry in cultured cortical astrocytes from wild-type and TRPC1 gene-deficient mice. (a) Fura-2 experiment showing changes in the cytoplasmic Ca^{2+} concentration recorded as F340/F380 ratio. In the absence of extracellular Ca^{2+} , 10 μM CPA was applied to deplete the ER which led to an increase in Ca^{2+} because of the Ca^{2+} leak out of the ER. Readdition of 2 mM

Ca^{2+} induced an increase in the cytoplasmic Ca^{2+} due to ORAI-dependent Ca^{2+} entry in wild-type astrocytes (black). TRPC1 deficient astrocytes (green) did exhibit a smaller response to CPA; however the ORAI-dependent Ca^{2+} seemed to be similar to wild-type cells. (b) Bar graphs of the area under the trace of Ca^{2+} release shows a significant reduction in the store depletion of TRPC1 deficient astrocytes compared to wild-type. (c) Bar graphs of the area under the trace of Ca^{2+} entry from both genotypes showing a slight significant increase in TRPC1 deficient astrocytes compared to the wild-type cells. Data represent mean \pm SEM of the indicated number of cells per number of experiments (* for ** for p value ≤ 0.01 and *** for p value ≤ 0.001 and).

3.8.2 Impact of TRPC1 VL on TRPC3 currents in HEK 293 cells

In the current work TRPC1 and TRPC3 were shown to be expressed in astrocytes and TRPC3 could be activated by OAG, however TRPC1 has so far no specific agonist or even a clear mechanism of activation. Nevertheless, it has been shown that TRPC1 could interact with other TRP proteins to form heterotetrameric channels. In some cases those heterotetrameric could show different currents and/or different selectivity towards Ca^{2+} and sodium when compared to the homomeric channels (Strubing et al., 2001). I studied by whole cell patch clamp whether TRPC1 could interact with TRPC3 by co-expressing the TRPC3 and TRPC1 VL cDNAs in HEK 293. First, I measured TRPC3 currents in HEK cells expressing only the TRPC3 cDNA. In contrast to Figure 3-12, where I studied the function of human TRPC3, in this new experiment the mouse TRPC3 cDNA was expressed. The reason for switching to the mouse cDNA is that we are studying the TRPC channels in mouse and we do want to be as close to the *in vivo* situation as possible. Currents were measured in the whole cell patch clamp configuration with voltage ramp from -100 mV to 100 mV. The application of 100 μM OAG did induce inward and outward currents similar than in Figure 3-12 and not in non-transfected HEK 293 (Figure 3-20-a-b-c-d). When the mouse TRPC3 cDNA was co-overexpressed in HEK cells stably expressing the mouse TRPC1 VL cDNA, OAG induced significantly reduced currents when compared to TRPC3 cDNA expression alone (Figure 3-20-a-b). However, the current-voltage relationship of this current was similar to the one obtained from cells expressing the TRPC3 cDNA alone. The application of OAG on TRPC1 VL cDNA expressing cells did

not induce any currents (Figure 3-20-e-f). These results show a negative effect of TRPC1 VL on TRPC3 activity.

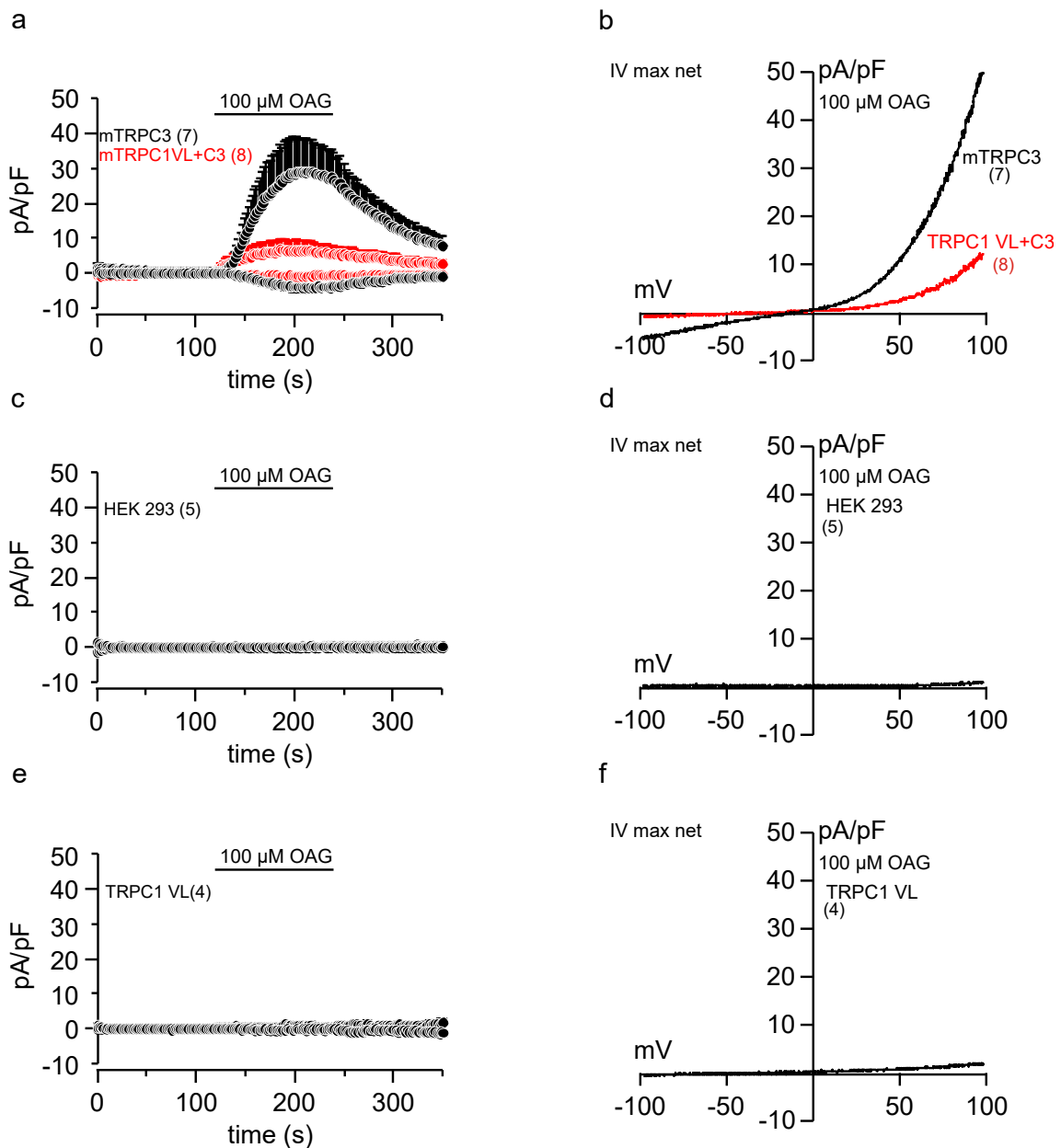


Figure 3-20 TRPC3 and TRPC3/TRPC1 VL currents in HEK293 cells. (a) Currents at -80 and 80 mV plotted versus time showing current before, during and after OAG application of TRPC3 currents in HEK cells transiently transfected with TRPC3 cDNA (black) and TRPC3/TRPC1 VL currents in TRPC1 VL-stably expressing HEK293 cells transfected with TRPC3 cDNA (red). (b) Current-voltage relationships were extracted from the maximum current during OAG application after having subtracted the basal current before application. HEK 293 cells (c,d) and TRPC1 VL HEK293 cells (e,f) did not show any OAG-induced currents. Data represent mean \pm SEM of the indicated number of measured cells.

3.8.3 Role of TRPC1 in OAG-induced Ca^{2+} oscillations in cultured cortical astrocytes

Following the findings from the patch clamp experiments where TRPC1 VL was found to have a negative effect on TRPC3 currents (Figure 3-20), and from the PCR results that both TRPC3 and TRPC1 VL transcripts are expressed in culture cortical astrocytes (Figure 3-5-a), the question came up whether the deletion of the TRPC1 would enhance the TRPC3 activity in astrocytes. In Fura-2 experiments, astrocytes isolated from TRPC1 gene-deficient mice were tested using the OAG protocol described before. After having the intracellular Ca^{2+} stores depleted (10 μM CPA in the presence of 2 mM extracellular Ca^{2+}) 100 μM OAG was applied on top of the steady state ORAI-dependent Ca^{2+} entry. Astrocytes isolated from TRPC1 gene-deficient mice showed a significant increase in the number of OAG-responding cells (Figure 3-21-a-b-c) and moreover the number of oscillations within the responding cells was also significantly increased as compared to the wild-type (Figure 3-21-a-b-d). These results show that deletion of TRPC1 did potentiate the OAG-induced Ca^{2+} influx via TRPC3 in astrocyte, and together with the patch clamp results hints for a possible interaction of TRPC1 with OAG-sensitive TRPC channels, i.e. TRPC3.

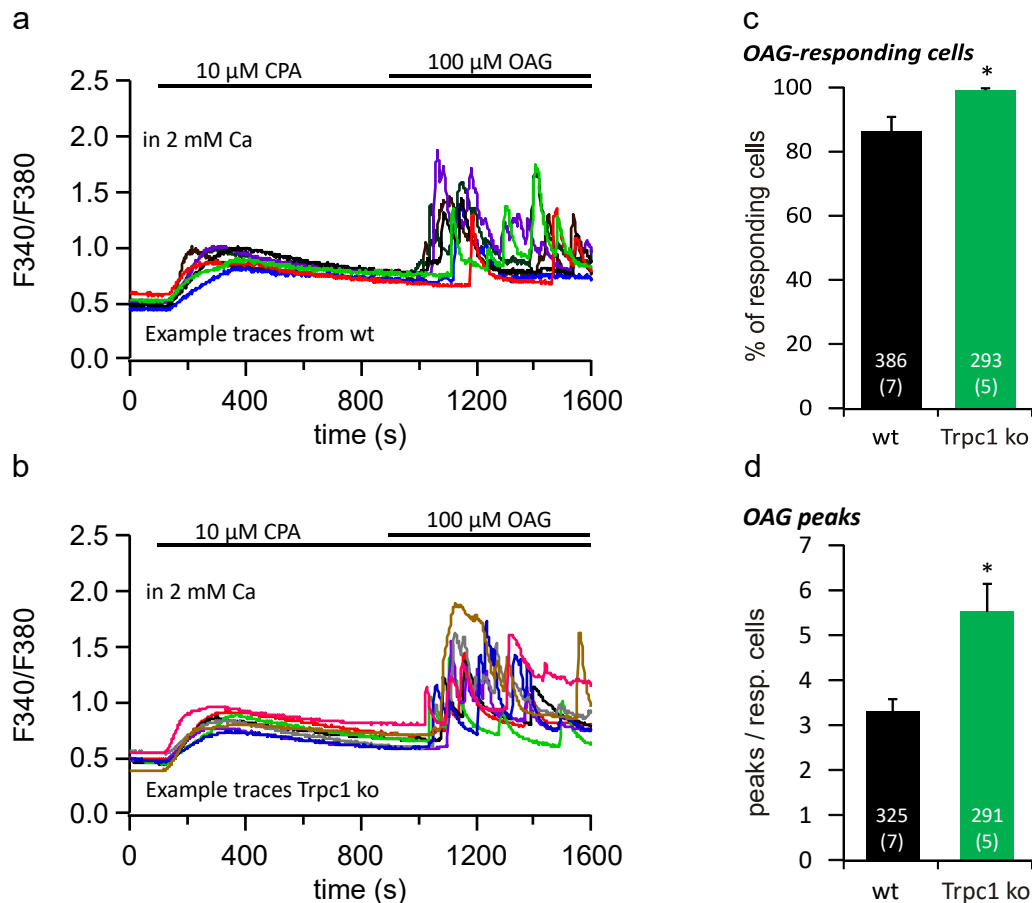


Figure 3-21 Deletion of TRPC1 increases the OAG-induced Ca^{2+} oscillations in astrocytes. Example traces (Fura-2 F340/F380) from the OAG response as established Figure 3-10 in astrocytes isolated from wild-type (“a” identical with Figure 3-10-d) and TRPC1 gene-deficient (b) mice. (c) The statistical analysis of the number of responding cells shows that almost all the cell from TRPC1 gene-deficient mice (green) did respond to the OAG application while around 85% of astrocytes from wild-type mice (black) responded to OAG. (d) Summary of the number of oscillations per cell shows ~5.5 oscillations per TRPC1 deficient astrocytes within the 700 s of OAG application and ~3.5 oscillations per OAG-responding astrocytes from wild-type. Data in c and d represent mean \pm SEM; from number cells per number of experiments (* for p value ≤ 0.05).

3.8.4 Impact of TRPC1 VL on the constitutive TRPC3 MWK

The data so far show that TRPC1 reduces TRPC3 currents in HEK293 cells, whereas in astrocytes isolated from TRPC1 gene-deficient mice revealed enhanced OAG-mediated TRPC3 dependent Ca^{2+} oscillations. To further investigate the effect of TRPC1 on TRPC3 activity, the TRPC1 VL cDNA was co-expressed in the tetracycline inducible TRPC3 MWK HEK cell line, using the

patch clamp technique under the same conditions as described above (Figure 3-12) for the optimum TRPC3 measurement. TRPC1 VL (48 h after transfection its cDNA) was found to significantly reduce the constitutive TRPC3 MWK (2 h on tetracycline induction) currents compared to control cell (only TRPC3 MWK). Co-expression of the TRPC3 cDNA in TRPC3 MWK inducible cells led also to a significant reduction of constitutive TRPC3 MWK currents (Figure 3-22-a-b-c). Similar results were obtained by Fura-2 measurement (Figure 3-22-c-d). The basal Ca^{2+} levels in TRPC3 MWK cells in the absence of extracellular Ca^{2+} were significantly reduced in the presence of TRPC1 VL overexpression but not in the presence of TRPC3. Upon readdition of 2 mM extracellular Ca^{2+} , the cytoplasmic Ca^{2+} increased under all these conditions. The steady state F340/F380ratio, i.e. 5 min after Ca^{2+} readdition, was lowest in TRPC1 VL/TRPC3 MWK cells and TRPC3/TRPC3 MWK cells and the highest in TRPC3 MWK cells (Figure 3-22-d-e). These results confirm the previous finding that TRPC1 VL suppresses the TRPC3 activity, and that also co-expression of the wild-type TRPC3 cDNA reduces the TRPC3 MWK activity.

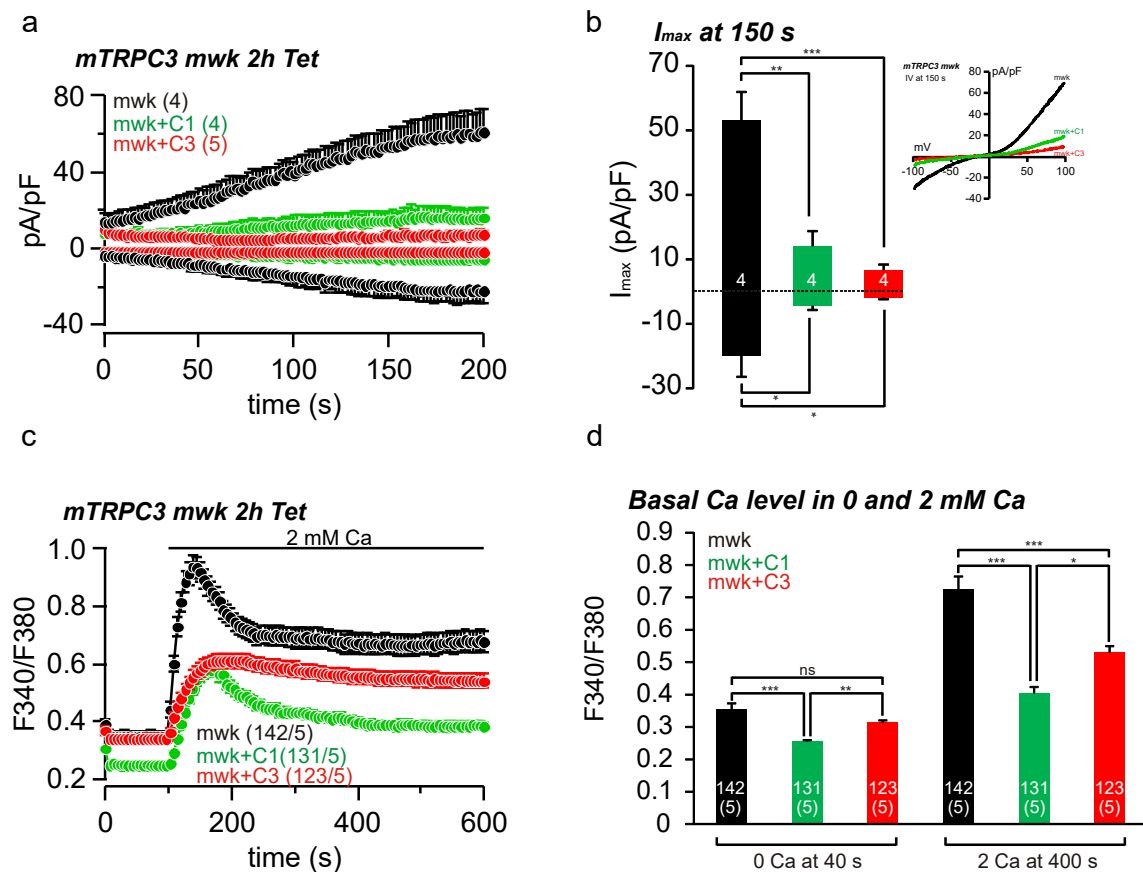


Figure 3-22 Effects of TRPC1 VL and TRPC3 on the constitutive TRPC3 MWK currents in HEK 293 cells. The expression of the TRPC3 MWK was induced by tetracycline 2 h before the measurement. The TRPC1 VL (green) and TRPC3 (red) cDNAs were transiently transfected 48 h prior to the measurement in TRPC3 MWK cell line. (a) Currents at -80 and +80 mV versus time showing that TRPC1 VL (green) and TRPC3 (red) reduced the TRPC3 MWK currents compared to control cells (black, identical as in Figure 3-16). (b) Summary of the currents at 80 mV and -80 mV at 150 s, and inset: showing current-voltage relationships of the currents in a 150 s after break-in. (d) Fura-2 experiment of TRPC3 MWK cells (black, identical as in Figure 3-16) plus TRPC1 VL (green) and TRPC3 (red) in the absence of extracellular Ca^{2+} and after application of 2 mM Ca^{2+} . Ca^{2+} readdition led to an increase in the F340/F380 ratio which was highest in TRPC3 MWK cells and lowest in TRPC1 VL/TRPC3 MWK cells. (d) Summary of the F340/F380 ratio in the absence of Ca^{2+} (basal Ca^{2+} at 40 s) and after readdition of 2 mM Ca^{2+} (400 s). Mean \pm SEM with number of cells in patch clamp and number of cells per number of experiments in Fura-2 (* for p value ≤ 0.05 , ** for p value ≤ 0.01 , *** for p value ≤ 0.001 and ns for non-significant)

3.8.5 Role of TRPC1 in astrocytes migration

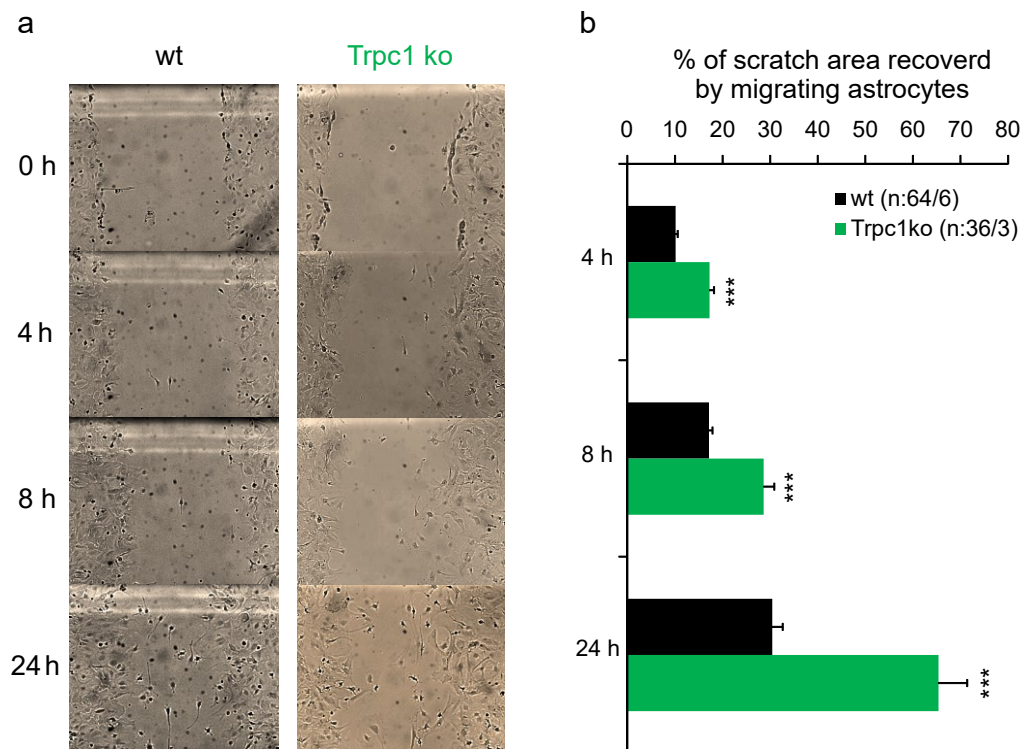


Figure 3-23 ***In vitro* migration of astrocytes from TRPC1 gene-deficient mice.** (a) Representative images of astrocytes at 0 and 4, 8 and 24 hours after scratch from wild-type (shown already in Figure 3-14) and TRPC1 gene-deficient mice. (b) Summary of the migration data. Scratch area at time “0” is 100%; area recovered by migrating astrocytes after 4, 8 and 24 h are indicated from wild-type (black) and TRPC1 deficient (green) astrocytes. Data represent mean \pm SEM of the indicated number of scratches per experiments (***) for p value ≤ 0.001 .

Since the deletion of the TRPC3 led to a reduced *in vitro* migration and because TRPC1 had a negative effect on TRPC3 channel activity, we investigated the effect of TRPC1 deletion on astrocyte migration. Astrocytes isolated from wild-type and TRPC1 gene-deficient mice were transferred into a 6-well plate and cultured until reached confluency. Thereafter, the cell monolayer was scratched as described in the methods and in Figure 3-14. The analysis of the migration 4 hours after the scratch revealed that astrocytes from TRPC1 gene-deficient mice have occupied around 17% of the scratched area, whereas wild-type cells (shown already in 3.6.6) occupied 10% of the scratched area. After 8 hours, ~28% of the scratch was covered by TRPC1 deficient astrocytes, and 18% of the scratch was covered by astrocytes from wild-type mice. At 24 hours, 65% was covered by TRPC1 deficient astrocytes and 30% by wild-type astrocytes

(Figure 3-23). These results and the results from patch clamp and Fura-2 experiments show that TRPC1 decreases TRPC3 function. If TRPC1 is absent, the TRPC3 activity increases, as a result migration is increased, and currents and Ca^{2+} entry are increased as well. Thus TRPC1 could have a significant impact on the astrogliosis after brain injury which is shown in Figure 3-15 to depend on the presence of TRPC3.

3.8.6 Astrogliosis and glial scar formation depends on TRPC1 gene-deficient mice

Next we studied the role of TRPC1 in astrogliosis and glial scar formation after brain injury. Because of the lack of TRPC1 gene-deficient mice at the time of the experiments and the consistent absence of TRPC5 transcripts in the PCR analysis of astrocytes (see 3.5), available TRPC1/TRPC5 gene-deficient mice were used for this experiment which was performed as described in the methods and Figure 3-15. 3 days after injury, mice were sacrificed and fixed with 4% PFA and 35 μm coronal sections were made from the injured brain region and stained for GFAP. Inspection of the GFAP-stained slices showed that the deletion of TRPC1/TRPC5 led to a significant increase in the area of reactive astrocytes, i.e. the GFAP positive area (3.8 mm^2) as compared to the corresponding wild-type mice (3 mm^2). This was further confirmed by the analysis of the anti-GFAP antibody fluorescence intensity which was measured from equally sized rectangles placed along the injured cortex (normalized to the contralateral). This analysis showed that a significant increase in the anti-GFAP antibody fluorescence intensity from injured hemisphere compared to the wild-type mice. Moreover, the width of the GFAP staining (i.e distribution of GFAP staining along the injured cortex) was wider in the TRPC1/TRPC5 gene-deficient mice compared to the wild-type. The analysis of the edema, quantified by measuring the cortex width of the injured hemisphere and normalized to the contralateral side, showed more cortical edema in the gene-deficient mice $\sim 17\%$, while wild-type mice had $\sim 10\%$ increase of the cortex width (Figure 3-24). These results indicate that deletion of TRPC1 suppresses the reactivity of astrocytes as well as in the inflammatory reaction following brain injury. It is to note that the independent groups of wild-type animals taken as controls for the TRPC3 gene-deficient mice and the TRPC1/TRPC5 gene-

deficient mice showed no significant difference in the analyzed parameters of the cortical stab wound protocol (n=7 for control1 and control2 respectively).

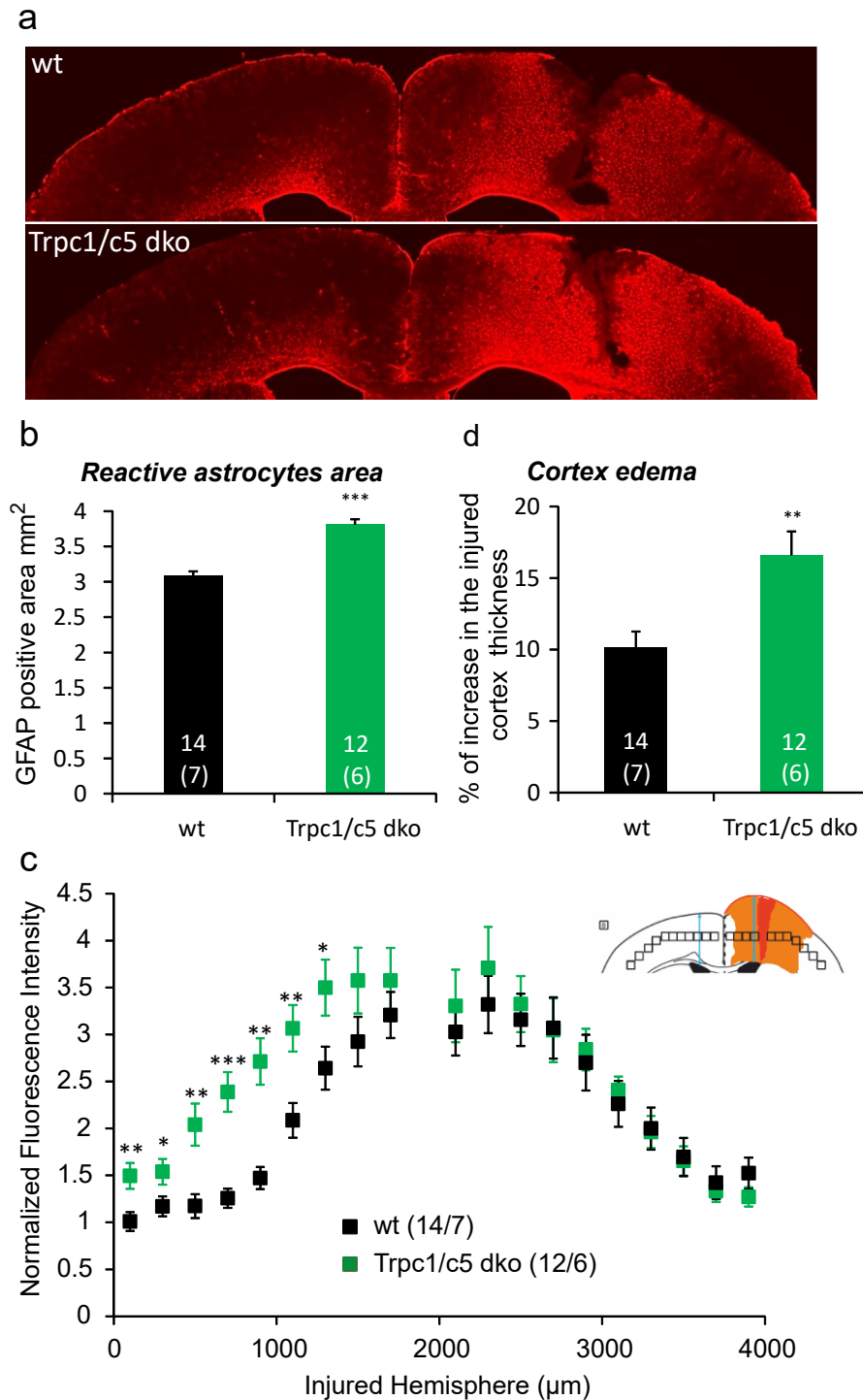


Figure 3-24 Cortical stab wound in TRPC1/TRPC5 gene-deficient mice. (a) Example images of the cortical stab injury from wild-type and TRPC1/TRPC5 gene-deficient mice as 35 μm sections stained anti-GFAP antibody to visualize the reactive astrocytes. (b) Summary of the area of reactive astrocytes (in mm²) showing significant larger area of GFAP staining in TRPC1/TRPC5 gene-deficient mice (green) compared to wild-type (black). (d) Analysis of the cortical

edema after brain injury measured from the cortical width where the TRPC1/TRPC5 gene-deficient mice had more cortical edema compared to wild-type mice. (c) Diagram showing the distribution of the reactive astrocytes obtained (inset) from measuring the anti-GFAP fluorescence intensities of rectangles along the cortex and normalized to the contralateral. Data shows again the TRPC1/TRPC5 gene-deficient mice had more intensity and distribution of astrocytes compared to wild-type. Data represent mean \pm SEM from 7 wild-type mice (14 sections) and 6 mice TRPC1/TRPC5 gene-deficient mice (12 sections) (** for p value ≤ 0.01 , and *** for p value ≤ 0.001).

3.9 Voltage-gated Ca^{2+} channels (CaVs) in astrocytes

3.9.1 Expression of CaVs subunits in cultured mouse cortical astrocytes

Astrocytes are generally considered to not express functional voltage-gated Ca^{2+} channels CaVs, even though many studies have shown that astrocytes do express mRNA of CaV subunits (Latour et al., 2003). In the present study transcriptome analysis from GLAST-sorted cultured mouse cortical astrocytes showed that indeed astrocytes do express various $\text{CaV}\alpha 1$ subunit genes. In addition, $\text{CaV}\beta$ subunit genes, but not $\text{CaV}\gamma 1$ subunit gene, $\text{CaV}\alpha 2\delta 2$ and $\text{CaV}\alpha 2\delta 4$ subunit genes were detectable (Figure 3-25). $\gamma 2$ to $\gamma 8$ are no CaV channel subunits but are involved in AMPA-receptor trafficking and therefore called transmembrane AMPA receptor regulating proteins (TARPs) (Nicoll et al., 2006). In addition, the FPKM values of $\gamma 2$ to $\gamma 8$ transcripts are higher than the $\text{CaV}\alpha 1$ subunit transcripts, but could correlate with the FPKM values of the AMPA transcripts shown in Figure 3-6. Interestingly, there are in sum more transcripts for the four $\text{CaV}\beta$ genes than for $\text{CaV}\alpha 1$ subunit genes or $\text{CaV}\alpha 2\delta$ subunit genes. This finding might indicate that in addition to the assumed 1:1:1 stoichiometry of $\text{CaV}\alpha 1$: $\text{CaV}\beta$: $\text{CaV}\alpha 2\delta$, additional functions and roles for $\text{CaV}\beta$ may be independent of the channel subunit function exist. However the mRNA levels do not necessarily reflect the functional presence of the channels.

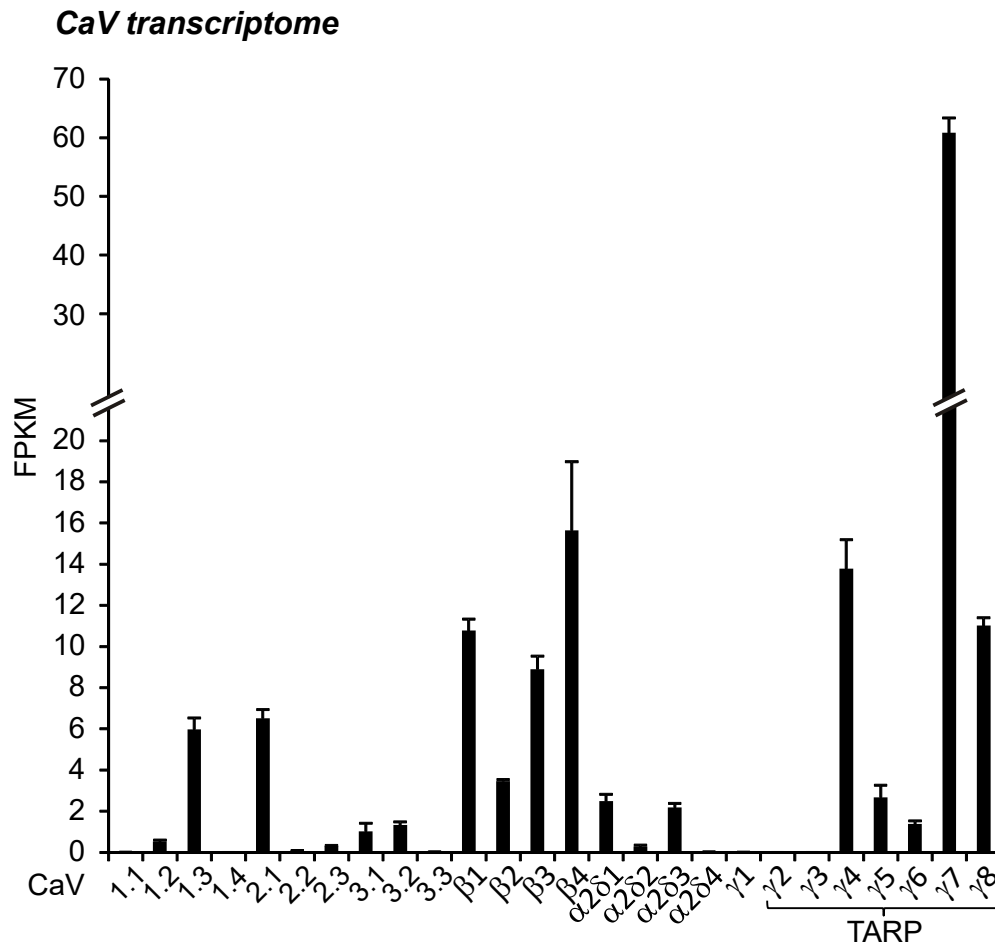


Figure 3-25 **Expression analysis of voltage-gated Ca^{2+} channel subunit genes in cultured cortical astrocytes.** Bar graph represents transcriptome data obtained from the GLAST-sorted astrocytes RNA, of the $\text{CaV}\alpha 1$ subunits, $\text{CaV}\beta$ subunit, $\text{CaV}\alpha 2\delta$ subunit, $\text{CaV}\gamma 1$ subunit and TARP $\gamma 2$ to $\gamma 8$ subunit genes. The values are expressed in Fragments Per Kilobase of transcript per Million mapped reads FPKM as mean \pm SEM of three independent RNA sequencing experiments from three independent FACS-sorted astrocyte cultures.

3.9.2 High potassium depolarization in astrocytes

CaVs are Ca^{2+} selective channels and their activity could be measured using Fura-2-based Ca^{2+} imaging. The CaVs are activated upon depolarization of the membrane potential which could be achieved by increasing the extracellular potassium concentrations. In Fura-2 experiments, the potassium concentration is set to 4 mM in which is not sufficient for depolarization needed to open CaVs . Increasing the potassium concentration to 50 mM led to a fast transient increase in the cytoplasmic Ca^{2+} which maybe mediated by voltage-gated Ca^{2+} channel opening (Figure 3-26-a). As shown by others (Beck et al., 2004), the

removal of extracellular potassium also causes cytoplasmic Ca^{2+} increase in astrocytes. This was explained that the potassium channels become Ca^{2+} permeable in the absence of potassium and is supposed to be specific mechanism for astrocytes. Microglia showed no response to neither potassium-free condition nor to the high potassium (Figure 3-26-b).

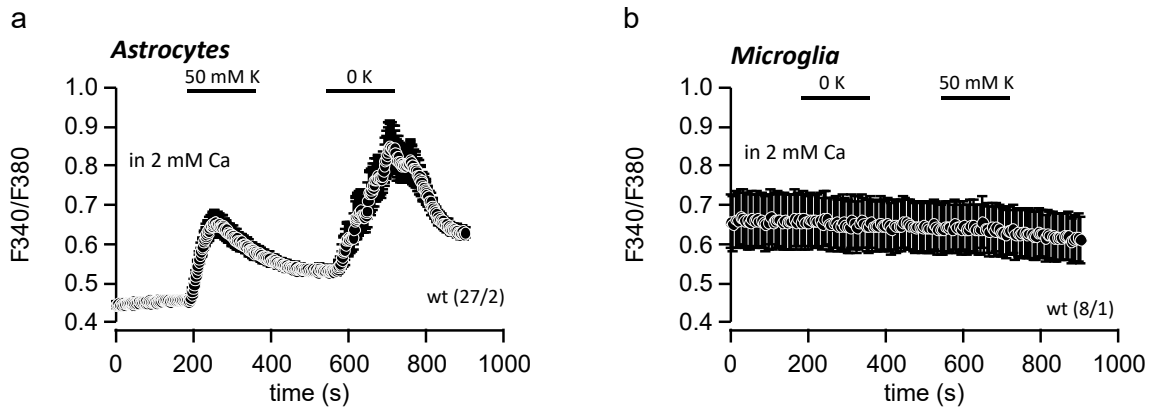


Figure 3-26 **Ca^{2+} influx induced by high potassium induced-depolarization in astrocytes.** (a) Fura-2 Ca^{2+} measurement (F_{340}/F_{380}) in astrocytes. Application of 50 mM cytoplasmic potassium led to subsequent Ca^{2+} influx, and removal of extracellular potassium also induced Ca^{2+} increase. Similar protocol was applied on microglia (b) did not lead to any Ca^{2+} increase. Data represent mean \pm SEM of the indicated number of cells per number of experiments.

3.9.3 Electrophysiological characterization of voltage-gated Ca^{2+} and Na^{+} channels in cultured cortical astrocytes

The Fura-2 experiment showed that voltage-gated Ca^{2+} channel activity might be present in astrocytes upon potassium depolarization. Patch clamp experiments offer the opportunity to characterize the CaVs in a more reliable manner. Due to the inhibitory effect of intracellular Ca^{2+} on the CaVs, the patch clamp experiments were carried out using an intracellular solution with Ca^{2+} buffered to 0 by BAPTA and extracellular Ca^{2+} was substituted by 10 mM barium (Ba^{2+}) since under this condition Ca^{2+} -dependent inactivation of CaV currents should be absent.

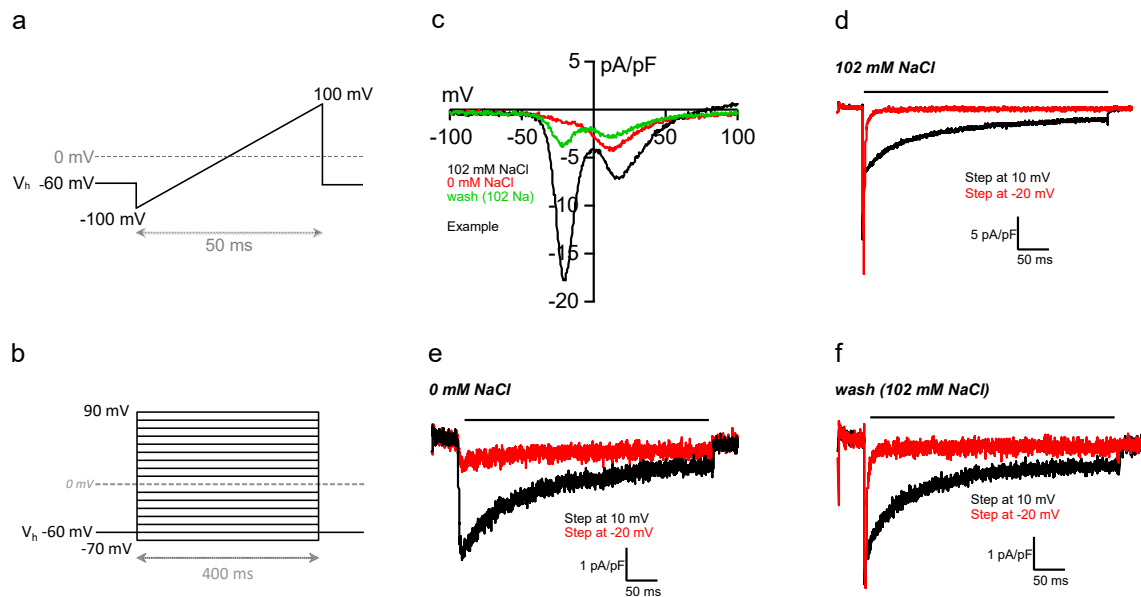


Figure 3-27 Voltage-gated cation channels in astrocytes. Scheme of the voltage ramp protocol (a) and step protocol (b) used to measure CaVs activity. Voltage ramps were applied every 2 s over a duration of 50 ms from -100 to 100 mV from a holding potential of -60 mV. The step protocol consist of voltage steps from -70 to 90 mV applied over a duration of 400 ms with 10 mV increment from a holding potential of -60 mV. (c) Current-voltage relationships extracted from the maximum current during the voltage ramp measurements in 102 mM Na^+ (Black), 0 Na^+ (substituted with cesium) (red) and the readdition of 102 mM Na^+ (green). Currents extracted from the 400 ms voltage step measurements at -20 mV (red) and at 10 mV (black) during 102 mM Na^+ (d), 0 Na^+ (e) and after the readdition of 102 mM Na^+ (f).

After break-in, astrocytes were clamped to -60 mV and voltage ramps from -100 to +100 mV of 50 ms duration were applied every 2 s (Figure 3-27-a). Under this condition, the astrocytes showed two distinct inward currents with a maximum at approximately -20 and +10 mV (Figure 3-27-c-black). To learn more about those currents, a step protocol was applied from -70 mV to +90 mV where every step last for 400 ms and steps escalated by 10 mV (Figure 3-27-b). This protocol showed that there are two different types of currents easily distinguishable by their peak voltage and their inactivation kinetics. The first type of currents had maximum amplitude at -20 mV and exhibited fast inactivation kinetics, while the second one had its maximum at +10 mV and showed a much slower inactivation. The shape of the current with its maximum at -20 mV strongly reflects the shape of a voltage-gated Na^+ channel, and the one at +10 mV rather indicates a voltage-gated Ca^{2+} channel (Figure 3-27-d).

Within the same cell, the extracellular Na^+ was substituted by cesium which does not pass Na^+ channels. As expected the current at -20 mV disappeared and only the current at +10 mV was present (Figure 3-27-c-red), in addition the step protocol showed no Ba^{2+} current with fast inactivation at -20 mV but the current at +10 mV did not change which strongly suggest that the first current was a voltage-gated Na^+ current (Figure 3-27-e). Readdition of extracellular Na^+ led to the reappearance of the Na^+ current, however the current amplitude was much smaller due to the duration of the measurement (Figure 3-27-c-green, f). Analyzing the transcriptome data obtained from the RNA extracted from the GLAST-sorted astrocytes, several transcripts of voltage-gated Na^+ $\alpha 1$ and β subunit genes were found to be expressed. The detectable members were the NaV 1.1, 1.2, 1.3, 1.5 and 1.6 with the 1.2 and the 1.5 transcripts showed the highest levels, while all NaV β subunit genes were detectable with NaV $\beta 1$ and $\beta 4$ subunit were the highest (Figure 3-28).

NaV transcriptome

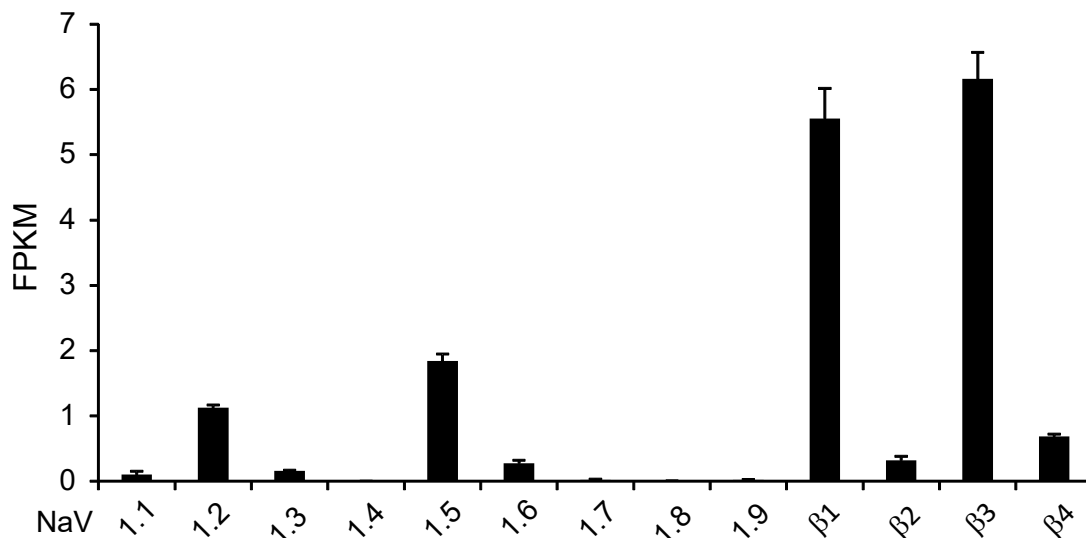


Figure 3-28 NaV subunit $\alpha 1$ and β transcripts of voltage-gated Na^+ channels in cultured cortical astrocytes. Bar graph represents transcriptome data obtained from the GLAST-sorted astrocytes RNA, of the NaV $\alpha 1$ and NaV β subunit genes. The values are expressed in Fragments Per Kilobase of transcript per Million mapped reads FPKM as mean \pm SEM of three independent RNA sequencing experiments from three independent FACS-sorted astrocyte cultures.

Tetrodotoxin (TTX) is a potent blocker of NaV channels; it is commonly used to block the NaVs when measuring CaVs activity. Using the same experimental conditions as before, but with addition of 10 μM TTX to the extracellular solution, the ramp protocol showed only one inward current which was almost completely blocked when the bath solution was replaced by a $\text{Ba}^{2+}/\text{Ca}^{2+}$ -free solution (Figure 3-29-a). Analyzing the maximum current from the step protocol revealed a current-voltage relationship which is typical for CaVs (Figure 3-29-b). Its maximum was at 10 mV and the current trace obtained by the depolarization at 10 mV showed the typical CaVs inactivation kinetics (Figure 3-29-c).

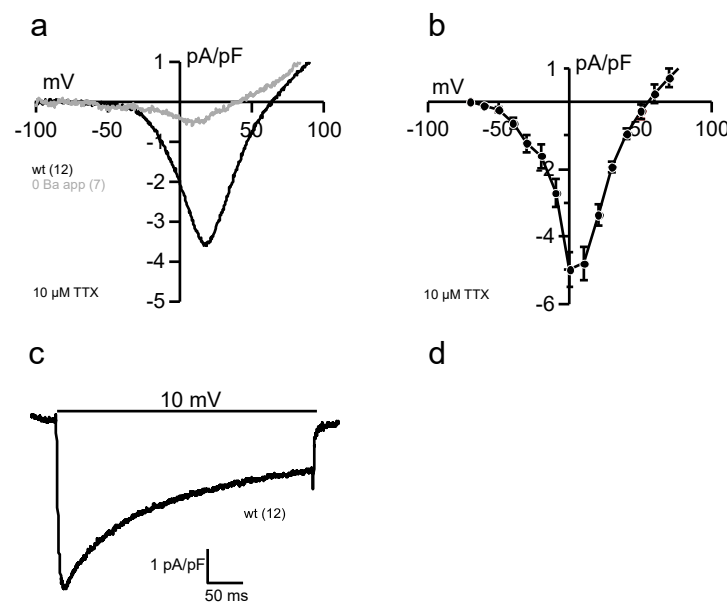


Figure 3-29 CaVs currents in cultured cortical astrocytes. (a) Current-voltage relationships extracted from the maximum current during the voltage ramp measurements of wild-type astrocytes in the presence of 10 mM Ba^{2+} and 10 μM TTX showing an inward current (black) which disappeared in the absence of Ba^{2+} (grey). (b) Current-voltage relationships extracted from the voltage steps measurements in 10 mM Ba^{2+} showing a current of -5 pA/pF at 10 mV depolarization. (c) Current induced by depolarizing to 10 mV for 400 ms shows the typical activation and inactivation kinetics of the CaV channels.

3.9.4 Impact of CaV β 3 deletion on CaVs activity in astrocytes

Cav β subunits are associated with the pore forming CaV α 1 subunit and they are involved in CaV α 1 trafficking to the plasma membrane and also in channel gating properties. The deletion of CaV β 3 subunit gene was shown, in a previous paper from our laboratory, to shift the Ca^{2+} current to more depolarized

potentials in dorsal root ganglion neurons (Murakami et al 2002). Astrocytes were isolated from CaV β 3 gene-deficient mice and used for electrophysiological measurements of dorsal root ganglion neurons currents. CaV β 3 deficient astrocytes exhibited similar CaV inward currents when compared with the corresponding wild-type cells in terms of current amplitude as well as activation and inactivation potentials (Figure 3-30-b-d). No significant difference could be identified, but a slightly higher but not significantly different current at -30 and -20 mV steps were observed in astrocytes CaV β 3 deficient astrocytes (Figure 3-30-b). The maximum currents (I_{max}) were achieved at 10 mV in both genotypes, and after normalizing the currents from the voltage steps to the maximum amplitude, CaV currents of CaV β 3 deficient astrocytes showed no difference in their activation and inactivation kinetics as compared to the corresponding currents of wild-type astrocytes (Figure 3-30-e-f). Thus the CaV β 3 subunit does not seem to play a role in the function of the CaV current in cultured cortical astrocytes.

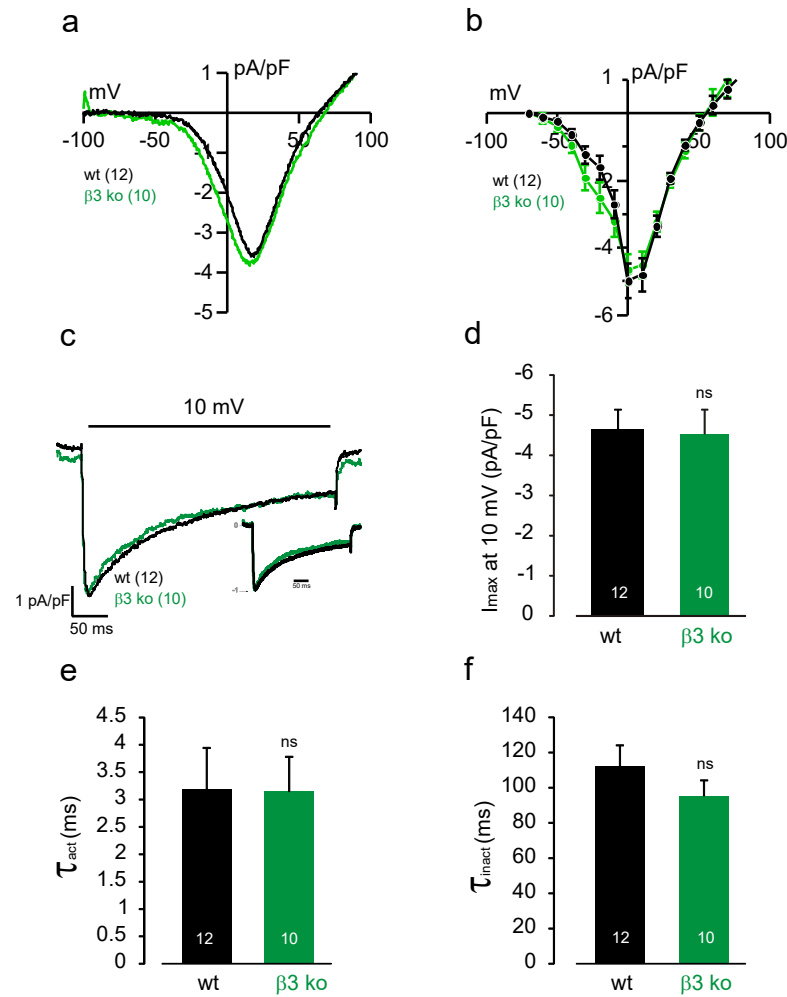


Figure 3-30 CaV currents in CaVβ3 deficient astrocytes. (a) Current-voltage relationships extracted from the current obtained by the voltage ramp protocol of wild-type astrocytes (black) and astrocytes from CaVβ3 gene-deficient mice (green). (b) Current-voltage relationships extracted as maximum current amplitudes from the voltage steps measurements of astrocytes from wild-type (black) and CaVβ3 gene-deficient mice (green). (c) Currents at 10 mV including as inset normalized currents to the maximum amplitude from both genotypes. (d) Maximal current density (I_{\max}) of the current at 10 mV from wild-type astrocytes (black) and CaVβ3 gene-deficient astrocytes (green). Analysis of the activation (e, τ_{act}) and inactivation (f, τ_{inact}) kinetics of the currents at 10 mV from wild-type astrocytes (black) and CaVβ3 gene-deficient astrocytes (green). Data represent mean \pm SEM of the indicated number of measured cells (ns for non-significant).

3.9.5 Impact of CaV β 2 deletion on CaVs activity in astrocytes

Similarly to CaV β 3, the deletion of CaV β 2 subunit was also shown to shift the L-type Ca²⁺ currents to more depolarizing potentials in embryonic cardiomyocytes, and in addition the amplitude of the current was reduced (Weissgerber et al., 2006). In the present work, astrocytes were also isolated from the extra-cardiomyocyte CaV β 2 gene-deficient mice generated in our laboratory. These mice carry a functional CaV β 2 gene in cardiomyocytes and are CaV β 2 gene-deficient in all other cell of their body (Katiyar et al., 2015). Ba²⁺ currents were measured using ramp protocols from -100 to +100 mV and step protocols from -70 to +90 mV with 10 mV increment as shown in Figure 3-27-a-b. The current amplitude in CaV β 2 deficient astrocytes was significantly reduced by ~40% compared to the corresponding wild-type cells (Figure 3-27-d). Moreover the activation curve tended to shift, but not significantly, towards more depolarized potentials in astrocytes isolated from CaV β 2 gene-deficient mice. The activation kinetics obtained from current at 10 mV showed no difference when CaV β 2 was deleted in astrocytes, but the inactivation kinetic at 10 mV current was significantly faster in CaV β 2 deficient astrocytes (Figure 3-31-e-f). Thus, in contrast to CaV β 3 the CaV β 2 has an impact on the CaV currents in cultured cortical astrocytes. The characteristics of the CaV currents were not significantly different in the two wild-type astrocytes used as a control for CaV β 3 and the CaV β 2 deficient astrocytes (black traces in Figure 3-30 and Figure 3-31).

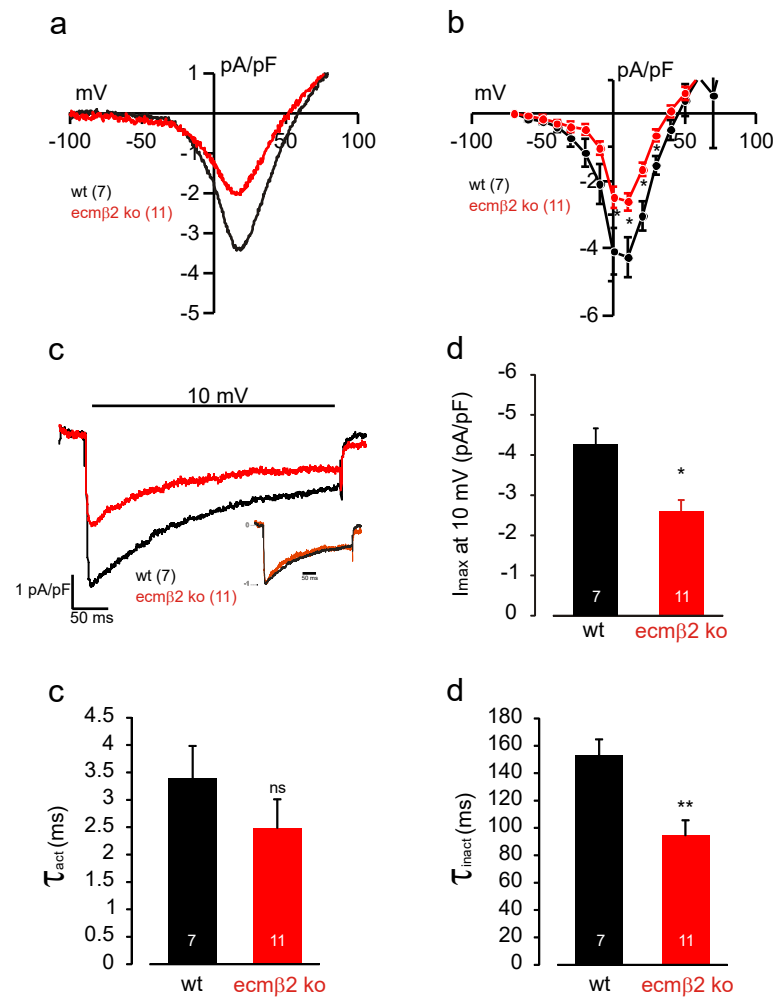


Figure 3-31 CaV currents in CaVβ2 deficient astrocytes. (a) Current-voltage relationships extracted from the current obtained by the voltage ramp protocol of wild-type astrocytes (black) and astrocytes from CaVβ2 gene-deficient mice (ecmβ2 ko red). (b) Current-voltage relationships extracted as maximum current amplitudes from the voltage steps measurements of astrocytes from wild-type (black) and CaVβ2 gene-deficient mice (red). (c) Currents at 10 mV including as inset normalized currents to the maximum amplitude from both genotypes. (d) Maximal current density (I_{max}) of the current at 10 mV from wild-type astrocytes (black) and CaVβ2 gene-deficient astrocytes (red). Analysis of the activation (e, τ_{act}) and inactivation (f, τ_{inact}) kinetics of the currents at 10 mV from wild-type astrocytes (black) and CaVβ2 gene-deficient astrocytes (green). Data represent mean \pm SEM of the indicated number of measured cells (* for p value ≤ 0.05 , ** for p value ≤ 0.01 and ns for non-significant).

3.9.6 Pharmacological characterization of CaVs in astrocytes

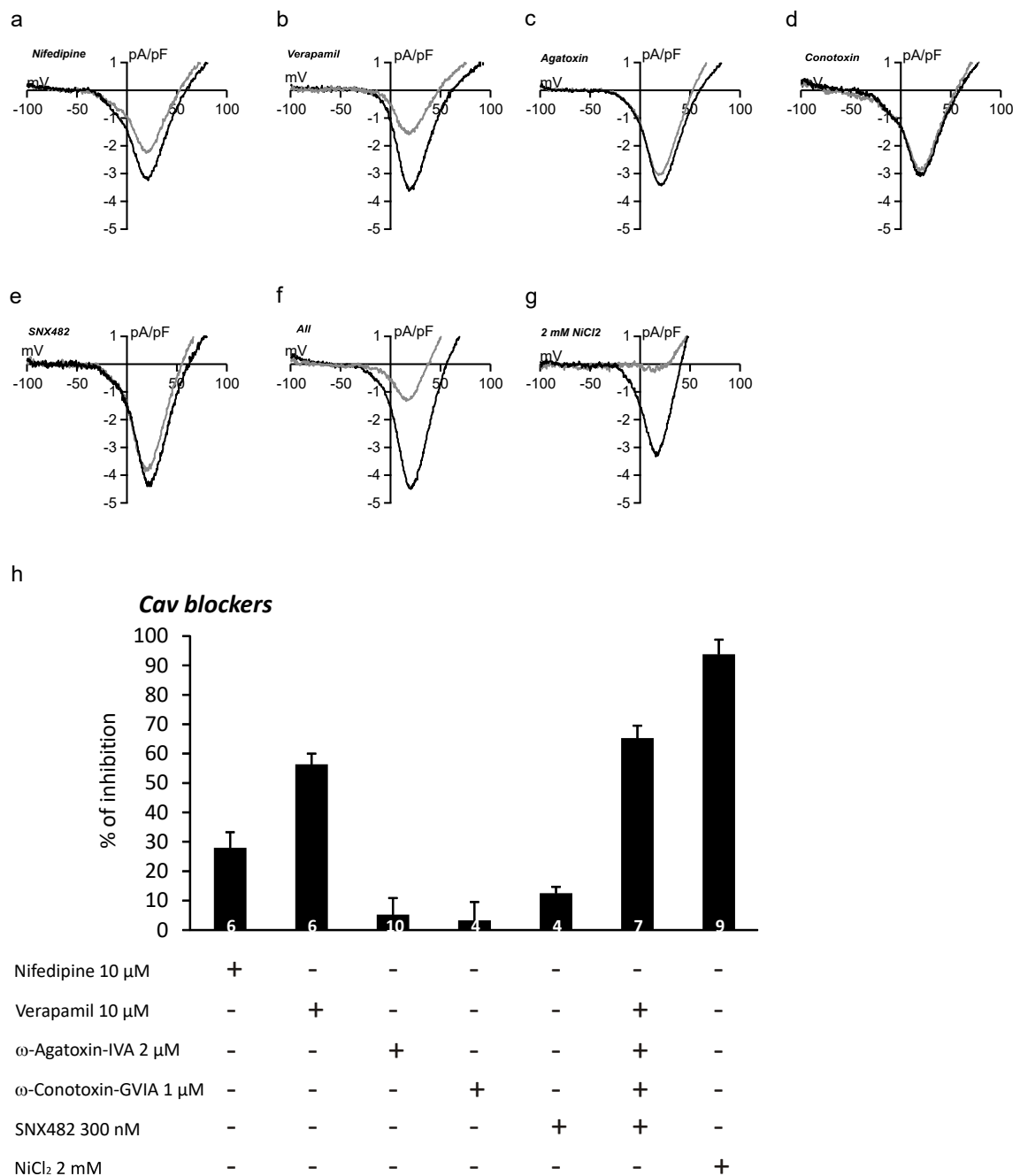


Figure 3-32 Pharmacological characterization CaVs in astrocytes. Current-voltage relations extracted from the I_{\max} (black) and after (grey) the application of nifedipine (a), verapamil (b), ω -agatoxin-IVA (c), ω -conotoxin-GVIA (d), SNX 482 (e), all agents (without nifedipine and NiCl_2) (f) and NiCl_2 (g). (h) Summary of mean \pm SEM with from the indicated number of measured cells.

The CaV I_{\max} measured in cultured mouse cortical astrocytes was obtained at 0 to 10 mV which indicates a contribution of high voltage-activated (HVA) CaVs rather than low voltage-activated (LVA) CaVs. These results are in good

agreement with the transcriptome data that shows the P/Q- and L-type channels to be expressed more prominently than the LVA CaVs (Figure 3-25-a). It is difficult to discriminate between the HVA CaVs in a cell that expresses a mixture of those channels by analyzing the current-voltage relationship. However, blockers of CaVs have been developed and tested, and some such as nimodipine and verapamil are in use to treat patients for more than 50 years. A set of different blockers of HVA CaVs were used in whole cell patch clamp experiments of astrocytes (Figure 3-32). The measurement started in the standard extracellular solution and after having the Ba^{2+} currents recorded for 2 min, blockers were applied, either separately or in combination, with an application pipette onto the measured cell. The percentage of blockage was calculated by dividing the decrease in the I_{max} after blocker application by the I_{max} before application ($(I_{\text{max}} - I_{\text{max blocker}}) \cdot 100 / I_{\text{max}}$). Application of 10 μM nifedipine, an L-type CaV blocker, led to a reduction of about 27% in the current (Figure 3-32-a), whereas another L-type blocker verapamil (10 μM) led to even higher blockage of about 56% (Figure 3-32-b). This indicates that many L-type Ca^{2+} channels are contributing to the astrocytic inward Ba^{2+} current. ω -agatoxin-IVA, a CaV2.1 blocker, was also used since there was a prominent expression of CaV2.1 RNA in the transcriptome, however only 5% blockage was observed using 2 μM (Figure 3-32-c). A CaV2.2 blocker, ω -conotoxin-GVIA, was also used, but 1 μM was able to block only 3% of the CaV current in astrocytes (Figure 3-32-d). The last HVA Ca^{2+} channel to be tested is the CaV2.3 channel using its specific blocker SNX 482, which blocks 12% of the current (Figure 3-32-e). The summed percentages of blockage from the different blockers resulted in 76% which reflects a residual current of 24% that was not blocked. Nevertheless, a cocktail of blockers was used including verapamil, ω -agatoxin-IVA, ω -conotoxin-GVIA and SNX 482 with same concentrations that were previously used. Again this cocktail was not able to fully block the inward current measured in astrocytes and resulted in a blockage of only 65% (Figure 3-32-f). Whereas NiCl_2 , a non-specific Ca^{2+} channels blocker at concentration of 2 mM, blocked almost completely the inward current (around 94%) (Figure 3-32-g). This finding indicates that maybe higher concentration of the CaV blockers have to be used to completely block all the CaVs.

In the transcriptome analysis of astrocytes, only CaV1.2 and CaV1.3 among the L-types were prominently expressed but the CaV1.3 transcripts were 10-fold higher than the CaV1.2. Therefore, a more sensitive CaV blocker was used. 10 μM of isradipine was able to block about 52% of the astrocytic inward current (Figure 3-33-b) which was very similar to what was obtained in the presence of 10 μM verapamil. When the concentration of isradipine was increased to 100 μM ~82% of the current was blocked (Figure 3-33-c), while 1 μM isradipine blocked ~25% of the current (Figure 3-33-a). Taken the summed percentages of inhibition by 100 μM isradipin (82%), ω -agatoxin-IVA (5%), ω -conotoxin-GVIA (3%) and SNX 482 (12%) revealed blockage of 102% of the Ca^{2+} current measured in astrocytes.

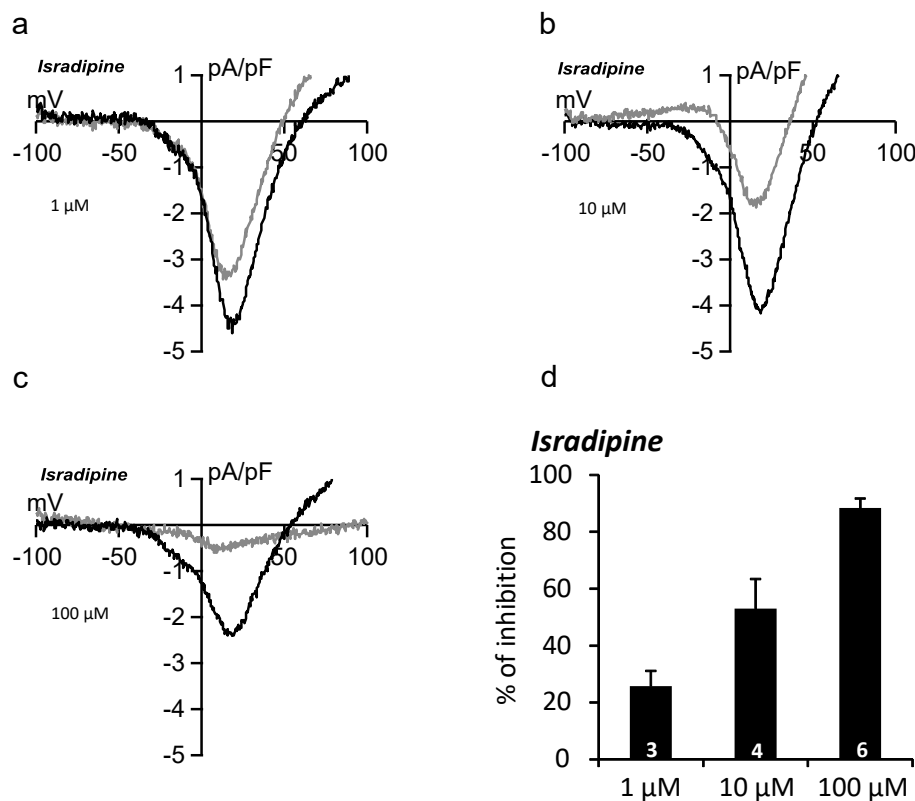


Figure 3-33 Block of CaV currents in astrocytes in the presence of increasing concentrations of isradipine. Current-voltage relationships extracted from the maximum current before (black) and during (grey) the application of isradipine 1 μM (a), 10 μM (b) and 100 μM (c). (d) Summary of means \pm SEM of the percentage of inhibition from the indicated number of measured cells.

4 Discussion

4.1 Characterization of cultured astrocytes and their transcript expression pattern

Astrocyte cultures obtained from the cerebral cortex of new born mice consist mainly of astrocytes and a very low number of microglia cells that grow on top of the astrocytes. Microglia cells can be removed by shaking the culture flask, but this procedure does not lead to full removal of the microglia. Such a culture is called enriched astrocytes culture. Using specific antibodies for astrocytes (anti-GFAP) and microglia (anti-CD11b) did reveal that a few cells of the enriched astrocyte culture were still positively labelled with the microglia marker but most of the cells were GFAP-positive. Most of the published studies, which used cultured astrocyte, have employed the enrichment method leading to more than 90% purity (Grimaldi et al., 2003; Yi et al., 2016). PCR analysis using RNA isolated from such astrocyte enriched cultures revealed that all the TRPC transcripts, except that of TRPC5, could be identified (Figure 3-2). These results are in agreement with results have been published by several groups on rat embryonic cortical astrocytes (Grimaldi et al., 2003; Liang et al., 2014). In addition, several groups have reported by the mean of western blot that astrocytes do express TRPC1, TRPC3, TRPC4 and TRPC6 (Grimaldi et al., 2003; Linde et al., 2011). However, the specificity and the sensitivity of the antibodies used in those studies against the TRPC proteins have not been shown. RT-PCR is a very sensitive technique where an RNA contamination from another cell type could easily lead to amplification of contaminating transcripts even if the number of contaminating cells is very low. In the case of the astrocyte cultures, which are contaminated by microglia cells, it is therefore very difficult to rely on the PCR results from the enriched culture. For this reason, isolation of pure astrocytes before any gene expression analysis is essential. Separating cells by fluorescence-activated cell sorting (FACS) is a technique which can be used to separate astrocytes from microglia cells. To sort living cells, surface markers which are labelled with fluorescent antibodies

are needed. The astrocytic marker GFAP is a cytoplasmic marker, and therefore using this marker to sort living cells is not possible. Alternatively, the glutamate aspartate transporter (GLAST) has been suggested to be an astrocytes marker protein which is located in the plasma membrane (Schmitt et al., 1997). Flow cytometry analysis of fixed and permeabilized cells from astrocyte cultures stained with both anti-GFAP-FITC and anti-GLAST-PE, revealed that the same cells were stained with both antibodies (Figure 3-3). Similarly as has been described (Jungblut et al., 2012). We therefore used anti-GLAST-PE antibody to sort pure living astrocytes for transcriptome analysis by next generation sequencing and RT-PCR. In addition, anti-CD11b-FITC antibody was used to label the microglia. Astrocytes were sorted for PCR analysis as GLAST-positive / CD11b-negative, and microglia as CD11b-positive / GLAST-negative (Figure 3-4). By RT-PCR using 100 sorted astrocytes, not all TRPC transcripts were amplified. Only TRPC3 was amplified in 13 independent PCRs from 5 independent sortings of 5 independent cultures, whereas TRPC1, TRPC2, TRPC4 were amplified more than 10 (TRPC1 and TRPC2) and 11 (TRPC4) times from the 13 performed PCRs (Figure 3-5-a). The difference in the expression pattern from the enriched and FACS-sorted astrocytes shows clearly how few contaminating cells could change the expression pattern of astrocytes. The RT-PCR results using 50 sorted microglia cells per reaction, showed that only TRPC4 was consistently amplified in the 3 performed PCRs (Figure 3-5-b). The expression patterns of the sorted astrocytes and microglia together do not fit the PCR results of the enriched astrocyte culture i.e. astrocytes and microglia are not the TRPC6- and TRPC7-expressing cells. This indicates that there is one (or more) other cell type (s) in the astrocyte cultures which could be the source of the TRPC6 and C7 detection. The FACS analysis revealed a third population of unstained cells i.e. GLAST-negative and CD11b-negative. Oligodendrocytes have been always reported to be present in the astrocytes culture in a low number (Chen et al., 2007b), and therefore oligodendrocytes could be the third cell population in the astrocytes cultures. In addition, a previous work has reported that TRPC6 is expressed in oligodendrocytes (Paez et al., 2011) which favor the possibility that oligodendrocytes are the (at least) TRPC6-expressing cells. However, this has to be further proved and confirmed by sorting separately the oligodendrocytes

and having them analyzed by PCR. Interestingly, comparing the RT-PCR results with the transcriptome data obtained from the GLAST-sorted astrocytes revealed more or less the same tendency, i.e. TRPC1. TRPC2 and TRPC3 were commonly detected with both methods (Figure 3-6). However, TRPC7 was detected in the transcriptome but not in the RT-PCR, even though the TRPC7 primers did amplify TRPC7 fragment using the enriched culture RNA which rule out the problem of primers (Figure 3-2). The reason behind this discrepancy is not clear yet. In addition, the expression levels of TRPC transcripts are comparable with the transcripts of other genes which are already described to play a role in Ca^{2+} signaling of astrocytes such as type 2 IP3R (Kanemaru et al., 2013), like TRPC1 and TRPC3 (Figure 3-6)

The present work focused on TRPC3 as I always could detect its transcripts in all performed RT-PCR from the GLAST-sorted astrocytes. In addition, TRPC1 was detected more than 10 times in a total of 13 PCRs. However, the amplified fragments in the RT-PCR are only 200 bp, therefore the full length cDNAs of TRPC3 and TRPC1 cDNAs were amplified from astrocytes, subcloned in pUC19 and sequenced (Figure 3-7). The sequencing of the TRPC1 clones revealed the presence of the extended TPRC1 variant, so called TRPC1 very long (VL), and a splice variant which has been published by Ong et al. (Ong et al., 2013) called TRPC1 ϵ lacking an EcoRV restriction cite due to the absence of 21 bp fragment in exon 5. However, the TRPC1 ϵ identified in astrocytes (Figure 3-7) lacks also the exon 3. In addition to the TRPC1 VL and TRPC1 $\epsilon\Delta$ exon3 variant, the TRPC1 VL Δ exon3 was identified. The presence of these TRPC variants in astrocytes could play a role in the Ca^{2+} homeostasis mediated by TRPC and ORAI channels.

4.2 Roles of TRPC1 and TRPC3 proteins in astrocytes

Upon a decrease in the ER Ca^{2+} concentrations, STIM proteins in the ER membrane assemble and interact with ORAI channels in the plasma membrane leading to Ca^{2+} influx into the cell from the extracellular space. Several TRPC channels have been discussed to be involved in the process (Venkatachalam et al., 2002). In pancreatic and salivary gland cells, the knockdown of TRPC3

gene expression reduced significantly Ca^{2+} entry when ER Ca^{2+} stores are depleted (Kim et al., 2011). Similarly, knockdown of TRPC3 gene expression in dorsal root ganglion cells gave similar results (Alkhani et al., 2014). In salivary gland acinar cells isolated from TRPC1 gene-deficient mice exhibited impaired Ca^{2+} entry (Liu et al., 2007). In the present work, astrocytes isolated from wild-type mice showed a prominent Ca^{2+} entry after store depletion with the SERCA pump blockers thapsigargin or cyclopiazonic acid followed by Ca^{2+} readdition (Figure 3-9). However, Ca^{2+} entry induced by store depletion / Ca^{2+} readdition protocol was not affected in astrocytes isolated from TRPC3/TRPC6 gene-deficient mice. On the other hand, astrocytes isolated from TRPC1 gene-deficient mice did have a reduced Ca^{2+} release in the presence of SERCA pump blocker and slightly increased Ca^{2+} entry (Figure 3-19). These results clearly indicate that TRPC3 plays no role in the ORAI-dependent Ca^{2+} entry in cultured mouse cortical astrocytes. However TRPC1 seem to affect negatively the ORAI-dependent Ca^{2+} entry in astrocytes, and moreover, the deletion of TRPC1 gene reduced the Ca^{2+} release in the presence of SERCA pump inhibitor. A Similar tendency was also observed in TRPC1 siRNA-treated SH-SY5Y cells where a smaller Ca^{2+} release after thapsigargin treatment was observed (Selvaraj et al., 2012). The reduction of Ca^{2+} release from the ER in TRPC1 deficient astrocytes (Figure 3-19) could indicate a possible role of TRPC1 in the Ca^{2+} homeostasis of the endoplasmic reticulum. Accordingly, my observation in the astrocytes could fit with what has been previously reported on TRPC1 by Berbey et al. that it localizes in the ER membrane of skeletal muscle cells and acts as a leak channel (Berbey et al., 2009).

4.3 Dissection of OAG-induced Ca^{2+} signals in astrocytes

DAG is an endogenous activator for TRPC2, TRPC3, TRPC6 and TRPC7 leading to the opening of these channels and a subsequent Ca^{2+} influx (Hofmann et al., 1999). DAG is formed by activation of PLC after activation of Gq protein coupled receptors or receptor tyrosine kinases. The DAG analogue OAG is an exogenous activator for DAG-sensitive TRPC channels (Hofmann et al., 1999), and it can be used externally in experiments. The application of 100 μM OAG on wild-type astrocytes led to Ca^{2+} oscillations in the presence of

extracellular Ca^{2+} (Figure 3-10-a). However, when extracellular Ca^{2+} was removed, OAG was still able to induce Ca^{2+} oscillations with smaller amplitudes (Figure 3-10-c). Hisatsun et al. suggested that the increase in cytoplasmic Ca^{2+} concentration observed after OAG stimulation in the absence of extracellular Ca^{2+} is mediated by the activation of PLC by OAG. Eventually, the activation of PLC leads to the cleavage of PIP₂ into DAG and IP₃ which then induces Ca^{2+} release from the ER via IP₃-receptor channels (Hisatsune et al., 2005). The question to be answered in my experiment was: Are the Ca^{2+} oscillation, in the presence of extracellular Ca^{2+} in cultured astrocytes, deriving from IP₃-induced Ca^{2+} release and subsequent Ca^{2+} influx through ORAI channels, or in addition to the IP₃/ORAI pathways, through TRPC channels? To exclude intracellular Ca^{2+} release as source for the OAG-mediated Ca^{2+} oscillations, intracellular Ca^{2+} stores were permanently emptied by blocking the SERCA pump, which also leads to constitutive activation of ORAI. Application of OAG on top of this condition led eventually to an additional Ca^{2+} influx (Figure 3-10-d), which was not mediated via PKC since the PMA, a PKC activator, had no influence (Figure 3-10-e). In the current study, several TRPC gene-deficient mice have been used to dissect the role of TRPCs in astrocytes and whether they are the target of OAG. In the RT-PCR from the GLAST-sorted astrocytes only TRPC2 and TRPC3 were detected from the TRPC members which can be activated via DAG or experimentally via OAG. Therefore the main focus was on TRPC3. Application of OAG protocol on astrocytes isolated from TRPC3 gene-deficient mice revealed a significant reduction in the number of responding cells as well as the number of oscillation per responding cell (Figure 3-11-b). The same was seen in astrocytes isolated from TRPC3/TRPC6 gene-deficient mice (Figure 3-11-d), whereas Ca^{2+} signals in astrocytes isolated from TRPC6 gene-deficient mice did not differ from those of wild-type astrocytes (Figure 3-11-c). However, in good agreement with the PCR results revealing no TRPC6 expression, the OAG-mediated Ca^{2+} signals were not affected in astrocytes from TRPC6 deficient mice. Thus the major Ca^{2+} influx mediated by OAG is TRPC3-dependent. The residual OAG-mediated Ca^{2+} oscillations in astrocytes from TRPC3 gene-deficient mice might have been mediated via TRPC2. A study on rat astrocytes showed that OAG induced Ca^{2+} signals in astrocytes, and TRPC3 was suggested to be involved (Grimaldi et al., 2003).

However, the efficiency of the siRNA used in this study was never shown. To further confirm the presence of a functional TRPC3 in astrocytes, whole cell patch clamp technique was employed. Before trying to isolate TRPC3 currents in astrocytes, the experimental conditions to record these currents were optimized in HEK293 cells expressing TRPC3 cDNA. Under conditions of 1 mM extracellular Ca^{2+} and 100 nM in the patch pipette, the OAG was not able to induce any measurable currents (Figure 3-12) even though many published work have been using those conditions (Trebak et al., 2003). Only after omitting the intra- and extracellular Ca^{2+} , OAG was able to induce consistently TRPC3 currents (Figure 3-12). This suggests that TRPC3 channel activity is highly Ca^{2+} sensitive and Ca^{2+} shows a negative feedback on TRPC3 activity which is more pronounced from the cytoplasmic side. A similar observation was reported for TRPC3 (Lintschinger et al., 2000) describing that TRPC3 activity depends on extracellular Ca^{2+} . Using our optimized conditions (0 Ca^{2+} intra- and extracellular) in whole cell patch clamp, OAG also induced currents in astrocytes (Figure 3-13) which revealed very similar current-voltage relation compared to the one from TRPC3 channel in HEK cells. However, the success rate is low. Endogenous TRP currents are very small, and in most measured astrocytes chloride currents were present which rendered the characterization of the endogenous TRPC3 current difficult. A complementary approach, astrocytes isolated from moonwalker (MWK) mice. They are heterozygous for a gain of function mutation in TRPC3 gene. Interestingly astrocytes isolated from these mice showed a higher basal Ca^{2+} levels and exhibited higher Ca^{2+} influx after readdition of extracellular Ca^{2+} (Figure 3-17). The observation that astrocytes from MWK mice have higher basal Ca^{2+} levels further confirms the fact that TRPC3 is functionally expressed in astrocytes.

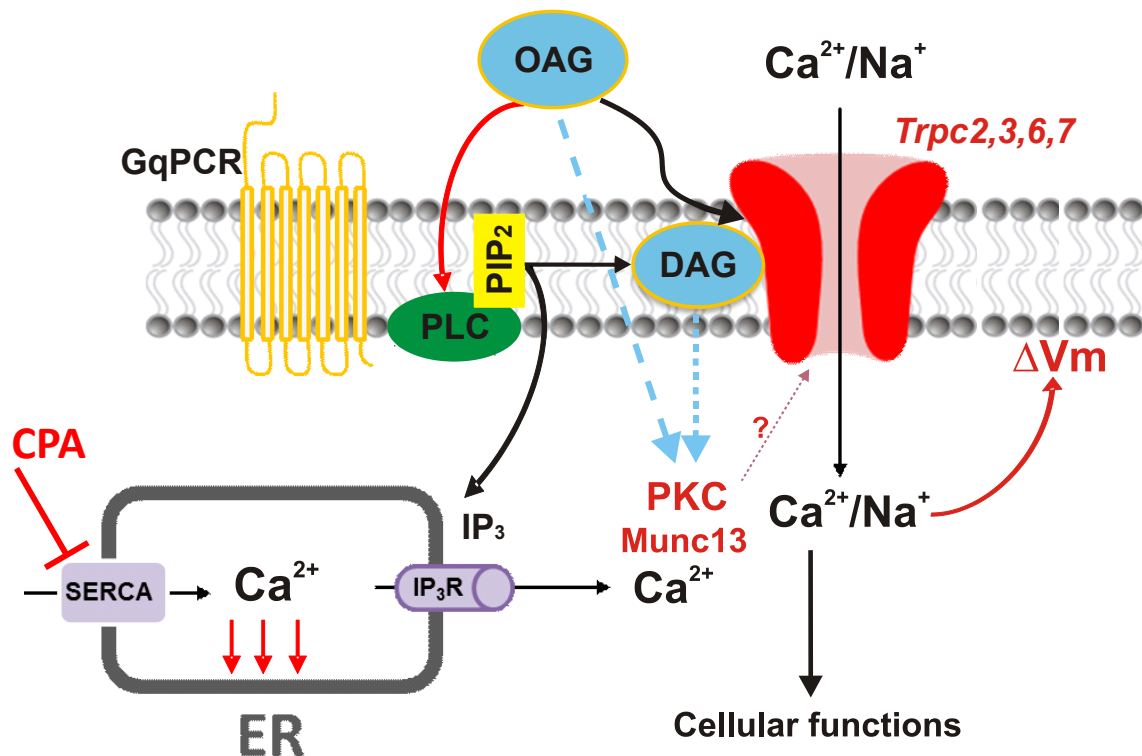


Figure 4-1 **OAG/DAG-dependent cation entry**. Representation of the possible OAG pathways, including: 1) OAG induces Ca²⁺ (and Na⁺) influx via DAG-sensitive TRPC channels similar to DAG (DAG results from the activation of PLC by Gq proteins). 2) OAG could activate the PLC which leads to IP₃-induced Ca²⁺ release which in turn activates ORAI. 3) OAG activates PKC which most probably has no effect of TRPC channels in astrocytes.

4.4 Role of TRPC1 in the OAG-induced TRPC3 channel activity

Although TRPC1 was the first mammalian TRP to be cloned; its mechanism of activation remains unclear. However, many reports have shown that TRPC1 could interact with TRPCs, and also with many other TRP and ORAI proteins (Dietrich et al., 2014). The well characterized interaction partners of TRPC1 are TRPC4 and TRPC5 at least in cell culture where TRPC1, if forming heterotetramers with TRPC4 or TRPC5, changes the current-voltage relationships (Strubing et al., 2001). TRPC1 has been shown to also interact with TRPC3 in skeletal muscle cells using co-immunoprecipitation (Cheung et al., 2011). In HEK cells TRPC1 did not change the current-voltage relationship of TRPC3 but shifted the reversal towards negative potentials and thus they concluded that it reduces its Ca²⁺ permeability (Storch et al., 2012). In the

current work, TRPC1 VL cDNA expressing cells did not show any currents when stimulated with OAG (Figure 3-20-e). However, when the TRPC3 cDNA was co-transfected with TRPC1 VL cDNA in HEK, the TRPC3 currents were significantly smaller compared to the pure TRPC3 current (Figure 3-20-a). Despite the reduction in the TRPC3 currents in presence of TRPC1 VL, the current-voltage relationships of TRPC3 with TRPC1 VL did not differ from the TRPC3 alone. This was further confirmed when TRPC1 VL cDNA was co-expressed with the TRPC3 MWK in HEK cells, where the constitutive TRPC3 MWK currents as well as the basal Ca^{2+} levels were reduced (Figure 3-22-a-c). Storch et al. observed only a slight decrease in the inward currents and a slight increase in the outward currents after co-transfection of TRPC1 and TRPC3 cDNAs, in contrast to the inhibitory effect of TRPC1 VL on TRPC3 channel activity presented in this work (Figure 3-20-a). The TRPC1 VL variant which includes a 5' extension and a new start codon CUG that adds 82 amino acids to the known sequence was used. The additional amino acid sequence of TRPC1 VL could be responsible for the effect on the TRPC3 current observed in this study. Astrocytes do express the TRPC1 VL variant, and in addition the TRPC1 VL Δ exon3 variant and TRPC1 ϵ Δ exon3 variant, which is a very long TRPC1 variant lacking exon3 and 21 bp within exon5 (Figure 3-7). The effect of TRPC1 VL was studied on the OAG-induced Ca^{2+} oscillations in astrocytes, in which TRPC3 was found to be involved. The results obtained from the OAG protocol in astrocytes isolated from TRPC1 gene-deficient mice showed that significantly more cells respond to OAG and more oscillations could be detected per cell when compared to wild-type astrocytes (Figure 3-21-b). This observation further enforces the fact that TRPC1 VL exerts a negative effect on TRPC3 activity. The exact mechanism of the TRPC1 effect is not clear yet, but several scenarios could be proposed. Since physical interaction of TRPC1 VL with TRPC3 was shown by co-immunoprecipitation (results from Laura Hofmann in our laboratory), it could be that: 1) both proteins form a heteromeric channel that is less active than the homomeric TRPC3, 2) TRPC1 VL acts as an additional non-conducting "beta" subunit for the homomeric TRPC3 channel and modulates its gating properties, or 3) TRPC1 VL reduces the membrane expression of TRPC3. All those possibilities have to be addressed with proper

biochemical techniques to have a deeper understanding on the TRPC1-TRPC3 interaction.

4.5 Role of TRPC1 and TRPC3 in astrocytes migration and astrogliosis

In healthy brain, astrocytes play critical roles in energy supply, homeostasis of ions and transmitters, synapse function, synaptic remodeling and blood flow. Astrocytes could enter into a reactive state called astrogliosis which is an abnormal increase in the migration and proliferation of astrocytes due to the damaged neurons (Silver and Miller, 2004). Moreover, traumatic brain injury results in the destruction of the brain-blood barrier which leaves the neurons and astrocytes exposed, in addition to molecules released from dead cells, to the blood fluid and blood cells. Many large and small molecules are involved in triggering the astrogliosis including cytokines and growth factors (IL6, LIF, CNTF, IL1, IL10, TGF β , TNF α , INF γ), mediators of innate immunity (LPS and other Toll-like receptor ligands), neurotransmitters and modulators (glutamate, noradrenalin), small molecules released by cell injury (ATP), and molecules of oxidative stress (nitric oxide, reactive oxygen species) (Sofroniew, 2009). Most of these molecules are modulators of the G protein coupled receptors which could involve an increase in the cytoplasmic Ca²⁺ concentration and therefore Ca²⁺ is closely related in the mechanism underlying the astrogliosis and glial scar formation after brain injury. As shown by Gao et al. that BAPTA-AM, a Ca²⁺ chelator, reduces the GFAP expression and the glial scar formation after brain injury, and concluded that the traumatic brain injury triggers Ca²⁺ influx which mediates in the end the astrogliosis (Gao et al., 2013). In the present study, several TRPC channels, which are activated downstream of Gq-coupled activation, are shown to be expressed in astrocytes. The deletion of TRPC3 gene resulted in reduced OAG- mediated Ca²⁺ influx in astrocytes, but deleting TRPC1 gene enhanced this Ca²⁺ influx (Figure 3-11 and Figure 3-21). Therefore, we investigated the role of TRPC3 and TRPC1 in astrocytes migration and astrogliosis. A scratch assay as an *in vitro* experiment for cell migration was applied as cells might behave similar in this *in vitro* experiment as they do after injury *in vivo*. Astrocytes isolated from TRPC3 gene-deficient mice

had a significant reduction in the migration rate as compared to wild-type astrocytes (Figure 3-14). However, astrocytes isolated from TRPC1 gene-deficient mice exhibited a significant increase in the migration rate as compared to wild-type astrocytes (Figure 3-23). The astrocytes migration results seem to correlate with the changes in the Ca^{2+} influx observed in TRPCs deficient astrocytes, i.e. the TRPC3 deficient astrocytes have less OAG-induced Ca^{2+} influx and less migration rate, and vice versa, TRPC1 deficient astrocytes have more OAG-induced Ca^{2+} influx and more migration rate. In the *in vivo* brain injury, the TRPC3 gene-deficient mice exhibited a significantly reduced area of astrogliosis (measured as area of GFAP-positive cells) and reduced cortical edema (Figure 3-15). Again the TRPC1/TRPC5 gene-deficient mice showed the opposite effects i.e. an increased astrogliosis area and increased cortical edema as compared to wild-type mice (Figure 3-24). This consistency observed in the TRPC3 and TRPC1 gene-deficient mice, respectively, strongly suggests that the Ca^{2+} influx via TRPC3 plays a critical role in the Ca^{2+} signaling required for astrogliosis. This Ca^{2+} influx is enhanced when TRPC1 is deleted and thereby astrogliosis is increased. The relation of Ca^{2+} signaling and astrogliosis was also reported by Kanemaru et al. where they showed that type 2 IP3 receptor gene-deficient mice had impaired reactive astrogliosis and concluded that the Ca^{2+} signaling via IP3 receptor type 2 is required for astrogliosis (Kanemaru et al., 2013). Next, we asked the question whether Ca^{2+} influx by itself could lead to astrogliosis without brain injury? To answer this question, we used the MWK mice, since astrocytes from these mice have increased basal Ca^{2+} (Figure 3-17). The analysis of non-injured brain slices from MWK mice did not show any signs of spontaneous astrogliosis when stained with anti-GFAP (Figure 3-18). Hence that Ca^{2+} influx alone is not sufficient to induce astrogliosis, but an injury is required to initiate the process. The findings of the current work strongly suggest that in particular TRPC3 channel is responsible for Ca^{2+} entry during brain injuries, and therefore is involved in the astrogliosis and glial scar formation after brain injury. Controlling the intensity of astrogliosis could help to ameliorate the outcome after brain injuries and TRPC channels could therefore be targeted to control astrogliosis.

4.6 Voltage-gated Na^+ (NaV) and Ca^{2+} (CaV) channels in astrocytes

Transcripts of genes encoding NaVs and CaVs have been identified in astrocytes by RNA sequencing (Figure 3-25 and Figure 3-28). Many transcripts from the genes encoding the ion conduction genes of L-type CaVs (CaV1.2 and CaV1.3) and P/Q-type CaV (CaV2.1) were identified, as well as transcripts of the CaV β and CaV α 2 δ genes (Figure 3-25). In rat astrocytes, only members of the CaV α 1 subunit genes have been investigated, but no functional analysis have been conducted in that study (Latour et al., 2003). Regarding the other auxiliary subunits, β , γ and α 2 δ subunits, little is known about their presence and function in astrocytes. The current study provides a complete overview about the expression pattern and expression levels of auxiliary CaV of the β and α 2 δ subunit genes in mouse cortical astrocytes. The first evidence for the presence of functional CaVs was obtained after increasing the extracellular $[\text{K}^+]$ concentration that leads to cell depolarization and CaVs should be activated. This is in fact the case as shown in Figure 3-26-a. Astrocytes used in this study exhibited Ca^{2+} response towards potassium depolarization in Fura-2 experiment which was absent in microglia cells. This type of astrocytic response to high potassium has been reported previously in brain slices but it was attributed to glutamate released by depolarized neurons which subsequently activates Ca^{2+} signals in astrocytes (Beck et al., 2004; Carmignoto et al., 1998). Neurons do not survive in the astrocyte culture within the first week of culturing (Schildge et al., 2013), and most of the conducted experiments were performed two to three weeks after the isolation. Therefore, it is highly unlikely that the Ca^{2+} signals observed in astrocytes after high potassium depolarization depend on neurons. To further investigate the source of the potassium-induced Ca^{2+} influx in astrocytes, whole cell patch clamp experiments were performed with conditions allowing to measure CaVs currents. As expected from the transcriptome analysis, inward Ba^{2+} (used instead of Ca^{2+}) currents were observed in astrocytes isolated from new born mice cortices. However, two types of inward currents were observed; one has maximum amplitude at -20 mV and the other one at 10 mV. When analyzing the currents at different voltage steps, the

current with a maximum at -20 mV had the typical shape of a voltage-gated Na^+ current with fast inactivation kinetics, and the one at 10 mV had slow inactivation kinetics which is characteristic for the voltage-gated Ca^{2+} channels. Moreover, the current at -20 mV disappeared when Na^+ was replaced by cesium which does not permeate NaVs, and the 10 mV current persisted under this condition (Figure 3-27). Additionally, the use of TTX, a specific blocker of the NaVs, did abolish the Na^+ current in cultured astrocytes. The removal of extracellular barium abolished the CaVs current (Figure 3-29). Those results correlate nicely with the transcriptome data from astrocytes where $\text{NaV}\alpha 1$ and $\text{NaV}\beta$ subunit genes were identified. In 1983, Nowak and colleagues have found evidence of Na^+ channels in cortical astrocytes using patch clamp experiments and specific activators like veratridine and scorpion toxin (Nowak et al., 1984). In 1987, the same group have shown again in a follow up study that the Na^+ currents measured in cortical astrocytes are TTX-sensitive but require a concentration more than 1 μM to achieve a complete block (Nowak et al., 1987). Later, another study showed the presence of the Na^+ channel genes in rat cortical astrocytes (Gautron et al., 1992). Despite the early discovery of Na^+ channels in astrocytes, very few studies have been conducted towards their functional role. Black et al. have shown that the $\text{NaV}1.5$ protein is upregulated in astrocytes from post-mortem multiple sclerosis patients (Black et al., 2010). Apparently, NaVs in astrocytes are also relevant under pathological conditions.

The HVA Ca^{2+} channels consist of L- ($\text{CaV}1.1$, $\text{CaV}1.2$, $\text{CaV}1.3$ and $\text{CaV}1.4$), P/Q- ($\text{CaV}2.1$), N- ($\text{CaV}2.2$) and R- ($\text{CaV}2.3$) types, and the LVA consists mainly of the T-type Ca^{2+} channels. However, the L-type $\text{CaV}1.3$ Ca^{2+} channel is activated at more negative potential than $\text{CaV}1.2$, therefore shares some properties with $\text{CaV}3$ channels (Koschak et al., 2001). The Ca^{2+} currents measured in this work from cortical astrocytes did open at -50 mV but had a maximum at 0 to 10 mV (Figure 3-29). This corresponds to the LVA channels on one hand since they open at a voltage less than -40 mV, and to HVA channels on the other hand because they had a maximum at positive potentials which is characteristic for the HVA members. This indicates that the Ca^{2+} currents in astrocytes are composed of more than one channel and most probably from $\text{CaV}1.2$, $\text{CaV}1.3$ and $\text{CaV}2.1$. In the transcriptome data, mainly

CaV1.2, CaV1.3 and CaV2.1 are detectable (Figure 3-25). Most probably the first component of the astrocytic Ca^{2+} current is maybe contaminated with some CaV3 channels. The second component could be Cav1.2 and / or Cav2.1. Specific Ca^{2+} channel blockers were employed to distinguish the currents, although for the CaV3 channels there are no specific antagonists available. 2 μM ω -agatoxin-IVA (CaV2.1) and 1 μM ω -conotoxin-GVIA (CaV2.2) blocked 5% and 3% respectively, while the CaV2.3 blocker SNX482 (300 nM) did block 12% and the L-type blocker verapamil (10 μM) blocked 56% of the Ca^{2+} current in astrocytes from wild-type mice. The combination of all blockers as one cocktail led to 65% blockade of the current; the residual current behaved similar in terms of current-voltage relationship which may indicate that no saturating concentrations of blockers were used. Although considerable CaV2.1 transcripts were identified, CaV2.1 seems to not contribute much to the overall current. On the other hand the L-type Ca^{2+} channel blocker verapamil blocked more than 50% of the current, while nifedipine (another L-type blocker) blocked less than 30%. isradipine, another L-type blocker, was used leading to 25% inhibition at 1 μM and 52% inhibition at 10 μM . However, at 100 μM isradipine blocked 82% of the current. The need of high isradipine concentrations to block the CaV currents in astrocytes suggests that CaV1.3 is one of the main functional CaVs in astrocytes, which correlates with the transcriptome data that CaV1.3 is highly expressed in astrocytes. The sensitivity of CaV1.3 towards the dihydropyridine derivatives is shown to be 20 fold less compared to CaV1.2 when nimodipine was used (Xu and Lipscombe, 2001). Summing up, the 82% isradipine block with the block by ω -agatoxin-IVA, ω -conotoxin-GVIA and SNX482, results in a complete block of CaV current in astrocytes, very similar to the block by the non-specific blocker Ni^{2+} . In summary, the different approaches suggest that CaV currents in cortical astrocytes are derived from mainly L-type Ca^{2+} channels (CaV1.2 and CaV1.3) and minor contribution of P/Q- (CaV2.1) and maybe R- /CaV2.3) types. This was seen differently by Burgos et al. (Burgos et al., 2007) who observed that the main CaV in the astrocytes is the P/Q-type (CaV2.1) (about 60%) and L-type (about 40%) Ca^{2+} channels.

CaV β 1, CaV β 2, CaV β 3 and CaV β 4 subunit genes of the voltage-gated Ca^{2+} channels were detected in the transcriptome from GLAST-sorted astrocytes.

Since CaV β subunits are shown to be associated with the HVA pore forming α 1 subunits (Dolphin, 2003) and involved in its trafficking to the plasma membrane and also gating properties. As mentioned above that the main component of the CaV currents in astrocytes is mediated via the L-type Ca $^{2+}$ channels (CaV1.2 and CaV1.3). Thus the role of CaV β 2 subunit in CaV currents in astrocytes were addressed since it is shown to associate preferentially with the L-type channels (Campiglio and Flucher, 2015). The role CaV β 3 subunit in the astrocytic CaV current was also analyzed, as it might preferentially associate with the CaV2 channels (Berrou et al., 2005). CaV current in astrocytes isolated from CaV β 3 gene-deficient mice did not show any significant difference as compared to the corresponding wild-type astrocytes in terms of amplitude and inactivation kinetics (Figure 3-30). In contrast, the astrocytes isolated from the CaV β 2 gene-deficient mice did have significantly reduced CaV current amplitude as well as significantly faster inactivation kinetics compared to astrocytes from wild-type mice (Figure 3-31). This fits with results from Weissgerber and colleagues (Weissgerber et al., 2006) in embryonic cardiomyocytes. They showed that the current amplitude was reduced and was faster inactivated in cells from CaV β 2 gene-deficient mice. The CaV current in astrocytes could have an impact on the physiological role of astrocytes either in healthy or in pathological conditions, similar to the effect of Ca $^{2+}$ influx via TRPC3. Ca $^{2+}$ has been suggested to play an important role in the traumatic brain injury where it accumulates in the astrocytes via the different cellular Ca $^{2+}$ sources and causes cell death and dysfunction (Gurkoff et al., 2013). However, clinical trials in the early nineties on patients with acute traumatic brain injury showed modest improvement of the outcome after treating the patients with the L-type Ca $^{2+}$ blocker nimodipine (Bailey et al., 1991), but those effect are in dispute (Vergouwen et al., 2006). On the other hand nimodipine is still approved for treatment of ischemic deficits following aneurysm hemorrhage in the brain (Fachinformation Nimodipin 2014). In the current work, the L-type CaVs were shown to contribute essentially to CaV currents in astrocytes. Under injury conditions gene expression and channel activity could become different than in healthy conditions and therefore other CaVs could be recruited in astrocytes. The blockers for CaV2.1, CaV2.2 and CaV2.3 are snail and spider toxins and

they are proteins. These properties limit their therapeutic use. Hopefully, small molecules will be developed, which do block these CaV2 channels and which may offer an option for treatment in traumatic brain injury.

5 References

1. Adebisi, A., Zhao, G., Narayanan, D., Thomas-Gatewood, C.M., Bannister, J.P., and Jaggar, J.H. (2010). Isoform-selective physical coupling of TRPC3 channels to IP3 receptors in smooth muscle cells regulates arterial contractility. *Circ Res* 106, 1603-1612.
2. Akbulut, Y., Gaunt, H.J., Muraki, K., Ludlow, M.J., Amer, M.S., Bruns, A., Vasudev, N.S., Radtke, L., Willot, M., Hahn, S., *et al.* (2015). (-)-Englerin A is a potent and selective activator of TRPC4 and TRPC5 calcium channels. *Angew Chem Int Ed Engl* 54, 3787-3791.
3. Alkhani, H., Ase, A.R., Grant, R., O'Donnell, D., Groschner, K., and Seguela, P. (2014). Contribution of TRPC3 to store-operated calcium entry and inflammatory transductions in primary nociceptors. *Mol Pain* 10, 43.
4. Ambudkar, I.S. (2014). Ca^{2+} signaling and regulation of fluid secretion in salivary gland acinar cells. *Cell Calcium* 55, 297-305.
5. Anderson, M.A., Ao, Y., and Sofroniew, M.V. (2014). Heterogeneity of reactive astrocytes. *Neurosci Lett* 565, 23-29.
6. Anderson, M.A., Burda, J.E., Ren, Y., Ao, Y., O'Shea, T.M., Kawaguchi, R., Coppola, G., Khakh, B.S., Deming, T.J., and Sofroniew, M.V. (2016). Astrocyte scar formation aids central nervous system axon regeneration. *Nature* 532, 195-200.
7. Arikath, J., and Campbell, K.P. (2003). Auxiliary subunits: essential components of the voltage-gated calcium channel complex. *Curr Opin Neurobiol* 13, 298-307.
8. Astori, S., Wimmer, R.D., Prosser, H.M., Corti, C., Corsi, M., Liaudet, N., Volterra, A., Franken, P., Adelman, J.P., and Luthi, A. (2011). The $\text{Ca}_v3.3$ calcium channel is the major sleep spindle pacemaker in thalamus. *Proc Natl Acad Sci U S A* 108, 13823-13828.
9. Bailey, I., Bell, A., Gray, J., Gullan, R., Heiskanen, O., Marks, P.V., Marsh, H., Mendelow, D.A., Murray, G., Ohman, J., *et al.* (1991). A trial of the effect of nimodipine on outcome after head injury. *Acta Neurochir (Wien)* 110, 97-105.
10. Barclay, J., Balaguero, N., Mione, M., Ackerman, S.L., Letts, V.A., Brodbeck, J., Canti, C., Meir, A., Page, K.M., Kusumi, K., *et al.* (2001). Ducky mouse phenotype of epilepsy and ataxia is associated with mutations in the *Cacna2d2* gene and decreased calcium channel current in cerebellar Purkinje cells. *J Neurosci* 21, 6095-6104.
11. Beck, A., Nieden, R.Z., Schneider, H.P., and Deitmer, J.W. (2004). Calcium release from intracellular stores in rodent astrocytes and neurons in situ. *Cell Calcium* 35, 47-58.
12. Beck, A., Speicher, T., Stoerger, C., Sell, T., Dettmer, V., Jusoh, S.A., Abdulmughni, A., Cavalie, A., Philipp, S.E., Zhu, M.X., *et al.* (2013). Conserved gating elements in TRPC4 and TRPC5 channels. *J Biol Chem* 288, 19471-19483.
13. Becker, E.B. (2014). The Moonwalker mouse: new insights into TRPC3 function, cerebellar development, and ataxia. *Cerebellum* 13, 628-636.

14. Becker, E.B., Oliver, P.L., Glitsch, M.D., Banks, G.T., Achilli, F., Hardy, A., Nolan, P.M., Fisher, E.M., and Davies, K.E. (2009). A point mutation in TRPC3 causes abnormal Purkinje cell development and cerebellar ataxia in moonwalker mice. *Proc Natl Acad Sci U S A* 106, 6706-6711.
15. Berbey, C., Weiss, N., Legrand, C., and Allard, B. (2009). Transient receptor potential canonical type 1 (TRPC1) operates as a sarcoplasmic reticulum calcium leak channel in skeletal muscle. *J Biol Chem* 284, 36387-36394.
16. Berggren, P.O., Yang, S.N., Murakami, M., Efanov, A.M., Uhles, S., Kohler, M., Moede, T., Fernstrom, A., Appelskog, I.B., Aspinwall, C.A., *et al.* (2004). Removal of Ca²⁺ channel beta3 subunit enhances Ca²⁺ oscillation frequency and insulin exocytosis. *Cell* 119, 273-284.
17. Berrou, L., Dodier, Y., Raybaud, A., Tousignant, A., Dafi, O., Pelletier, J.N., and Parent, L. (2005). The C-terminal residues in the alpha-interacting domain (AID) helix anchor CaV beta subunit interaction and modulation of CaV2.3 channels. *J Biol Chem* 280, 494-505.
18. Black, J.A., Newcombe, J., and Waxman, S.G. (2010). Astrocytes within multiple sclerosis lesions upregulate sodium channel Nav1.5. *Brain* 133, 835-846.
19. Boulay, G., Zhu, X., Peyton, M., Jiang, M., Hurst, R., Stefani, E., and Birnbaumer, L. (1997). Cloning and expression of a novel mammalian homolog of Drosophila transient receptor potential (Trp) involved in calcium entry secondary to activation of receptors coupled by the Gq class of G protein. *J Biol Chem* 272, 29672-29680.
20. Brechard, S., Melchior, C., Plancon, S., Schenten, V., and Tschirhart, E.J. (2008). Store-operated Ca²⁺ channels formed by TRPC1, TRPC6 and Orai1 and non-store-operated channels formed by TRPC3 are involved in the regulation of NADPH oxidase in HL-60 granulocytes. *Cell Calcium* 44, 492-506.
21. Brixel, L.R., Monteilh-Zoller, M.K., Ingenbrandt, C.S., Fleig, A., Penner, R., Enklaar, T., Zabel, B.U., and Prawitt, D. (2010). TRPM5 regulates glucose-stimulated insulin secretion. *Pflügers Arch* 460, 69-76.
22. Brose, N., and Rosenmund, C. (2002). Move over protein kinase C, you've got company: alternative cellular effectors of diacylglycerol and phorbol esters. *J Cell Sci* 115, 4399-4411.
23. Buraei, Z., and Yang, J. (2013). Structure and function of the beta subunit of voltage-gated Ca²⁺ channels. *Biochim Biophys Acta* 1828, 1530-1540.
24. Burgess, D.L., Jones, J.M., Meisler, M.H., and Noebels, J.L. (1997). Mutation of the Ca²⁺ channel beta subunit gene Cchb4 is associated with ataxia and seizures in the lethargic (lh) mouse. *Cell* 88, 385-392.
25. Burgos, M., Pastor, M.D., Gonzalez, J.C., Martinez-Galan, J.R., Vaquero, C.F., Fradejas, N., Benavides, A., Hernandez-Guijo, J.M., Tranque, P., and Calvo, S. (2007). PKCepsilon upregulates voltage-dependent calcium channels in cultured astrocytes. *Glia* 55, 1437-1448.
26. Cabezas, R., Avila, M., Gonzalez, J., El-Bacha, R.S., Baez, E., Garcia-Segura, L.M., Jurado Coronel, J.C., Capani, F., Cardona-Gomez, G.P., and Barreto, G.E. (2014). Astrocytic modulation of blood brain barrier: perspectives on Parkinson's disease. *Front Cell Neurosci* 8, 211.

27. Camacho Londono, J.E., Tian, Q., Hammer, K., Schroder, L., Camacho Londono, J., Reil, J.C., He, T., Oberhofer, M., Mannebach, S., Mathar, I., *et al.* (2015). A background Ca^{2+} entry pathway mediated by TRPC1/TRPC4 is critical for development of pathological cardiac remodelling. *Eur Heart J* 36, 2257-2266.
28. Campiglio, M., and Flucher, B.E. (2015). The role of auxiliary subunits for the functional diversity of voltage-gated calcium channels. *J Cell Physiol* 230, 2019-2031.
29. Cao, E., Liao, M., Cheng, Y., and Julius, D. (2013). TRPV1 structures in distinct conformations reveal activation mechanisms. *Nature* 504, 113-118.
30. Carmignoto, G., Pasti, L., and Pozzan, T. (1998). On the role of voltage-dependent calcium channels in calcium signaling of astrocytes in situ. *J Neurosci* 18, 4637-4645.
31. Catterall, W.A., Perez-Reyes, E., Snutch, T.P., and Striessnig, J. (2005). International Union of Pharmacology. XLVIII. Nomenclature and structure-function relationships of voltage-gated calcium channels. *Pharmacol Rev* 57, 411-425.
32. Cens, T., Rousset, M., Leyris, J.P., Fesquet, P., and Charnet, P. (2006). Voltage- and calcium-dependent inactivation in high voltage-gated Ca^{2+} channels. *Prog Biophys Mol Biol* 90, 104-117.
33. Chang, B., Heckenlively, J.R., Bayley, P.R., Brecha, N.C., Davisson, M.T., Hawes, N.L., Hirano, A.A., Hurd, R.E., Ikeda, A., Johnson, B.A., *et al.* (2006). The nob2 mouse, a null mutation in *Cacna1f*: anatomical and functional abnormalities in the outer retina and their consequences on ganglion cell visual responses. *Vis Neurosci* 23, 11-24.
34. Chaudhari, N. (1992). A single nucleotide deletion in the skeletal muscle-specific calcium channel transcript of muscular dysgenesis (mdg) mice. *J Biol Chem* 267, 25636-25639.
35. Chaudhuri, P., Colles, S.M., Damron, D.S., and Graham, L.M. (2003). Lysophosphatidylcholine inhibits endothelial cell migration by increasing intracellular calcium and activating calpain. *Arterioscler Thromb Vasc Biol* 23, 218-223.
36. Chen, C.C., Lamping, K.G., Nuno, D.W., Barresi, R., Prouty, S.J., Lavoie, J.L., Cribbs, L.L., England, S.K., Sigmund, C.D., Weiss, R.M., *et al.* (2003). Abnormal coronary function in mice deficient in $\alpha 1\text{H}$ T-type Ca^{2+} channels. *Science* 302, 1416-1418.
37. Chen, R.S., Deng, T.C., Garcia, T., Sellers, Z.M., and Best, P.M. (2007a). Calcium channel gamma subunits: a functionally diverse protein family. *Cell Biochem Biophys* 47, 178-186.
38. Chen, Y., Balasubramanian, V., Peng, J., Hurlock, E.C., Tallquist, M., Li, J., and Lu, Q.R. (2007b). Isolation and culture of rat and mouse oligodendrocyte precursor cells. *Nat Protoc* 2, 1044-1051.
39. Cheung, K.K., Yeung, S.S., Au, S.W., Lam, L.S., Dai, Z.Q., Li, Y.H., and Yeung, E.W. (2011). Expression and association of TRPC1 with TRPC3 during skeletal myogenesis. *Muscle Nerve* 44, 358-365.
40. Chomczynski, P., and Sacchi, N. (1987). Single-step method of RNA isolation by acid guanidinium thiocyanate-phenol-chloroform extraction. *Anal Biochem* 162, 156-159.

41. Clapham, D.E. (2003). TRP channels as cellular sensors. *Nature* 426, 517-524.
42. Clapham, D.E. (2007). Calcium signaling. *Cell* 131, 1047-1058.
43. Colasoul, B., Schraenen, A., Lemaire, K., Quintens, R., Van Lommel, L., Segal, A., Owsianik, G., Talavera, K., Voets, T., Margolskee, R.F., *et al.* (2010). Loss of high-frequency glucose-induced Ca^{2+} oscillations in pancreatic islets correlates with impaired glucose tolerance in *Trpm5*^{-/-} mice. *Proc Natl Acad Sci U S A* 107, 5208-5213.
44. Conti, F., DeBiasi, S., Minelli, A., and Melone, M. (1996). Expression of NR1 and NR2A/B subunits of the NMDA receptor in cortical astrocytes. *Glia* 17, 254-258.
45. Cosens, D.J., and Manning, A. (1969). Abnormal electroretinogram from a *Drosophila* mutant. *Nature* 224, 285-287.
46. Davies, A., Kadurin, I., Alvarez-Laviada, A., Douglas, L., Nieto-Rostro, M., Bauer, C.S., Pratt, W.S., and Dolphin, A.C. (2010). The $\alpha 2\delta$ subunits of voltage-gated calcium channels form GPI-anchored proteins, a posttranslational modification essential for function. *Proc Natl Acad Sci U S A* 107, 1654-1659.
47. Dietrich, A., Fahlbusch, M., and Gudermann, T. (2014). Classical Transient Receptor Potential 1 (TRPC1): Channel or Channel Regulator? *Cells* 3, 939-962.
48. Dietrich, A., and Gudermann, T. (2014). TRPC6: physiological function and pathophysiological relevance. *Handb Exp Pharmacol* 222, 157-188.
49. Dietrich, A., Kalwa, H., Storch, U., Mederos y Schnitzler, M., Salanova, B., Pinkenburg, O., Dubrovskaya, G., Essin, K., Gollasch, M., Birnbaumer, L., *et al.* (2007). Pressure-induced and store-operated cation influx in vascular smooth muscle cells is independent of TRPC1. *Pflugers Arch* 455, 465-477.
50. Dietrich, A., Mederos, Y.S.M., Gollasch, M., Gross, V., Storch, U., Dubrovskaya, G., Obst, M., Yildirim, E., Salanova, B., Kalwa, H., *et al.* (2005). Increased vascular smooth muscle contractility in TRPC6^{-/-} mice. *Mol Cell Biol* 25, 6980-6989.
51. Dolphin, A.C. (2003). Beta subunits of voltage-gated calcium channels. *J Bioenerg Biomembr* 35, 599-620.
52. Dolphin, A.C. (2013). The $\alpha 2\delta$ subunits of voltage-gated calcium channels. *Biochim Biophys Acta* 1828, 1541-1549.
53. Dutton, R.P., and McCunn, M. (2003). Traumatic brain injury. *Curr Opin Crit Care* 9, 503-509.
54. Eberst, R., Dai, S., Klugbauer, N., and Hofmann, F. (1997). Identification and functional characterization of a calcium channel gamma subunit. *Pflugers Arch* 433, 633-637.
55. Eckel, J., Lavin, P.J., Finch, E.A., Mukerji, N., Burch, J., Gbadegesin, R., Wu, G., Bowling, B., Byrd, A., Hall, G., *et al.* (2011). TRPC6 enhances angiotensin II-induced albuminuria. *J Am Soc Nephrol* 22, 526-535.
56. Ellis, S.B., Williams, M.E., Ways, N.R., Brenner, R., Sharp, A.H., Leung, A.T., Campbell, K.P., McKenna, E., Koch, W.J., Hui, A., *et al.* (1988). Sequence and expression of mRNAs encoding the $\alpha 1$ and $\alpha 2$ subunits of a DHP-sensitive calcium channel. *Science* 241, 1661-1664.
57. Ertel, E.A., Campbell, K.P., Harpold, M.M., Hofmann, F., Mori, Y., Perez-Reyes, E., Schwartz, A., Snutch, T.P., Tanabe, T., Birnbaumer, L., *et al.*

- (2000). Nomenclature of voltage-gated calcium channels. *Neuron* 25, 533-535.
58. Fan, D., Grooms, S.Y., Araneda, R.C., Johnson, A.B., Dobrenis, K., Kessler, J.A., and Zukin, R.S. (1999). AMPA receptor protein expression and function in astrocytes cultured from hippocampus. *J Neurosci Res* 57, 557-571.
59. Fawcett, J.W., and Asher, R.A. (1999). The glial scar and central nervous system repair. *Brain Res Bull* 49, 377-391.
60. Feske, S., Gwack, Y., Prakriya, M., Srikanth, S., Puppel, S.H., Tanasa, B., Hogan, P.G., Lewis, R.S., Daly, M., and Rao, A. (2006). A mutation in Orai1 causes immune deficiency by abrogating CRAC channel function. *Nature* 441, 179-185.
61. Flockerzi, V. (2007). An introduction on TRP channels. *Handb Exp Pharmacol*, 1-19.
62. Flockerzi, V., Oeken, H.J., Hofmann, F., Pelzer, D., Cavalie, A., and Trautwein, W. (1986). Purified dihydropyridine-binding site from skeletal muscle t-tubules is a functional calcium channel. *Nature* 323, 66-68.
63. Freichel, M., Almering, J., and Tsvilovskyy, V. (2012). The Role of TRP Proteins in Mast Cells. *Front Immunol* 3, 150.
64. Freichel, M., Suh, S.H., Pfeifer, A., Schweig, U., Trost, C., Weissgerber, P., Biel, M., Philipp, S., Freise, D., Droogmans, G., *et al.* (2001). Lack of an endothelial store-operated Ca^{2+} current impairs agonist-dependent vasorelaxation in TRP4-/- mice. *Nat Cell Biol* 3, 121-127.
65. Freichel, M., Tsvilovskyy, V., and Camacho-Londono, J.E. (2014). TRPC4- and TRPC4-containing channels. *Handb Exp Pharmacol* 222, 85-128.
66. Freise, D., Held, B., Wissenbach, U., Pfeifer, A., Trost, C., Himmerkus, N., Schweig, U., Freichel, M., Biel, M., Hofmann, F., *et al.* (2000). Absence of the gamma subunit of the skeletal muscle dihydropyridine receptor increases L-type Ca^{2+} currents and alters channel inactivation properties. *J Biol Chem* 275, 14476-14481.
67. Gao, K., Wang, C.R., Jiang, F., Wong, A.Y., Su, N., Jiang, J.H., Chai, R.C., Vatcher, G., Teng, J., Chen, J., *et al.* (2013). Traumatic scratch injury in astrocytes triggers calcium influx to activate the JNK/c-Jun/AP-1 pathway and switch on GFAP expression. *Glia* 61, 2063-2077.
68. Gao, Y., Cao, E., Julius, D., and Cheng, Y. (2016). TRPV1 structures in nanodiscs reveal mechanisms of ligand and lipid action. *Nature* 534, 347-351.
69. Gautron, S., Dos Santos, G., Pinto-Henrique, D., Koulakoff, A., Gros, F., and Berwald-Netter, Y. (1992). The glial voltage-gated sodium channel: cell- and tissue-specific mRNA expression. *Proc Natl Acad Sci U S A* 89, 7272-7276.
70. Gregg, R.G., Messing, A., Strube, C., Beurg, M., Moss, R., Behan, M., Sukhareva, M., Haynes, S., Powell, J.A., Coronado, R., *et al.* (1996). Absence of the beta subunit (cchb1) of the skeletal muscle dihydropyridine receptor alters expression of the alpha 1 subunit and eliminates excitation-contraction coupling. *Proc Natl Acad Sci U S A* 93, 13961-13966.
71. Grimaldi, M., Maratos, M., and Verma, A. (2003). Transient receptor potential channel activation causes a novel form of $[\text{Ca}^{2+}]$ oscillations

- and is not involved in capacitative Ca^{2+} entry in glial cells. *J Neurosci* 23, 4737-4745.
72. Gross, S.A., Guzman, G.A., Wissenbach, U., Philipp, S.E., Zhu, M.X., Bruns, D., and Cavalie, A. (2009). TRPC5 is a Ca^{2+} activated channel functionally coupled to Ca^{2+} -selective ion channels. *J Biol Chem* 284, 34423-34432.
 73. Grynkiewicz, G., Poenie, M., and Tsien, R.Y. (1985). A new generation of Ca^{2+} indicators with greatly improved fluorescence properties. *J Biol Chem* 260, 3440-3450.
 74. Gurkoff, G., Shahlaie, K., Lyeth, B., and Berman, R. (2013). Voltage-gated calcium channel antagonists and traumatic brain injury. *Pharmaceuticals (Basel)* 6, 788-812.
 75. Harteneck, C., and Gollasch, M. (2011). Pharmacological modulation of diacylglycerol-sensitive TRPC3/6/7 channels. *Curr Pharm Biotechnol* 12, 35-41.
 76. Hartmann, J., Dragicevic, E., Adelsberger, H., Henning, H.A., Sumser, M., Abramowitz, J., Blum, R., Dietrich, A., Freichel, M., Flockerzi, V., *et al.* (2008). TRPC3 channels are required for synaptic transmission and motor coordination. *Neuron* 59, 392-398.
 77. Hirschler-Laszkiewicz, I., Zhang, W., Keefer, K., Conrad, K., Tong, Q., Chen, S.J., Bronson, S., Cheung, J.Y., and Miller, B.A. (2012). Trpc2 depletion protects red blood cells from oxidative stress-induced hemolysis. *Exp Hematol* 40, 71-83.
 78. Hisatsune, C., Nakamura, K., Kuroda, Y., Nakamura, T., and Mikoshiba, K. (2005). Amplification of Ca^{2+} signaling by diacylglycerol-mediated inositol 1,4,5-trisphosphate production. *J Biol Chem* 280, 11723-11730.
 79. Hofmann, F., Biel, M., and Flockerzi, V. (1994). Molecular basis for Ca^{2+} channel diversity. *Annu Rev Neurosci* 17, 399-418.
 80. Hofmann, T., Obukhov, A.G., Schaefer, M., Harteneck, C., Gudermann, T., and Schultz, G. (1999). Direct activation of human TRPC6 and TRPC3 channels by diacylglycerol. *Nature* 397, 259-263.
 81. Hofmann, T., Schaefer, M., Schultz, G., and Gudermann, T. (2000). Transient receptor potential channels as molecular substrates of receptor-mediated cation entry. *J Mol Med (Berl)* 78, 14-25.
 82. Iglesias, J., Morales, L., and Barreto, G.E. (2016). Metabolic and Inflammatory Adaptation of Reactive Astrocytes: Role of PPARs. *Mol Neurobiol*.
 83. Jun, K., Piedras-Renteria, E.S., Smith, S.M., Wheeler, D.B., Lee, S.B., Lee, T.G., Chin, H., Adams, M.E., Scheller, R.H., Tsien, R.W., *et al.* (1999). Ablation of P/Q-type Ca^{2+} channel currents, altered synaptic transmission, and progressive ataxia in mice lacking the $\alpha(1A)$ -subunit. *Proc Natl Acad Sci U S A* 96, 15245-15250.
 84. Jungblut, M., Tiveron, M.C., Barral, S., Abrahamsen, B., Knobel, S., Pennartz, S., Schmitz, J., Perraut, M., Pfrieger, F.W., Stoffel, W., *et al.* (2012). Isolation and characterization of living primary astroglial cells using the new GLAST-specific monoclonal antibody ACSA-1. *Glia* 60, 894-907.
 85. Kanemaru, K., Kubota, J., Sekiya, H., Hirose, K., Okubo, Y., and Iino, M. (2013). Calcium-dependent N-cadherin up-regulation mediates reactive

- astrogliosis and neuroprotection after brain injury. *Proc Natl Acad Sci U S A* 110, 11612-11617.
86. Katiyar, R., Weissgerber, P., Roth, E., Dorr, J., Sothilingam, V., Garcia Garrido, M., Beck, S.C., Seeliger, M.W., Beck, A., Schmitz, F., *et al.* (2015). Influence of the beta2-Subunit of L-Type Voltage-Gated Cav Channels on the Structural and Functional Development of Photoreceptor Ribbon Synapses. *Invest Ophthalmol Vis Sci* 56, 2312-2324.
 87. Kim, D., Park, D., Choi, S., Lee, S., Sun, M., Kim, C., and Shin, H.S. (2003). Thalamic control of visceral nociception mediated by T-type Ca^{2+} channels. *Science* 302, 117-119.
 88. Kim, M.S., Lee, K.P., Yang, D., Shin, D.M., Abramowitz, J., Kiyonaka, S., Birnbaumer, L., Mori, Y., and Muallem, S. (2011). Genetic and pharmacologic inhibition of the Ca^{2+} influx channel TRPC3 protects secretory epithelia from Ca^{2+} -dependent toxicity. *Gastroenterology* 140, 2107-2115, 2115 e2101-2104.
 89. Kim, Y.J., and Kang, T.C. (2015). The role of TRPC6 in seizure susceptibility and seizure-related neuronal damage in the rat dentate gyrus. *Neuroscience* 307, 215-230.
 90. Kimelberg, H.K., and Nedergaard, M. (2010). Functions of astrocytes and their potential as therapeutic targets. *Neurotherapeutics* 7, 338-353.
 91. Kiselyov, K., van Rossum, D.B., and Patterson, R.L. (2010). TRPC channels in pheromone sensing. *Vitam Horm* 83, 197-213.
 92. Kiyonaka, S., Kato, K., Nishida, M., Mio, K., Numaga, T., Sawaguchi, Y., Yoshida, T., Wakamori, M., Mori, E., Numata, T., *et al.* (2009). Selective and direct inhibition of TRPC3 channels underlies biological activities of a pyrazole compound. *Proc Natl Acad Sci U S A* 106, 5400-5405.
 93. Koschak, A., Reimer, D., Huber, I., Grabner, M., Glossmann, H., Engel, J., and Striessnig, J. (2001). α 1D (Cav1.3) subunits can form I-type Ca^{2+} channels activating at negative voltages. *J Biol Chem* 276, 22100-22106.
 94. Kraft, R. (2015). STIM and ORAI proteins in the nervous system. *Channels (Austin)* 9, 245-252.
 95. Latour, I., Hamid, J., Beedle, A.M., Zamponi, G.W., and Macvicar, B.A. (2003). Expression of voltage-gated Ca^{2+} channel subtypes in cultured astrocytes. *Glia* 41, 347-353.
 96. Leuner, K., Kazanski, V., Muller, M., Essin, K., Henke, B., Gollasch, M., Harteneck, C., and Muller, W.E. (2007). Hyperforin--a key constituent of St. John's wort specifically activates TRPC6 channels. *Faseb J* 21, 4101-4111.
 97. Liang, C., Du, T., Zhou, J., Verkhatsky, A., and Peng, L. (2014). Ammonium increases Ca^{2+} signalling and up-regulates expression of TRPC1 gene in astrocytes in primary cultures and in the in vivo brain. *Neurochem Res* 39, 2127-2135.
 98. Liao, M., Cao, E., Julius, D., and Cheng, Y. (2013). Structure of the TRPV1 ion channel determined by electron cryo-microscopy. *Nature* 504, 107-112.
 99. Liao, Y., Erxleben, C., Yildirim, E., Abramowitz, J., Armstrong, D.L., and Birnbaumer, L. (2007). Orai proteins interact with TRPC channels and

- confer responsiveness to store depletion. *Proc Natl Acad Sci U S A* 104, 4682-4687.
100. Lichtenegger, M., and Groschner, K. (2014). TRPC3: a multifunctional signaling molecule. *Handb Exp Pharmacol* 222, 67-84.
 101. Linde, C.I., Baryshnikov, S.G., Mazzocco-Spezia, A., and Golovina, V.A. (2011). Dysregulation of Ca^{2+} signaling in astrocytes from mice lacking amyloid precursor protein. *Am J Physiol Cell Physiol* 300, C1502-1512.
 102. Lintschinger, B., Balzer-Geldsetzer, M., Baskaran, T., Graier, W.F., Romanin, C., Zhu, M.X., and Groschner, K. (2000). Coassembly of Trp1 and Trp3 proteins generates diacylglycerol- and Ca^{2+} -sensitive cation channels. *J Biol Chem* 275, 27799-27805.
 103. Lipscombe, D., Helton, T.D., and Xu, W. (2004). L-type calcium channels: the low down. *J Neurophysiol* 92, 2633-2641.
 104. Liu, X., Cheng, K.T., Bandyopadhyay, B.C., Pani, B., Dietrich, A., Paria, B.C., Swaim, W.D., Beech, D., Yildirim, E., Singh, B.B., *et al.* (2007). Attenuation of store-operated Ca^{2+} current impairs salivary gland fluid secretion in TRPC1(-/-) mice. *Proc Natl Acad Sci U S A* 104, 17542-17547.
 105. Lucas, P., Ukhanov, K., Leinders-Zufall, T., and Zufall, F. (2003). A diacylglycerol-gated cation channel in vomeronasal neuron dendrites is impaired in TRPC2 mutant mice: mechanism of pheromone transduction. *Neuron* 40, 551-561.
 106. MacVicar, B.A., and Tse, F.W. (1988). Norepinephrine and cyclic adenosine 3':5'-cyclic monophosphate enhance a nifedipine-sensitive calcium current in cultured rat astrocytes. *Glia* 1, 359-365.
 107. Malarkey, E.B., Ni, Y., and Papura, V. (2008). Ca^{2+} entry through TRPC1 channels contributes to intracellular Ca^{2+} dynamics and consequent glutamate release from rat astrocytes. *Glia* 56, 821-835.
 108. Mangoni, M.E., Traboulsie, A., Leoni, A.L., Couette, B., Marger, L., Le Quang, K., Kupfer, E., Cohen-Solal, A., Vilar, J., Shin, H.S., *et al.* (2006). Bradycardia and slowing of the atrioventricular conduction in mice lacking $\text{CaV}3.1/\alpha 1\text{G}$ T-type calcium channels. *Circ Res* 98, 1422-1430.
 109. Maragakis, N.J., and Rothstein, J.D. (2006). Mechanisms of Disease: astrocytes in neurodegenerative disease. *Nat Clin Pract Neurol* 2, 679-689.
 110. Miller, B.A. (2014). Trpc2. *Handb Exp Pharmacol* 222, 53-65.
 111. Miyano, K., Morioka, N., Sugimoto, T., Shiraishi, S., Uezono, Y., and Nakata, Y. (2010). Activation of the neurokinin-1 receptor in rat spinal astrocytes induces Ca^{2+} release from IP_3 -sensitive Ca^{2+} stores and extracellular Ca^{2+} influx through TRPC3. *Neurochem Int* 57, 923-934.
 112. Montell, C., and Rubin, G.M. (1989). Molecular characterization of the *Drosophila* trp locus: a putative integral membrane protein required for phototransduction. *Neuron* 2, 1313-1323.
 113. Montgomery, D.L. (1994). Astrocytes: form, functions, and roles in disease. *Vet Pathol* 31, 145-167.
 114. Muller, C.S., Haupt, A., Bildl, W., Schindler, J., Knaus, H.G., Meissner, M., Rammner, B., Striessnig, J., Flockerzi, V., Fakler, B., *et al.*

- (2010). Quantitative proteomics of the Cav2 channel nano-environments in the mammalian brain. *Proc Natl Acad Sci U S A* 107, 14950-14957.
115. Munakata, M., Shirakawa, H., Nagayasu, K., Miyanohara, J., Miyake, T., Nakagawa, T., Katsuki, H., and Kaneko, S. (2013). Transient receptor potential canonical 3 inhibitor Pyr3 improves outcomes and attenuates astrogliosis after intracerebral hemorrhage in mice. *Stroke* 44, 1981-1987.
 116. Murakami, M., Fleischmann, B., De Felipe, C., Freichel, M., Trost, C., Ludwig, A., Wissenbach, U., Schwegler, H., Hofmann, F., Hescheler, J., *et al.* (2002). Pain perception in mice lacking the beta3 subunit of voltage-activated calcium channels. *J Biol Chem* 277, 40342-40351.
 117. Nakao, K., Shirakawa, H., Sugishita, A., Matsutani, I., Niidome, T., Nakagawa, T., and Kaneko, S. (2008). Ca²⁺ mobilization mediated by transient receptor potential canonical 3 is associated with thrombin-induced morphological changes in 1321N1 human astrocytoma cells. *J Neurosci Res* 86, 2722-2732.
 118. Neary, J.T., and Zhu, Q. (1994). Signaling by ATP receptors in astrocytes. *Neuroreport* 5, 1617-1620.
 119. Neely, G.G., Hess, A., Costigan, M., Keene, A.C., Goulas, S., Langeslag, M., Griffin, R.S., Belfer, I., Dai, F., Smith, S.B., *et al.* (2010). A genome-wide *Drosophila* screen for heat nociception identifies alpha2delta3 as an evolutionarily conserved pain gene. *Cell* 143, 628-638.
 120. Nesin, V., and Tsiokas, L. (2014). Trpc1. *Handb Exp Pharmacol* 222, 15-51.
 121. Newton, R.A., Bingham, S., Case, P.C., Sanger, G.J., and Lawson, S.N. (2001). Dorsal root ganglion neurons show increased expression of the calcium channel alpha2delta-1 subunit following partial sciatic nerve injury. *Brain Res Mol Brain Res* 95, 1-8.
 122. Nicoll, R.A., Tomita, S., and Brecht, D.S. (2006). Auxiliary subunits assist AMPA-type glutamate receptors. *Science* 311, 1253-1256.
 123. Niemeyer, M.I., and Lummis, S.C. (2001). The role of the agonist binding site in Ca(2+) inhibition of the recombinant 5-HT(3A) receptor. *Eur J Pharmacol* 428, 153-161.
 124. Nilius, B., and Flockerzi, V. (2014). Mammalian transient receptor potential (TRP) cation channels. Preface. *Handb Exp Pharmacol* 223, v - vi.
 125. Nishizuka, Y. (1984). The role of protein kinase C in cell surface signal transduction and tumour promotion. *Nature* 308, 693-698.
 126. Nowak, L., Ascher, P., and Berwald-Netter, Y. (1987). Ionic channels in mouse astrocytes in culture. *J Neurosci* 7, 101-109.
 127. Nowycky, M.C., Fox, A.P., and Tsien, R.W. (1985). Three types of neuronal calcium channel with different calcium agonist sensitivity. *Nature* 316, 440-443.
 128. Okada, T., Inoue, R., Yamazaki, K., Maeda, A., Kurosaki, T., Yamakuni, T., Tanaka, I., Shimizu, S., Ikenaka, K., Imoto, K., *et al.* (1999). Molecular and functional characterization of a novel mouse transient receptor potential protein homologue TRP7. Ca(2+)-permeable cation channel that is constitutively activated and enhanced by

- stimulation of G protein-coupled receptor. *J Biol Chem* 274, 27359-27370.
129. Olivera, B.M., Miljanich, G.P., Ramachandran, J., and Adams, M.E. (1994). Calcium channel diversity and neurotransmitter release: the omega-conotoxins and omega-agatoxins. *Annu Rev Biochem* 63, 823-867.
130. Ong, E.C., Nesin, V., Long, C.L., Bai, C.X., Guz, J.L., Ivanov, I.P., Abramowitz, J., Birnbaumer, L., Humphrey, M.B., and Tsiokas, L. (2013). A TRPC1 protein-dependent pathway regulates osteoclast formation and function. *J Biol Chem* 288, 22219-22232.
131. Paez, P.M., Fulton, D., Spreuer, V., Handley, V., and Campagnoni, A.T. (2011). Modulation of canonical transient receptor potential channel 1 in the proliferation of oligodendrocyte precursor cells by the golli products of the myelin basic protein gene. *J Neurosci* 31, 3625-3637.
132. Parpura, V., and Verkhratsky, A. (2012). Astrocytes revisited: concise historic outlook on glutamate homeostasis and signaling. *Croat Med J* 53, 518-528.
133. Paulsen, C.E., Armache, J.P., Gao, Y., Cheng, Y., and Julius, D. (2015). Structure of the TRPA1 ion channel suggests regulatory mechanisms. *Nature* 525, 552.
134. Pereverzev, A., Mikhna, M., Vajna, R., Gissel, C., Henry, M., Weiergraber, M., Hescheler, J., Smyth, N., and Schneider, T. (2002). Disturbances in glucose-tolerance, insulin-release, and stress-induced hyperglycemia upon disruption of the Ca(v)2.3 (alpha 1E) subunit of voltage-gated Ca(2+) channels. *Mol Endocrinol* 16, 884-895.
135. Phelan, K.D., Shwe, U.T., Abramowitz, J., Birnbaumer, L., and Zheng, F. (2014). Critical role of canonical transient receptor potential channel 7 in initiation of seizures. *Proc Natl Acad Sci U S A* 111, 11533-11538.
136. Phelan, K.D., Shwe, U.T., Abramowitz, J., Wu, H., Rhee, S.W., Howell, M.D., Gottschall, P.E., Freichel, M., Flockerzi, V., Birnbaumer, L., *et al.* (2013). Canonical transient receptor channel 5 (TRPC5) and TRPC1/4 contribute to seizure and excitotoxicity by distinct cellular mechanisms. *Mol Pharmacol* 83, 429-438.
137. Philipp, S., Cavalie, A., Freichel, M., Wissenbach, U., Zimmer, S., Trost, C., Marquart, A., Murakami, M., and Flockerzi, V. (1996). A mammalian capacitative calcium entry channel homologous to Drosophila TRP and TRPL. *Embo J* 15, 6166-6171.
138. Philipp, S., Hambrecht, J., Braslavski, L., Schroth, G., Freichel, M., Murakami, M., Cavalie, A., and Flockerzi, V. (1998). A novel capacitative calcium entry channel expressed in excitable cells. *Embo J* 17, 4274-4282.
139. Platzter, J., Engel, J., Schrott-Fischer, A., Stephan, K., Bova, S., Chen, H., Zheng, H., and Striessnig, J. (2000). Congenital deafness and sinoatrial node dysfunction in mice lacking class D L-type Ca²⁺ channels. *Cell* 102, 89-97.
140. Reuter, H. (1967). The dependence of slow inward current in Purkinje fibres on the extracellular calcium-concentration. *J Physiol* 192, 479-492.

141. Reuter, H. (1983). Calcium channel modulation by neurotransmitters, enzymes and drugs. *Nature* **301**, 569-574.
142. Reuter, H. (1986). Voltage-dependent mechanisms for raising intracellular free calcium concentration: calcium channels. *Ciba Found Symp* **122**, 5-22.
143. Rhodes, K.E., and Fawcett, J.W. (2004). Chondroitin sulphate proteoglycans: preventing plasticity or protecting the CNS? *J Anat* **204**, 33-48.
144. Riccio, A., Li, Y., Moon, J., Kim, K.S., Smith, K.S., Rudolph, U., Gapon, S., Yao, G.L., Tsvetkov, E., Rodig, S.J., *et al.* (2009). Essential role for TRPC5 in amygdala function and fear-related behavior. *Cell* **137**, 761-772.
145. Riccio, A., Li, Y., Tsvetkov, E., Gapon, S., Yao, G.L., Smith, K.S., Engin, E., Rudolph, U., Bolshakov, V.Y., and Clapham, D.E. (2014). Decreased anxiety-like behavior and Galphq/11-dependent responses in the amygdala of mice lacking TRPC4 channels. *J Neurosci* **34**, 3653-3667.
146. Ruth, P., Rohrkasten, A., Biel, M., Bosse, E., Regulla, S., Meyer, H.E., Flockerzi, V., and Hofmann, F. (1989). Primary structure of the beta subunit of the DHP-sensitive calcium channel from skeletal muscle. *Science* **245**, 1115-1118.
147. Saadoun, S., Papadopoulos, M.C., Watanabe, H., Yan, D., Manley, G.T., and Verkman, A.S. (2005). Involvement of aquaporin-4 in astroglial cell migration and glial scar formation. *J Cell Sci* **118**, 5691-5698.
148. Saegusa, H., Kurihara, T., Zong, S., Kazuno, A., Matsuda, Y., Nonaka, T., Han, W., Toriyama, H., and Tanabe, T. (2001). Suppression of inflammatory and neuropathic pain symptoms in mice lacking the N-type Ca^{2+} channel. *Embo J* **20**, 2349-2356.
149. Saotome, K., Singh, A.K., Yelshanskaya, M.V., and Sobolevsky, A.I. (2016). Crystal structure of the epithelial calcium channel TRPV6. *Nature* **534**, 506-511.
150. Schachtrup, C., Ryu, J.K., Helmrick, M.J., Vagena, E., Galanakis, D.K., Degen, J.L., Margolis, R.U., and Akassoglou, K. (2010). Fibrinogen triggers astrocyte scar formation by promoting the availability of active TGF-beta after vascular damage. *J Neurosci* **30**, 5843-5854.
151. Schildge, S., Bohrer, C., Beck, K., and Schachtrup, C. (2013). Isolation and culture of mouse cortical astrocytes. *J Vis Exp*.
152. Schleifer, H., Doleschal, B., Lichtenegger, M., Oppenrieder, R., Derler, I., Frischauf, I., Glasnov, T.N., Kappe, C.O., Romanin, C., and Groschner, K. (2012). Novel pyrazole compounds for pharmacological discrimination between receptor-operated and store-operated Ca^{2+} entry pathways. *Br J Pharmacol* **167**, 1712-1722.
153. Schmitt, A., Asan, E., Puschel, B., and Kugler, P. (1997). Cellular and regional distribution of the glutamate transporter GLAST in the CNS of rats: nonradioactive in situ hybridization and comparative immunocytochemistry. *J Neurosci* **17**, 1-10.
154. Scimemi, A. (2013). A TRP among the astrocytes. *J Physiol* **591**, 9-15.

155. Seisenberger, C., Specht, V., Welling, A., Platzner, J., Pfeifer, A., Kuhbandner, S., Striessnig, J., Klugbauer, N., Feil, R., and Hofmann, F. (2000). Functional embryonic cardiomyocytes after disruption of the L-type $\alpha 1C$ (Cav1.2) calcium channel gene in the mouse. *J Biol Chem* 275, 39193-39199.
156. Sell, T.S., Belkacemi, T., Flockerzi, V., and Beck, A. (2014). Protonophore properties of hyperforin are essential for its pharmacological activity. *Sci Rep* 4.
157. Selvaraj, S., Sun, Y., Watt, J.A., Wang, S., Lei, S., Birnbaumer, L., and Singh, B.B. (2012). Neurotoxin-induced ER stress in mouse dopaminergic neurons involves downregulation of TRPC1 and inhibition of AKT/mTOR signaling. *J Clin Invest* 122, 1354-1367.
158. Silver, J., and Miller, J.H. (2004). Regeneration beyond the glial scar. *Nat Rev Neurosci* 5, 146-156.
159. Sofroniew, M.V. (2009). Molecular dissection of reactive astrogliosis and glial scar formation. *Trends Neurosci* 32, 638-647.
160. Song, X., Zhao, Y., Narcisse, L., Duffy, H., Kress, Y., Lee, S., and Brosnan, C.F. (2005). Canonical transient receptor potential channel 4 (TRPC4) co-localizes with the scaffolding protein ZO-1 in human fetal astrocytes in culture. *Glia* 49, 418-429.
161. Storch, U., Forst, A.L., Philipp, M., Gudermann, T., and Mederos y Schnitzler, M. (2012). Transient receptor potential channel 1 (TRPC1) reduces calcium permeability in heteromeric channel complexes. *J Biol Chem* 287, 3530-3540.
162. Stowers, L., Holy, T.E., Meister, M., Dulac, C., and Koentges, G. (2002). Loss of sex discrimination and male-male aggression in mice deficient for TRP2. *Science* 295, 1493-1500.
163. Streifel, K.M., Gonzales, A.L., De Miranda, B., Mouneimne, R., Earley, S., and Tjalkens, R. (2014). Dopaminergic neurotoxicants cause biphasic inhibition of purinergic calcium signaling in astrocytes. *PLoS One* 9, e110996.
164. Striedinger, K., and Scemes, E. (2008). Interleukin-1 β affects calcium signaling and in vitro cell migration of astrocyte progenitors. *J Neuroimmunol* 196, 116-123.
165. Strubing, C., Krapivinsky, G., Krapivinsky, L., and Clapham, D.E. (2001). TRPC1 and TRPC5 form a novel cation channel in mammalian brain. *Neuron* 29, 645-655.
166. Tagliaferri, F., Compagnone, C., Korsic, M., Servadei, F., and Kraus, J. (2006). A systematic review of brain injury epidemiology in Europe. *Acta Neurochir (Wien)* 148, 255-268; discussion 268.
167. Tanabe, T., Takeshima, H., Mikami, A., Flockerzi, V., Takahashi, H., Kangawa, K., Kojima, M., Matsuo, H., Hirose, T., and Numa, S. (1987). Primary structure of the receptor for calcium channel blockers from skeletal muscle. *Nature* 328, 313-318.
168. Tang, J., Lin, Y., Zhang, Z., Tikunova, S., Birnbaumer, L., and Zhu, M.X. (2001). Identification of common binding sites for calmodulin and inositol 1,4,5-trisphosphate receptors on the carboxyl termini of trp channels. *J Biol Chem* 276, 21303-21310.
169. Templeton, N.S. (1992). The polymerase chain reaction. History, methods, and applications. *Diagn Mol Pathol* 1, 58-72.

170. Tong, Q., Chu, X., Cheung, J.Y., Conrad, K., Stahl, R., Barber, D.L., Mignery, G., and Miller, B.A. (2004). Erythropoietin-modulated calcium influx through TRPC2 is mediated by phospholipase Cgamma and IP3R. *Am J Physiol Cell Physiol* 287, C1667-1678.
171. Trebak, M., St, J.B.G., McKay, R.R., Birnbaumer, L., and Putney, J.W., Jr. (2003). Signaling mechanism for receptor-activated canonical transient receptor potential 3 (TRPC3) channels. *J Biol Chem* 278, 16244-16252.
172. Ulbricht, W. (2005). Sodium channel inactivation: molecular determinants and modulation. *Physiol Rev* 85, 1271-1301.
173. Varga-Szabo, D., Authi, K.S., Braun, A., Bender, M., Ambily, A., Hassock, S.R., Gudermann, T., Dietrich, A., and Nieswandt, B. (2008). Store-operated Ca(2+) entry in platelets occurs independently of transient receptor potential (TRP) C1. *Pflugers Arch* 457, 377-387.
174. Venkatachalam, K., van Rossum, D.B., Patterson, R.L., Ma, H.T., and Gill, D.L. (2002). The cellular and molecular basis of store-operated calcium entry. *Nat Cell Biol* 4, E263-272.
175. Vergouwen, M.D., Vermeulen, M., and Roos, Y.B. (2006). Effect of nimodipine on outcome in patients with traumatic subarachnoid haemorrhage: a systematic review. *Lancet Neurol* 5, 1029-1032.
176. Weissgerber, P., Held, B., Bloch, W., Kaestner, L., Chien, K.R., Fleischmann, B.K., Lipp, P., Flockerzi, V., and Freichel, M. (2006). Reduced cardiac L-type Ca²⁺ current in Ca(V)beta2-/- embryos impairs cardiac development and contraction with secondary defects in vascular maturation. *Circ Res* 99, 749-757.
177. Weissgerber, P., Kriebs, U., Tsvilovskyy, V., Olausson, J., Kretz, O., Stoerger, C., Mannebach, S., Wissenbach, U., Vennekens, R., Middendorff, R., *et al.* (2012). Excision of Trpv6 gene leads to severe defects in epididymal Ca²⁺ absorption and male fertility much like single D541A pore mutation. *J Biol Chem* 287, 17930-17941.
178. Wes, P.D., Chevesich, J., Jeromin, A., Rosenberg, C., Stetten, G., and Montell, C. (1995). TRPC1, a human homolog of a Drosophila store-operated channel. *Proc Natl Acad Sci U S A* 92, 9652-9656.
179. Wu, J., Yan, Z., Li, Z., Yan, C., Lu, S., Dong, M., and Yan, N. (2015). Structure of the voltage-gated calcium channel Cav1.1 complex. *Science* 350, aad2395.
180. Wu, L.J., Sweet, T.B., and Clapham, D.E. (2010). International Union of Basic and Clinical Pharmacology. LXXVI. Current progress in the mammalian TRP ion channel family. *Pharmacol Rev* 62, 381-404.
181. Wycisk, K.A., Zeitz, C., Feil, S., Wittmer, M., Forster, U., Neidhardt, J., Wissinger, B., Zrenner, E., Wilke, R., Kohl, S., *et al.* (2006). Mutation in the auxiliary calcium-channel subunit CACNA2D4 causes autosomal recessive cone dystrophy. *Am J Hum Genet* 79, 973-977.
182. Xu, W., and Lipscombe, D. (2001). Neuronal Ca(V)1.3alpha(1) L-type channels activate at relatively hyperpolarized membrane potentials and are incompletely inhibited by dihydropyridines. *J Neurosci* 21, 5944-5951.
183. Yi, M., Dou, F., Lu, Q., Yu, Z., and Chen, H. (2016). Activation of the KCa3.1 channel contributes to traumatic scratch injury-induced

- reactive astrogliosis through the JNK/c-Jun signaling pathway. *Neurosci Lett* 624, 62-71.
184. Yue, D.T. (2004). The dawn of high-resolution structure for the queen of ion channels. *Neuron* 42, 357-359.
185. Zeng, S., Li, B., and Chen, S. (2009). Simulation of spontaneous Ca^{2+} oscillations in astrocytes mediated by voltage-gated calcium channels. *Biophys J* 97, 2429-2437.
186. Zhang, X., and Trebak, M. (2014). Transient receptor potential canonical 7: a diacylglycerol-activated non-selective cation channel. *Handb Exp Pharmacol* 222, 189-204.
187. Zholos, A.V. (2014). Trpc5. *Handb Exp Pharmacol* 222, 129-156.
188. Zhu, X., Chu, P.B., Peyton, M., and Birnbaumer, L. (1995). Molecular cloning of a widely expressed human homologue for the *Drosophila* trp gene. *FEBS Lett* 373, 193-198.
189. Zhu, X., Jiang, M., Peyton, M., Boulay, G., Hurst, R., Stefani, E., and Birnbaumer, L. (1996). trp, a novel mammalian gene family essential for agonist-activated capacitative Ca^{2+} entry. *Cell* 85, 661-671.
190. Zubcevic, L., Herzik, M.A., Jr., Chung, B.C., Liu, Z., Lander, G.C., and Lee, S.Y. (2016). Cryo-electron microscopy structure of the TRPV2 ion channel. *Nat Struct Mol Biol* 23, 180-186.

6 Supplementary Figures

Figure S1

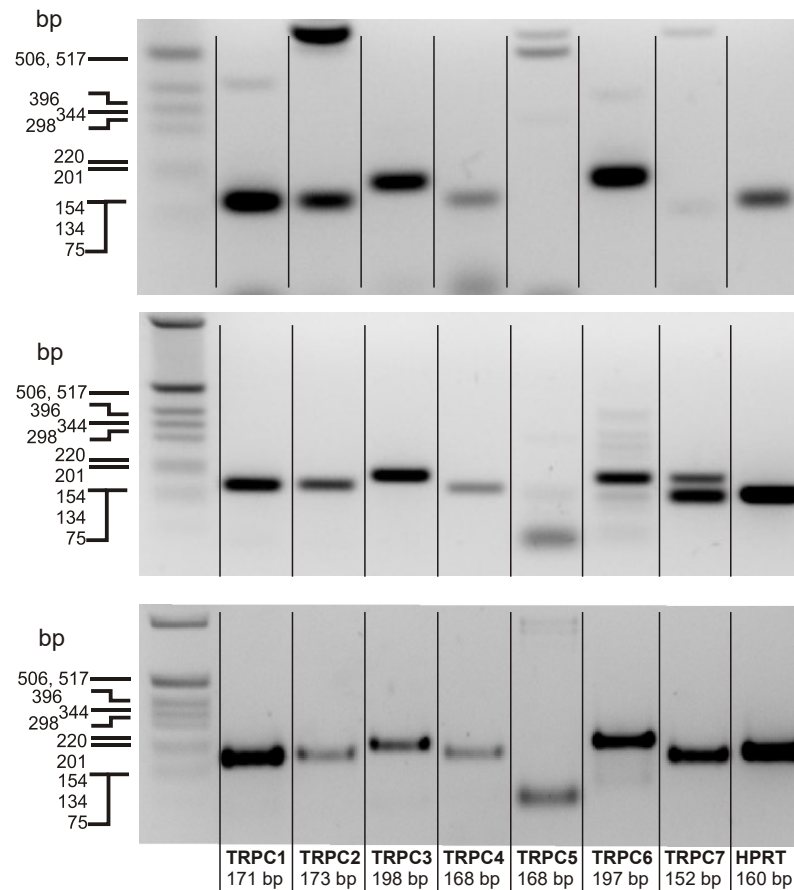


Figure 6-1 TRPC transcripts expression in enriched astrocyte culture. 3 independent RT-PCRs performed from enriched astrocyte culture RNA showing the amplification of TRPC1, TRPC2, TRPC3, TRPC4, TRPC6, TRPC7 and HPRT DNA fragments of the expected sizes.

Figure S2

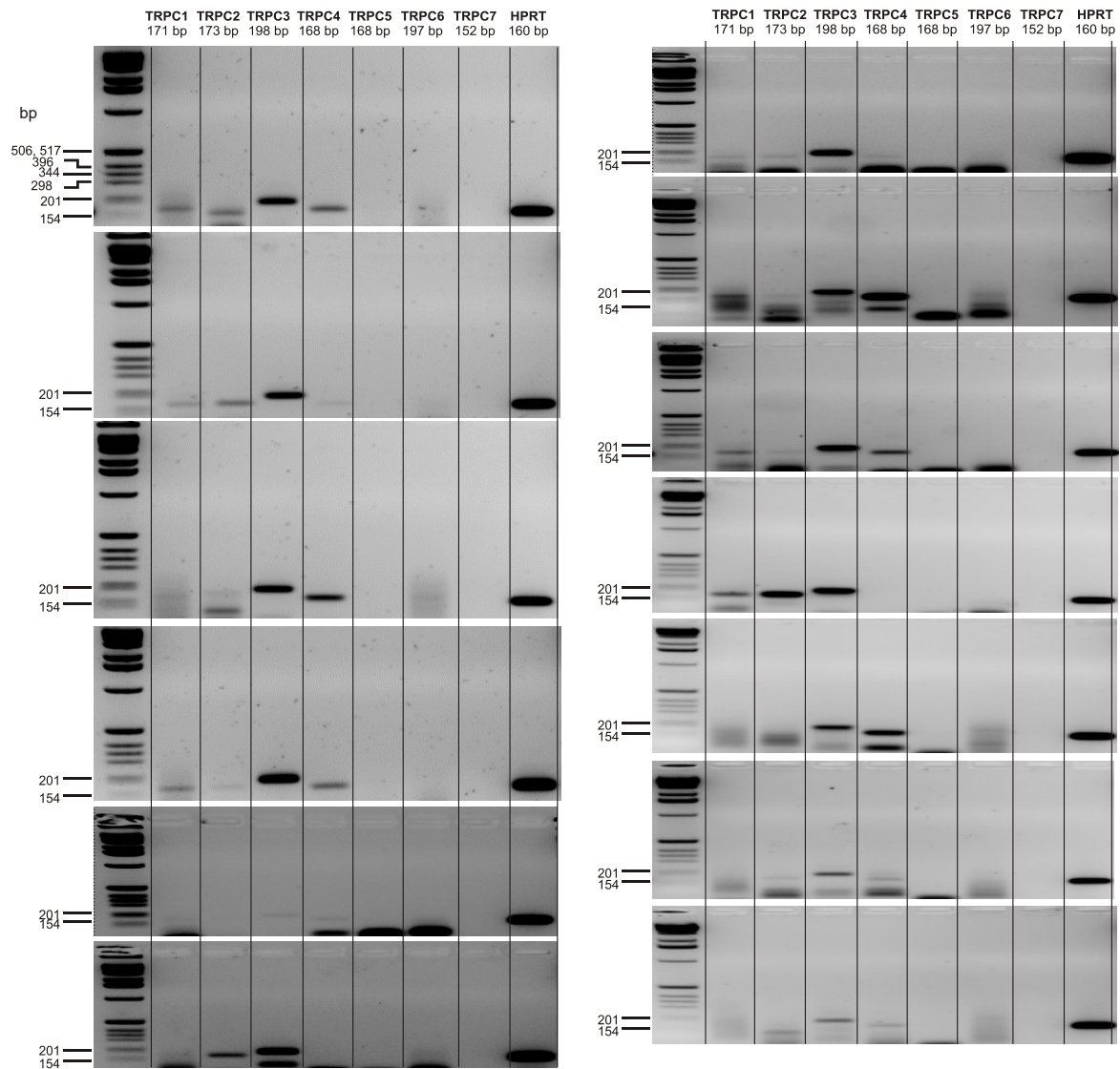


Figure 6-2 **TRPC transcripts expression in GLAST-sorted astrocytes.** 13 independent RT-PCRs performed from GLAST-sorted astrocytes showing the amplification of TRPC1, TRPC2, TRPC3, TRPC4 and HPRT DNA fragments of the expected sizes.

Figure S3

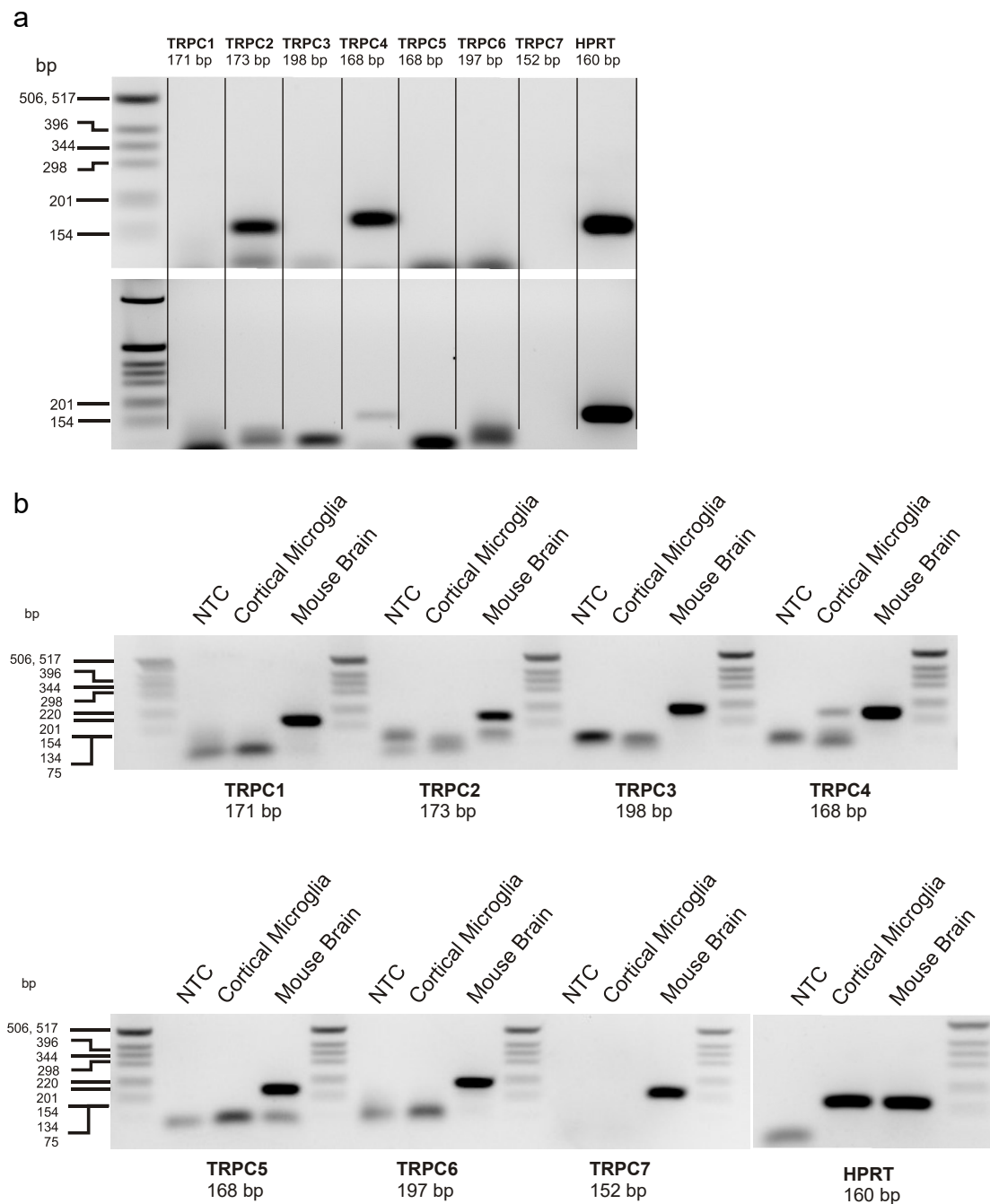


Figure 6-3 **TRPC transcripts expression in CD11b-sorted microglia.** (a and b) 3 independent RT-PCRs performed from CD11b-sorted microglia showing the amplification of TRPC2, TRPC4 and HPRT DNA fragments of the expected sizes. TRPC6 in (b) is shown in (Sell et al., 2014).

Curriculum Vitae

Personal Data

Name: Thabet Belkacemi
Date and place of birth: 22.07.1986
Manchester, United Kingdom
Email: thabet.belkacemi@yahoo.com

Education and work experience

2012-2016	PhD student and research associate at the Institute of Experimental and Clinical Pharmacology and Toxicology, Saarland University. Member of the DFG-funded research training group (Graduiertenkolleg) 1326 "Calcium-Signaling and Cellular Nanodomains".
2011-2012	Master equivalent thesis at the Institute of Experimental and Clinical Pharmacology and Toxicology, Medical Faculty, Saarland University.
2009-2011	- Assistant teacher for the laboratory sessions at the Pharmacy Department, Batna University in Algeria - Pharmacist at a private pharmacy in Batna, Algeria.
2004-2009	Pharmacist degree from the University of Batna in Algeria
2004	Secondary school certificate "Natural Sciences" Albaha, Kingdom of Saudi Arabia

Publications

Sell, T.S., **Belkacemi, T.**, Flockerzi, V., and Beck, A. (2014). Protonophore properties of hyperforin are essential for its pharmacological activity. *Sci Rep* 4.

Conferences

Poster selected for a talk: Belkacemi, T., Philipp, SE., Weissgerber, P., Flockerzi, V., and Beck, A. TRPC channels are involved in glial Ca^{2+} signaling and migration. Frühjahrstagung der Deutschen Gesellschaft für Experimentelle und Klinische Pharmakologie und Toxikologie (DGPT) 2014 Hannover, Germany.

Poster: Sell, T.S., **Belkacemi, T.**, Flockerzi, V., and Beck, A. Hyperforin is a protonophore and mediates significant H^+ currents. Frühjahrstagung der Deutschen Gesellschaft für Experimentelle und Klinische Pharmakologie und Toxikologie (DGPT) 2014 Hannover, Germany.

Poster: Belkacemi, T., Philipp, SE., Weissgerber, P., Flockerzi, V., and Beck, A. Contribution of TRPC channels on Ca^{2+} influx and migration of astrocytes. Internationales Symposium des Deutschen Zentrums für Herz-Kreislauf-Forschung (DZHK): Receptors, G Proteins and Integration of Ca^{2+} Signaling in the Cardiovascular System. 2014 Berlin, Germany.

Poster selected for a talk: Belkacemi, T., Philipp, SE., Weissgerber, P., Flockerzi, V., and Beck, A. TRPC channels mediate Ca^{2+} influx and facilitate migration of astrocytes. 2nd European Calcium Channel Conference (ECCC) 2015 Alpbach, Austria.

Manuscripts in preparation

Belkacemi, T., Hofmann, L., Wissenbach, U., Backes, C., Meese, E., Keller, A., Philipp, SE., Weissgerber, P., Flockerzi, V., and Beck, A. "TRPC1 and TRPC3 in cortical astrocytes opposingly affect astrogliosis after traumatic brain injury."

Belkacemi, T., Belkacemi A., Niermann, A., Flockerzi, V., and Beck, A. "CaV and NaV channels in cortical astrocytes: Expression and functional characterization."